VIT-AP UNIVERSITY

Proceedings of

International Conference on Advances in Transport Phenomena

(ICATP 2022)

July 16 – 18, 2022

Organized by
School of Advanced Sciences
VIT- AP University

OPEN BOOK PUBLISHER

Dr. Rashmi Dubey
Dr. Nikunja Bihari Barik
Dr. Anil Negi
Editors

ABOUT ICATP

The International Conference on Advances in Transport Phenomena (ICATP 2022) is proposed to bring along the notable speakers from across India and globe who have years of research experience in the different areas of Transport Phenomena and Applied Mathematics, and to provide our local research community with a platform where all can share and get to know about each other's research. The conference aims at providing in depth knowledge about the recent advances in a wide range of areas of Transport Phenomena which can be used to solve a plethora of real world problems. Transport phenomena can be found from nano-scale to macro-scale, from single-phase to multiphase, from non-reactive to reacting flows, and for applications in different space and domains. Some of the scientific areas covered under this topic are Convective Heat and Mass Transfer, Physiological Fluid Mechanics, Micro-fluidics, Rheology, and other related areas. The speakers invited for talks in the conference are eminent researchers from top institutions with expertise in different areas of Transport Phenomena and Fluid Mechanics. This conference would benefit post-graduate students, research scholars and young faculty members to get exposure on various areas of Transport Phenomena and would also give them the opportunity to collaborate with top researchers from these fields worldwide.

ICATP 2022, ISBN 978-81-952903-0-7

CONTENTS

ICATP 2022, ISBN 978-81-952903-0-7

Welcome Message from the Chancellor & Founder, VIT

VIT UNIVERSITY
(Estd. u/s. 3 of UGC Act 1956)

Dr. G. VISWANATHAN
Founder & Chancellor
Former Member of Parliament
Former Minister, Govt. of Tamil Nadu
President, Education Promotion Society for India, New Delhi

CHANCELLOR'S MESSAGE

With gratitude in my heart, I welcome the participants of the International Conference on Advances in Transport Phenomena (ICATP 2022) to VIT-AP University at Amaravati.

VIT-AP aims at providing quality education on par with international standards and continuously seeks to be one of its kinds by adopting innovative methods to ameliorate the quality of higher education.

Conferences such as ICATP also aim to scaffold learners and researchers for a better future and I believe that this conference will serve as a great platform to share the latest and required developments in the field of Transport Phenomena. I believe this conference will connect the world with intriguing discussions and recommendations and elevate the knowledge in this field.

I am extremely delighted that the eminent speakers, skilled researchers, dedicated faculty members, research scholars and ambitious students have added value to ICATP.

I share my congratulatory message to the organizing team for their profound efforts and wishing the conference a great success.

With best wishes,

Dr. G. Viswanathan
Founder & Chancellor

October 14, 2022

Vellore – 632 014, Tamil Nadu, India; Tel.: + 91 416 224 3100; E-mail: chancellor@vit.ac.in
Chennai Campus: Vandalur - Kelambakkam Road, Chennai - 600 127, Tamil Nadu, India; Tel.: + 91 44 3993 1555
VIT - AP University, Near AP Secretariat, Amaravati - 522 237, Andhra Pradesh, India Tel.: + 91 863 237 0555
VIT - Bhopal University, Bhopal-Indore Highway, Kothrikalan, Sehore - 466 114, Madhya Pradesh, India; Tel.: + 91 7560 254545
www.vit.ac.in

Welcome Message from Vice-Chancellor, VIT-AP University

Dr. S. V. Kota Reddy
Vice Chancellor
VIT-AP University

With great delectation, I write this message for the International Conference on Advances in Transport Phenomena (ICATP 2022) to VIT-AP University at Amaravati

I feel immense euphoria that several distinguished speakers across India and the globe associated with top institutes and universities are sharing knowledge at ICATP. More than 100 papers are going to be presented in the areas of Transport Phenomena.

I am confident that the conference will lay better avenues for researchers, academicians and students to exchange their research findings in the field of Transport Phenomena. I am extremely delighted to say that the School of Advanced Sciences (SAS) will succeed in achieving the main objective of propagating knowledge and information in the most effective manner through this conference. I am sure that this conference will fulfil the objective of driving the student community to the academic/research realm.

I appreciate the efforts and hard work put in by the entire ICATP organizing team for their wonderful contribution in organizing this conference. The efforts of the editorial board are commendable for their excellent contribution towards preparing the conference souvenir. I am sure conference souvenir as ICATP will set the standards for future editions.

Dr. S. V. Kota Reddy
Vice Chancellor
VIT-AP University

Welcome Message from Registrar, VIT-AP, University

Dr. Jagadish Chandra Mudiganti

Registrar,

VIT-AP, University

Dear Participants of ICATP 2022,

This conference on ‘Transport Phenomena’ is of great importance in the field of advanced sciences. I am sure this conference will bring forward the current trends, challenges and future prospects in the subject area. I appreciate the efforts made by the entire organizing team in inviting experts and technocrats from top universities and institutions in the country and across the globe.

Lastly, I wish the School of Advanced Sciences a grand success in achieving the conference goals and kindle curious minds.

Dr. Jagadish Chandra Mudiganti

Registrar

VIT-AP, University

Welcome Message from Convener and Co-Convener

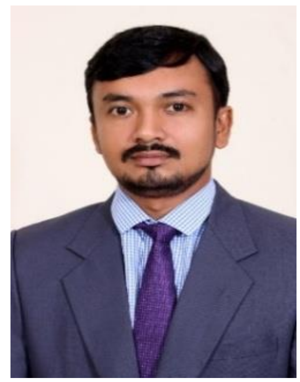

Dr. Rashmi Dubey, General Chair **Prof. S. Srinivas, Co-Chair** **Dr. Santanu Mandal, Co-Chair**

Dear Participants of ICATP 2022,
With great contentment, we the Convener and Co-Conveners of the International Conference on Transport Phenomena (ICATP 2022) welcome you all to the conference that is to be held during July 16-18, 2022 at VIT-AP University, Amaravati, Andhra Pradesh.
Through this conference, we foresee a rally for sharing insights into new research in the domain of Transport Phenomena. We hope that this conference will stimulate ideas, exchange and facilitate networking among all researchers, participants and students. We are delighted that ICATP 2022 received many submissions from eight different countries. It was a challenging task for the reviewing committee to select more than one hundred quality papers where authors will be sharing their outstanding ideas and latest research results.
The conference will offer invited talks and plenary. S ocial events will also take place to foster networking among the participants in a friendly atmosphere. We trust that you will find the ICATP 2022 professionally rewarding and stimulating as well as socially enjoyable.
Finally, we would like to express our utmost gratitude to all speakers, authors, presenters, panellists, reviewers, advisory and organising committee members for their hard work, passion and commitment to shape a high-quality conference called ICATP 2022.

Rashmi Dubey

Dr. Rashmi Dubey, Ph.D.
General Chair, ICATP-2022
Assistant Professor,
School of Advanced Sciences,
VIT-AP University,
Andhra Pradesh, India

Prof. S. Srinivas, Ph.D.
Co-Chair, ICATP-2022
Professor (HAG),
School of Advanced Sciences,
VIT-AP University,
Andhra Pradesh, India

Dr. Santanu Mandal
Co-Chair, ICATP-2022
Associate Professor & Dean,
School of Advanced Sciences,
VIT-AP University,
Andhra Pradesh, India

ADVISORY COMMITTEES

Prof. Vemuri Balakotaiah	University of Houston, USA
Prof. Andrew Rees	University of Bath, UK
Prof. Helen Wilson	University College London, UK
Prof. Alan Jaffrey Giacomin	Queen's University, Canada
Dr. Muhammad Fazal Ijaz,	Sejong University, South Korea
Prof. Peeyush Chandra	Professor (Retired), IIT Kanpur
Prof. Pradeep G. Siddheswar	Christ (Deemed to be University), Banglore
Prof. B. V. Rathish Kumar,	IIT Kanpur
Prof. P. V. S. N. Murthy,	IIT Kharagpur
Prof. T. V. S. Sekhar,	IIT Bhubaneswar
Prof. Satyajit Roy,	IIT Madras
Dr. Thirupathi Gudi,	Associate Professor, IISc Bangalore
Prof. Satyanarayana Nandury,	Former Chief Scientist and Head, Energy & Enviromental Engineering, CSIR-IICT
Prof. Karthikeyan Rajagopal,	Center for Nonlinear Systems, Chennai Institute of Technoogy

ICATP 2022, ISBN 978-81-952903-0-7

ORGANISING COMMITTEES

CHIEF PATRON

Dr. G. Viswanathan	Chancellor, VIT Group of Institutions

PATRONS

Shri Sankar Viswanathan	Vice President, VIT-AP, University
Dr. Sekar Viswanathan	Vice President, VIT-AP, University
Shri G. V. Selvam	Vice President, VIT-AP, University

CO-PATRONS

Prof. S. V. Kota Reddy	Vice Chancellor, VIT-AP, University
Prof. Jagadish C. Mudiganti	Registrar, VIT-AP, University

GENERAL CHAIR

Dr. Rashmi Dubey	School of Advanced Sciences, VIT-AP, University

JOINT CO-CHAIRS

Prof. S. Srinivas	Sr. Professor, School of Advanced Sciences, VIT-AP, University
Dr. Santanu Mandal	Dean, School of Advanced Sciences, VIT-AP, University

TECHNICAL PROGRAMME COMMITTEE

Dr. Nikunja Bihari Barik (Chair)	School of Advanced Sciences, VIT-AP, University
Dr. Satyanarayana Badeti	School of Advanced Sciences, VIT-AP, University
Dr. M. Phani Kumar	School of Advanced Sciences, VIT-AP, University
Dr. Sudhakar Matle	School of Advanced Sciences, VIT-AP, University

Dr. V. Ramakrishna Reddy	School of Advanced Sciences, VIT-AP, University
Dr. Prashanth Maroju	School of Advanced Sciences, VIT-AP, University
Dr. Manoj Kumar Mishra	School of Advanced Sciences, VIT-AP, University
Dr. Anil Negi	School of Advanced Sciences, VIT-AP, University
Dr. Kiran Kumar Patra	School of Advanced Sciences, VIT-AP, University
Dr. Yada Nandukumar	School of Advanced Sciences, VIT-AP, University
Dr. Gaddam Sharat	School of Advanced Sciences, VIT-AP, University
Dr. Chandan Kr. Thakur	School of Advanced Sciences, VIT-AP, University
Dr. Shah Parth Mukeshbhai	School of Advanced Sciences, VIT-AP, University

REGISTRATION COMMITTEE

Dr. Tanuj Kumar (Chair)	School of Advanced Sciences, VIT-AP, University
Dr. Pratik Premdarshi Ray	School of Advanced Sciences, VIT-AP, University
Dr. Sukanta Nayak	School of Advanced Sciences, VIT-AP, University
Dr. Ajith Jubilson	School of Computer Science & Engineering, VIT-AP, University

FINANCE COMMITTEE

Dr. Manoj Kumar Mishra (Chair)	School of Advanced Sciences, VIT-AP, University
Dr. V. Raja	School of Advanced Sciences, VIT-AP, University

WEBSITE AND PUBLICITY COMMITTEE

Dr. Yada Nandukumar (Chair-Website Committee)	School of Advanced Sciences, VIT-AP, University
Dr. Aswathy R. K. (Chair-Publicity Committee)	School of Advanced Sciences, VIT-AP, University
Dr. Lisna P. C.	School of Advanced Sciences, VIT-AP, University
Dr. Shah Parth Mukeshbhai	School of Advanced Sciences, VIT-AP, University

Dr. Arenkala Kichu	VIT-AP School of Social Sciences and Humanities, VIT-AP University
Dr. Ranjan Kumar	School of Advanced Sciences, VIT-AP, University
Dr. Siba Prasad Panda	GITAM University

LOGISTIC ARRANGEMENT COMMITTEE

Mr. N. Saikiran	VIT-AP University
Mr. A. Sekhar	VIT-AP University
Mr. M. Sreenivasu	VIT-AP University
Mrs. V. Nagamani	VIT-AP University
Mr. Ravikumar Thota	VIT-AP University

SPEAKERS

About the speaker

Prof. Alan Jeffrey Giacomin is editor-in-chief of Physics of Fluids since 2016. He Holds the Tier 1 Canada Chair in Rheology from the Canadian government's Natural Sciences and Engineering Research Council. Since 2017, he has been President of the Canadian Society of Rheology

Title of the talk: Recent Advances in Polymer Viscoelasticity from General Rigid Bead-Rod Theory

Co-author: Mona A. Kanso, Research Assistant, Polymers Research Group, Chemical Engineering Department, Queen's University, 19 Division Street, Kingston, ON, Canada K7L 2N9

Abstract: One good way to explain the elasticity of a polymeric liquid, is to just consider the orientation distribution of the macromolecules. When exploring how macromolecular architecture affects the elasticity of a polymeric liquid, we find general rigid bead-rod theory to be both versatile and accurate. This theory sculpts macromolecules using beads and rods. Whereas beads represent points of Stokes flow resistances, the rods represent rigid separations. In this way, how the shape of the macromolecule affects its rheological behavior in suspension is determined. Our work shows the recent advances in polymer viscoelasticity using general rigid bead-rod theory, including advances applied on the coronavirus.

Till recently, general rigid bead- rod theory has neglected interferences of the Stokes flow velocity profiles between nearby beads. We call these hydrodynamic interactions, and we here employ our new method for exploring how these interactions affect the complex viscosity of suspensions of multi-bead rods. We find that for shish-kebabs, hydrodynamic interactions (i) increase zero-shear viscosity, (ii) increase zero-shear first normal stress coefficient, (iii) decrease the real part of the dimensionless complex viscosity, (iv) and increase minus the dimensionless imaginary part. We find that the combination of (iii) and (iv) explains crossovers of the parts of the complex viscosity. We find that the combination of (iii) and (iv) explains crossovers of the parts of the complex viscosity.

ICATP 2022, ISBN 978-81-952903-0-7

About the speaker

Prof. Antonia Barletta obtained his Degree (*Laurea*) in Physics, *cum laude*, at the School of Mathematical, Physical and Natural Sciences at the University of Bologna on March 21st 1987. From November 1st 2003, Antonio Barletta is Full Professor of Industrial Technical Physics at Alma Mater Studiorum Università di Bologna.

Title of the talk: Convective, absolute and spatial instability in porous media: Three different views on the linear analysis of the onset of convection

The onset of convection heat transfer in a horizontal porous layer takes place as a manifestation of the Rayleigh–Bénard instability. A vertical downward–oriented temperature gradient causes an unstable thermal stratification so that the thermal buoyancy force may cause the emergence of a cellular flow. Bénard cells can, in fact, be observed in an unstably stratified porous layer saturated with a fluid [1]. The usual way to exploit the theoretical modelling and analysis of the onset of convection in a porous medium flow is through a stability analysis which can be either linear or nonlinear [2]. By restricting the scope of this talk to the linear stability analysis, there can be three different approaches: convective, absolute or spatial. The first two approaches are diversified deployments for the Lyapunov concept of instability in dynamical systems, namely the response of a system to an alteration in the initial condition set at time $t = 0$ [3]. The third approach, i.e., the spatial stability analysis, is based on a non–Lyapunov scheme for instability where the system response is evaluated to an input perturbation source localized at a given spatial position, say $x = 0$, instead of a given time, say $t = 0$ [4]. In other words, if the Lyapunov scheme envisages a perturbation at time $t = 0$ that undergoes either amplification or attenuation in its time evolution, the non–Lyapunov scheme underpinning the spatial stability analysis devises a normal mode perturbation at position $x = 0$ whose spatial evolution along x, either upstream or downstream, may undergo amplification or attenuation along its direction of propagation. The three approaches to the flow linear instability are first illustrated with a toy system governed by a one–dimensional Burgers' PDE. Then, such concepts are employed for the exploration of different views on the linear thermal instability of the stationary and uniform flow in a horizontal fluid–saturated porous layer heated from below, also known as Prats' problem [5]. If the convective instability for Prats' problem occurs with a Darcy–Rayleigh number, R, larger than $4\pi^2$, the absolute instability takes place with $R > Ra$, where $Ra \geq 4\pi^2$ is a monotonic increasing function of the Péclet number associated with the basic flow rate. Finally, the emergence of the spatial instability appears for every positive Darcy–Rayleigh number [4].

REFERENCE

[1] Nield D. A., Bejan A.: Convection in Porous Media. Springer, New York (2017)
[2] Straughan B.: Stability and Wave Motion in Porous Media. Springer, New York (2008)
[3] Barletta A.: Routes to Absolute Instability in Porous Media. Springer, New York (2019)
[4] Barletta A.: Time–evolving to space–evolving Rayleigh–B´enard instability of a horizontal porous medium flow. Phys. Fluids 33, 124106 (2021)
[5] Prats M.: The effect of horizontal fluid flow on thermally induced convection currents in porous mediums. J. Geophys. Res. 71, 4835–4838 (1966)

ICATP 2022, ISBN 978-81-952903-0-7

About the speaker
Prof. Suman Chakraborty
Department of Mechanical Engineering at the Indian Institute of Technology (IIT) in Kharagpur, India. He is also Sir J. C. Bose National Fellow Institute and National Academy of Engineering chair professor.

Title of the talk: Flipping with the Flow - Perspectives of Puzzling Fluid Dynamics and Human Health

Abstract: Leonardo da Vinci (1452 – 1519) was a genius of the High Renaissance and was recognized as one among the greatest painters in the history of art, having apparently no great influence as recognized by modern fluid dynamists. However, with numerous lost, unpublished and unfinished works that were premised to disrupt human knowledge—he created some of the most influential paintings that reflected supreme technological ingenuity, including understanding the functionalities of individual parts of the body, delving into the internal organs that were interpreted by him to act as the motors orchestrating human life. William Harvey (1578-1657), by training a medical doctor, focused much of his work on the mechanics of blood flow in the human body. He first showed that valves in the veins, discovered by his teacher Fabricius, permit the blood to flow only in the direction of the heart and act as lifelines of the circulatory system. He also postulated the existence of tiny capillaries between arteries and veins, that were later discovered in 1661 by Marcello Malpighi. Jean Léonard Marie Poiseuille (1797 –1869) was a French physicist who delved deeply into the understanding of the flow of human blood in narrow tubes, and in 1840’s, disseminated the celebrated Poiseuille's law. All these developments took place in an era when fluid dynamics research was not colonised by the present-day snobbery of distinguishing great mastery in solving complex partial differential equations relating idealized problems that may not otherwise address mundane quests of understanding realities of life and nature. Despite the subject being taken over by illustrious mathematicians and physicists who have revolutionized the subsequent understanding of fluid dynamics, an apparently simple proposition of understanding the mechanics of blood flow in physiological pathways in human bodies remained to be an unsolved proposition. Over the past century, advancements in fluid dynamics hallmarked deeper studies on complex fluids, though. Fluid dynamics of blood, possibly the most critical complex fluid impacting human lives, is primarily dictated by red blood cells (RBCs) that are flexible biconcave discs spending their lives suspended in blood plasma that is elusively more complex than simple water. Commonly, RBCs stack together to form structures called rouleaux like cylindrical packs of coins that reform continuously. Contrary to intuition, instead of clogging, such reforms result in easier flow of blood as it passes through extremely narrow channels. An influential theoretical premise of blood flow has been rationalizing this by drawing analogies of RBCs with compound liquid droplets in which the cytoplasm is more viscous than the outer fluid that triggers a series of complex shape transitions. However, a stiffening of RBC membranes under certain conditions contradicts this analogy and may alter ATP release that happens due to shape deformation. This may signify specific diseased conditions and influence a plethora of ailments ranging from cardiovascular irregularities to cancer metastasis. The role of unique flexibility of microvasculature and morphology of the microenvironment, dynamical signals of pressure pulsation and disease-specific blood rheology make it extremely deceptive and patient-specific and difficult to model within the known territories of expertise of fluid dynamics. I discuss here various computational, in-vitro and in-vivo studies conducted in my group that have attempted to address some of the pertinent outstanding questions, unresolved paradoxes, and present a deeper challenge that makes even a ‘simple’ blood flow strikingly more complicated than its intuitive analogy of pipe flow in engineering fluid mechanics. I also suggest a way forward with a convergence of physics-based modelling and data science, where blood flow is not merely perceived as an ‘inert’ physical phenomenon but recognized as an exclusive hallmark of ‘life’ with all individualism intrinsic to humans.

About the speaker

Prof. P.V. S.N. Murty currently working as professor in Department of Mathematics Indian Institute of Technology Kharagpur. He completed his Ph.D. in Fluid mechanics from Department of Mathematics, Indian Institute of Technology Kanpur. He has more than 120 research papers in the leading journals as Journal of Fluid Mechanics, Proceedings of the Royal Society, Physics of Fluids, International Journal of Heat and Mass Transfer, Transactions of ASME-Journal of Heat Transfer, Transport in Porous Media, etc.

Title of the talk: Solute dispersion in non-Newtonian fluid flow in blood vessels with wall absorption - deviation from the Gaussianity

Co-author: Shalini Singh, Department of Mathematics, Indian Institute of Technology Kharagpur
West Bengal 721302, India

INTRODUCTION

The study of non-Newtonian flow solute dispersion has implications in biomedical engineering, physiological fluid dynamics, etc. The Herschel-Bulkley fluid model is a three-parameter model that includes yield stress, viscosity, and the power-law index. The ability to combine Newtonian, Bingham, and power-law fluid models is a virtue of this model. The axial solute dispersion in a straight circular tube in a pulsatile Herschel-Bulkley fluid flow was investigated by Rana and Murthy (2016). The steady case of the Taylor dispersion in laminar Newtonian flow with surface absorption was examined by Wang and Chen in (2017), taking into consideration the first four moments. The current research examines the impact of skewness and kurtosis on solute dispersion in non-Newtonian pulsatile fluid flow.

MATHEMATICAL MODEL

Consider the unsteady, fully developed, and axisymmetric pulsatile flow of non-Newtonian fluid in a circular cylindrical tube. A solute slug is initially delivered into this stream, and the solute is absorbed in the tube wall.
The unsteady transport of solute concentration with initial and boundary conditions is governed by

$$\frac{\partial C'}{\partial t'} + w'(r',t')\frac{\partial C'}{\partial z'} = \frac{1}{r'}\frac{\partial}{\partial r'}\left(r'\frac{\partial C'}{\partial r'}\right) + \frac{1}{Pe^2}\frac{\partial^2 C'}{\partial z'^2}, \quad C'(r',z',0) = \frac{\delta(z')}{Pe}, \qquad (1)(a)$$

$$\frac{\partial C'}{\partial r'}(1,z',t') = -\beta C'(1,z',t'), C'(r',\infty,t') = \frac{\partial C'}{\partial z'}(r',\infty,t') = 0, \qquad (1)(b)$$

where, C' is solute concentration, w' is axial velocity, r' is radial coordinate, z' is axial coordinate, t' is time, Pe is Peclet number and β is wall absorption parameter.

Constitutive equation of the momentum equation and H-B fluid model with the boundary conditions are

$$\epsilon\frac{\partial w'}{\partial t'} = 4[1 + e\sin(\alpha^2 Sct')] - \frac{1}{r'}\frac{\partial(r'\tau')}{\partial r'}, \qquad (2)(a)$$

$$\tau' = \tau_y + \left(-\frac{\partial w'}{\partial r'}\right)^k, \quad \text{if } \tau' \geq \tau_y, \quad \text{and} \quad \frac{\partial w'}{\partial r'} = 0, \quad \text{if } \tau' \leq \tau_y, \qquad (2)(b)$$

$$w'(1,t') = 0, \quad \text{and} \quad \tau'(0,t') \text{ is finite}. \qquad (2)(c)$$

where Sc is Schmidt number, τ' is shear stress, τ_y is yield stress, k is power law index, α is Womersley frequency parameter, e is amplitude of fluctuating pressure component, and r_p is plug flow radius. The velocity profile of the governing non-linear partial differential equation is obtained using the regular perturbation method with parameter ϵ = 1/Sc.

ICATP 2022, ISBN 978-81-952903-0-7

METHOD OF SOLUTION

Barton (1983) method of moments has been used and the m^{th} moment of concentration is $C'_m(r,t) = \int_{-\infty}^{+\infty} z'^m C'(r',z',t')\,dz$ and cross-sectional averaged m^{th} moment is $\langle C'_m(t)\rangle = \int_0^1 2\,r' C'_m(r',t')dr'$. The m^{th} central moment about the mean concentration distribution is $X_m(t') = \left(\int_0^1\int_{-\infty}^{+\infty} 2\,r'(z'-\mu)^m C'\,dz'dr'\right) / \left(\int_0^1\int_{-\infty}^{+\infty} 2\,r' C'\,dz'dr'\right)$ and centroid is $\mu = \left(\int_0^1\int_{-\infty}^{+\infty} 2\,r' z' C'\,dz'dr'\right) / \left(\int_0^1\int_{-\infty}^{+\infty} 2\,r' C'\,dz'dr'\right)$.

The exchange coefficient $\nu_0(t') = d(\log\langle C'_0(t')\rangle)/dt'$ convection coefficient $\nu_1(t') = -d\mu_g/dt'$, dispersion coefficient $\nu_2(t') = (dX_2/dt')/2$, skewness $\nu_3(t') = X_3/X_2^{3/2}$, kurtosis $\nu_4(t') = X_4/X_2^2 - 3$.

The mean concentrations distribution with the Hermite polynomials H_k is specified as

$$C_{mean}(z',t') = \langle C'_0(t')\rangle e^{-\psi^2} \sum_{m=0}^{\infty} A_m(t') H_m\big(\psi(t')\big), \tag{3}$$

Where $H_{k+1}(\psi) = 2\psi H_k(\psi) - 2kH_{k-1}(\psi), \psi(t') = \big(z-\mu(t')\big)/\sqrt{2X_2(t')},\ H_0(\psi) = 1,$
$a_0(t') = 1/\sqrt{2\pi X_2(t')}, A_1 = A_2 = 0, A_3(t') = \sqrt{2}A_0\nu_3(t')/24, A_4(t') = A_0\nu_4(t')/96.$

RESULTS AND DISCUSSION

Figure 1 depicts the axial mean concentration C_{mean} distribution in the tube, taking into account up to the second X_2 and third moments X_3, as well as all four moments X_4 (or in other words, with the dispersion coefficient ν_2, skewness ν_3, and kurtosis ν_4). The skewness ν_3 shifting the mean concentration curve to the left, while the kurtosis ν_4 minimising the peak of the mean concentration curve. A Gaussian distribution is obtained by pure solute diffusion.

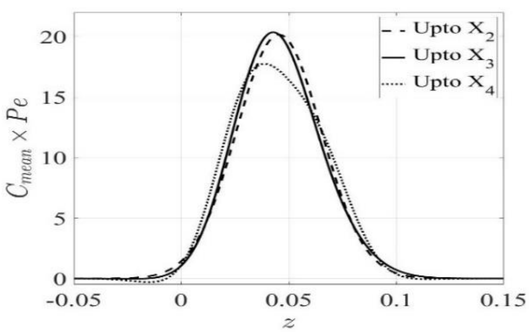

Figure 1. Axial mean concentration $C_{mean} \times Pe$ variation with z' including second moment, third moment and fourth moment at time t' =0.1, when k=0.9, e=0.5, α =0.5, τ_y =0.05 and β =0.01.

CONCLUSION

The combined time-dependent data of exchange ν_0, convection ν_1, and dispersion ν_2 coefficients do not offer comprehensive information regarding unsteady solute distribution in any fluid flow. Higher moments, whether for Newtonian or non-Newtonian fluids, offer more detailed information on the unsteady solute dispersion in the flow field.

REFERENCES

Jyotirmoy Rana and PVSN Murthy. 2016. Unsteady solute dispersion in Herschel-Bulkley fluid in a tube with wall absorption. Physics of Fluids, 28(11):111903.

NG Barton. 1983. On the method of moments for solute dispersion. Journal of Fluid Mechanics, 126:205–218.

Ping Wang and GQ Chen. 2017. Basic characteristics of Taylor dispersion in a laminar tube flow with wall absorption: Exchange rate, advection velocity, dispersivity, skewness and kurtosis in their full time dependance. International Journal of Heat and Mass Transfer, 109:844–852.

About the speaker
Prof. Jitesh Gajjar is currently working as Professor of Applied Mathematics at the University of Manchester since 2007. He is also Director of Social Responsibility in the School of Mathematics since 2016.

Title of the talk: Cancellation of Tollmien-Schlichting waves with localised surface heating

Co-author: [1]Brennan, G., [2]Hewitt, R.E.
[1, 2]Mathematics Department, University of Manchester, Manchester M13 9PL, UK
[2]Mathematical Institute, University of Oxford, Oxford OX2 6GG

INTRODUCTION

In studying the inviscid stability of parallel flows, Rayleigh's inflexion point criterion states that a necessary condition for instability is that the basic flow must have a point of inflexion. However fully developed channel flows with the Poiseuille profile, and boundary layers over flat plates do not have a point of inflexion and so are inviscidly stable. The theoretical work of Heisenberg, Tollmien and Schlichting in the early part of the 20th century however suggested that channel flows as well as boundary layer flows were unstable to an instability stemming from viscous effects, but this work was largely ignored by many fluid dynamicists including G.I. Taylor because viscosity was seen as a damping mechanism and not one likely to cause instability. There was no experimental evidence to back up the work of the German scientists. However, it wasn't until the 1940s through the pioneering experiments of Shubauer & Skramstad (1948) who demonstrated for the first time that two-dimensional boundary layers were unstable to a type of instability now known as Tollmien-Schlichting (TS) instability that this work gained credibility. In the experimental work of Shubauer & Skramstad (1948) instability waves were triggered by disturbances generated by a vibrating ribbon and their experiments were successful in being able to observe instability waves because of the low turbulence wind tunnels in which the experiments were performed. This allowed instability waves which were amplified downstream to be picked up by the instruments placed downstream of the vibrator, and the waves were seen to be directly responsible for causing transition to turbulence.

There are many different mechanisms through which the TS instability is excited and not just via vibrating ribbons. In fact, free-stream turbulence wall roughness, as well as surface heating can all introduce disturbances which lead to the growth of TS waves. In many aerodynamic applications such as flow over aircraft wings, controlling and eliminating TS waves is important if one is interested in maintaining laminar flow with reduced drag and other favorable flow properties. In this paper, we discuss how localised surface heating can be used to control three-dimensional TS instability. Our theoretical approach is able to explain the experimental work of Liepmann et al. (1982), Liepmann & Nosenchuck (1982) who showed how it is possible to reduce unstable Tollmien-Schlichting wave amplitudes using unsteady surface heating. In their experiments one heating strip was used to generate an unstable wave and another heating strip positioned further downstream with a suitably phase-controlled signal, could be used to either reinforce or cancel the generated wave via a feedback loop.

METHODOLOGY

In the current work we consider a two-dimensional compressible boundary layer flow encountering a three-dimensional vibrator and with localised surface heating present. The Reynolds number is assumed to be large and we choose the scalings and sizes of the vibrator such that they align with the triple-deck scales. It is now well known that the unsteady triple-deck equations govern the linear and nonlinear development of disturbances in boundary layers, see for example Smith (1979). In the current work using matched asymptotic expansions, the governing equations are shown to reduce to the three-dimensional unsteady triple-deck equations with thermal effects included. The full equations and boundary conditions are given in Brennan et al. (2021). We study the linearized version of these equations both analytically and numerically for small disturbance amplitudes.

RESULTS AND CONCLUSION

From the analysis it is possible to deduce an exact formula for TS wave cancellation with an appropriate choice of wall heating function. The application of this formula is shown in Figure 1 for an unstable frequency $\omega = 2.5$ and zero Mach number. The formula is shown to work equally well for non-zero Mach numbers as well. This is the first time such a formula has been explicitly derived and shown to work, albeit for a model problem.

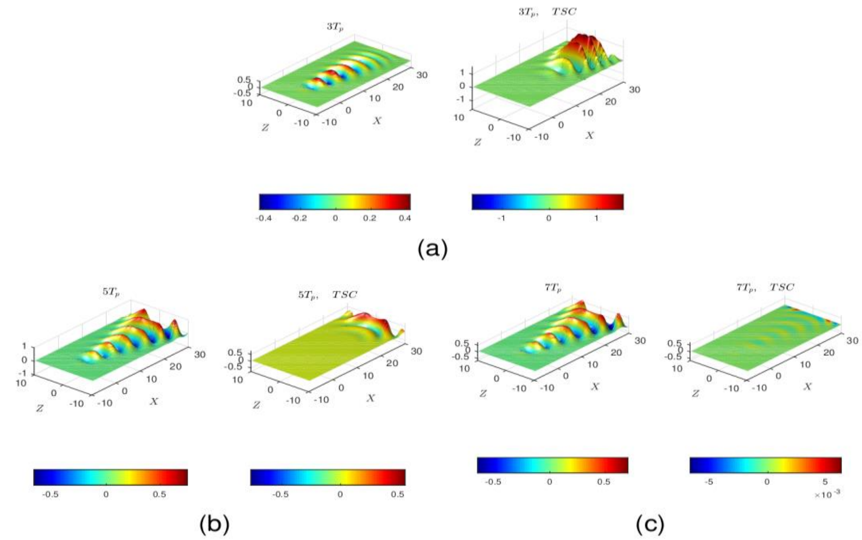

Figure 1. Results from numerical simulation showing development of unstable TS waves at an unstable frequency at various time periods (a) 3Tp, (b) 5Tp, (c) 7Tp . In a),b) c) the left hand figure shows the wave developing with no cancellation formula, the right hand side shows wave development with cancellation active.

REFERENCES

Brennan, G.S., Gajjar, J.S.B., Hewitt, R.E.: Cancellation of Tollmien-Schlichting wave cancellation with surface heating. Journal of Eng. Maths. Vol. 128, No. 1, (2021).

Liepmann, H., Brown, G., Nosenchuck, D.: Control of laminar instability waves using a new technique. Journal of Fluid Mechanics 118, 187–200 (1982).

Liepmann, H.W., Nosenchuck, D.M.: Active control of laminar turbulent transition. Journal of Fluid Mechanics 118, 201–204 (1982).

Schubauer, G.B., Skramstad, H.K.: Laminar boundary layer oscillations and transition on a flat plate. NACA Rep. 909 (1948).

Smith, F.T.: On the non-parallel flow stability of the Blasius boundary layer. Proc. Roy. Soc. London Ser. A 366, 91–109 (1979).

About the speaker

Dr. Vemuri Balakotaiah is currently working as Professor in Cullen College of Engineering, University of Houston. He completed his Ph.D. from University of Huston and passed his B.Tech from IIT, Madras.

Title of the talk: *Multi-scale Coarse-graining of Diffusion-Convection-Reaction Models*

INTRODUCTION

Due to the fact that the length and time scales associated with continuum models of diffusion-convection-reaction (DCR) type vary from the molecular scale ($\sim 10^{-10}$ m in length and 10^{-9} s in time) to the process scale ($\sim 10^{0}$ m in length and 10^{4} s in time), for most cases of practical interest, even with the present day computational power, it is impractical to solve the detailed models of these systems (consisting of several nonlinear partial differential equations) and explore all the different types of solutions that exist in the multi-dimensional parameter spaces. Accurate coarse-grained reduced order models that retain the multi-scale physics and expressed in terms of measurable variables (such as mixing-cup temperature or concentrations) are desired for the purpose of design, control, optimization, and real time simulations of these systems.

We have shown that the Liapunov-Schmidt (L-S) technique of classical bifurcation theory is an excellent multi-scale averaging technique for DCR models that describe many physical systems of interest to engineers and scientists [Balakotaiah & Chang, 2003; Balakotaiah & Chakraborty, 2003]. This procedure starts with detailed models based on the fundamental laws and takes advantage of the separation of the length or time scales (expressed in terms of one or more small parameters in the dimensionless form of the model) to reduce the spatial and/or temporal degrees of freedom and to obtain multi-mode multi-scale low-dimensional models in terms of measurable quantities (such as cup-mixing concentration or phase averaged temperature). This procedure is rigorous and is equivalent to the Taylor expansion of a more detailed fundamental model in terms of one or more small parameters representing separation of length/time scales in the original model. In such an expansion, the lowest order term represents the conservation law at the macro scale while higher order corrections modify the model by including the physical phenomena at smaller and smaller length scales.

In earlier work, we have also discussed the convergence and accuracy of various truncated coarse-grained models, and their connection to the two important concepts in transport phenomena, namely, the dispersion coefficient and transfer coefficient [Ratnakar & Balakotaiah, 2010]. It was shown that even when there is scale separation in the physical problem, the range of validity of the truncated averaged models is limited by the high frequency components present in the initial /inlet conditions or point sources/sinks and/or fast volumetric or wall reactions. Because of this limitation, the use of dispersion coefficient concept (with a single or fewer than a minimum number of modes) and a parabolic description can lead to many conceptual difficulties (such as negative dispersion coefficients, upstream propagation of signals even in convection dominated systems, and so forth). In contrast, truncated multi-mode reduced order models derived by the L-S method with the transfer coefficient concept and a hyperbolic description retain the physics at all length and time scales, even though the accuracy may be limited. We have illustrated these concepts using examples from various applications in the areas of catalytic reaction engineering, chromatographic theory and tracer dispersion [Ratnakar & Balakotaiah, 2011].

In the present work, we discuss various extensions of the LS method of averaging to diffusion-reaction, convection-reaction and diffusion-convection-reaction models describing single and multi-phase systems.

ICATP 2022, ISBN 978-81-952903-0-7

RESULTS AND DISCUSSION

In the first part of this work, we discuss the theoretical/mathematical aspects of the L-S reduction with focus on how to include the initial/inlet/boundary conditions in the averaging procedure, proper scaling of the model, the use of multiple modes to write the global and local equations and the convergence and accuracy aspects of the averaged model. We also present some specific examples of rigorously derived low-dimensional models (e.g. laminar dispersion with point sources in time/space, monolithic catalytic reactors, and transport in porous media). In the second part, we extend the multi-scale averaging technique to multi-phase systems with reactions in one or more phases. These reduced order models are expressed in terms of phase averaged concentration/temperature modes with inter as well as intra-phase (dispersion) fluxes. The various fluxes are determined by the local equations that are linear in these modes and fluxes, similar to the Maxwell-Stefan equations of multi-component diffusion. It is also found that the structure of these multi-phase averaged models is fundamentally different from the traditional models. We provide physical interpretation of the various inter and intra-phase transfer coefficients appearing in the reduced order models and also methods for evaluating them. The accuracy of the reduced order models is illustrated by comparing with the exact solutions for selected cases and also with other models in the literature. In the third part, we present further extensions of the method to coupled heterogeneous reacting systems and detailed micro-kinetics corresponding to extremely small length and time scales [Tu et al., 2022]. We determine the mesh size independent solutions of the detailed models and compare the same with those obtained with the reduced order models. We show that the reduced order model has the same accuracy as the mesh size independent detailed solution while speeding up calculations by three orders of magnitude for the example studied, and possibly by several more orders of magnitude for more complex real systems. Finally, we show some applications of reduced order models for real time (and faster than real time) simulations of physical systems on a desktop computer.

ACKNOWLEDGMENT

I would like to thank the Robert A. Welch Foundation, The Dow Chemical Company, SABIC Americas Inc., and University of Houston for support of my work on multi-scale averaging. I also thank my former students Drs. S. Chakraborty, M. Bhattacharya, R. Ratnakar, B. Sarkar, I. Alam, and M. Tu as well as collaborators D. H. West and Professors H.-C. Chang and M. Harold.

REFERENCES

Balakotaiah, V. and H.-C. Chang. 2003. Hyperbolic Homogenized Models for Thermal and Solutal Dispersion, SIAM J. Appl. Math., 63, 1231-1258.

Balakotaiah, V. and S. Chakraborty, 2003. Averaging Theory and Low-dimensional Models for Chemical Reactors and Reacting Flows, Chem. Engng. Sci., 58, 4769-4786.

Ratnakar, R. R and V. Balakotaiah, 2010. On the Use of Transfer and Dispersion Coefficient Concepts in Low-dimensional Diffusion-Convection-Reaction Models, Chemical Engineering Research and Design, 88, 342-361.

Ratnakar, R. R and V. Balakotaiah, 2011. Exact Averaging of Laminar Dispersion", Physics of Fluids, 23, 023601-1 to 023601-23.

Mingjie Tu, R. Ratnakar and V. Balakotaiah, "Multi-mode reduced order models for real time simulations of monolith reactors with micro-kinetics", Chemical Engineering Journal, 430, (2022), 132532.

About the speaker

Prof. Pradeep G. Siddheshwar is a senior professor at Christ University, Bangalore. His interested area of research are applied mathematics and fluid dynamics.

Title of the talk: Cylindrical Rayleigh-Bénard convection: Study of regular, periodic and chaotic convection

Abstract: Cylindrical analog of 'Rayleigh-Bénard convection in a rectangular enclosure' is studied by considering the linear and weakly nonlinear realms of convection for investigation. Emphasis in the work is on making an analytical study using Bessel functions as part of the eigenfunctions in the conductive and convective modes. The analysis then is classical in nature with the normal mode used for the linear theory and the minimal Fourier-Bessel series representation used for the non-linear theory. The linearized version of the cylindrical-Lorenz model yields information on regular convection in the form of either direct or Hopf bifurcation. The full model with nonlinearities similar to that seen in the classical Lorenz model is analysed to extract information on periodic and chaotic regimes of convection. The similarities and differences between the cylindrical and rectangular counterparts of Rayleigh-Bénard convection are brought out and discussed. Knot instability and emergence of turbulence are not for the present a part of this work. Possible applications of the study shall be highlighted.

About the speaker

Prof. Manoranjan Mishra obtained his doctoral degree from Indian Institute of Science (IISc), Bangalore. He carried out post-doctoral studies at INLN, University of Nice Sophia Antipolis, France (2005-2006) obtaining a fellowship from French National Ministry of Education and Research and also at Université Libre de Bruxelles, Brussels (2006-2007). His area of research is fluid dynamics.

Title of the talk: Reaction-induced hydrodynamic instability in miscible fluids

Abstract: Hydrodynamic instabilities of fingering patterns are observed while displacing a less viscous fluid by another more viscous one through porous media or Hele-Shaw cell, which is called viscous fingering instability. Such instability is pervasive in the transport phenomena in several applications in porous media flow type, e.g., enhanced oil recovery, liquid chromatography, CO_2 sequestration, etc. Moreover, instabilities at the fluid-fluid interface in enhanced oil recovery processes such as polymer flooding remain a significant challenge. Also, this instability is likely to be detrimental to the separation efficiency in the separation process. Depending on the application, either a stable or an unstable pattern is desirable, and therefore understanding to control such interfacial fingering instabilities is very important. This talk discusses modeling and the possible mechanism to control the instability pattern through a second-order chemical reaction. The linear stability analysis and non-linear simulation based on an efficient scheme of finite difference and spectral methods will be presented in comparison to the corresponding experimental investigations.

ICATP 2022, ISBN 978-81-952903-0-7

About the speaker
Prof. S. V. Raghurama Rao is currently working as a Professor in the Department of Aerospace Engineering, IISC Bangalore. His research interest are developing efficient CFD algorithms for fluid flows, including central schemes, kinetic schemes and relaxation schemes, exact capturing of shocks and contact discontinuities, low numerical diffusion methods, meshless or grid-free methods, Lattice Boltzman method, non-standard finite difference methods, aerodynamic shape optimization, algorithms for turbulence simulations

Title of the talk: Fluid flow simulations through Discrete Velocity Models

Abstract: Kinetic theory of gases has been an efficient foundational framework for generating computational models and numerical algorithms for simulating fluid flows. Research in the past few decades has shown that discrete velocity models simplify the existing frameworks and yet are flexible enough to introduce the required accuracy in the algorithms. A review of the discrete velocity based computational algorithms generated over the past few decades in our CFD lab will be presented. Topics covered include the mesoscopic modelling through Lattice Boltzmann Method as well as finite volume methods.

About the speaker
Prof. Katepalli Sreenivasan is the professor of physics in Dpeartment of Mathematics, New York University. He has the distinction of being a University Professor, a title conferred upon scholars whose work is interdisciplinary and reflects exceptional breadth. Some of his achievements include the Guggenheim Fellowship, Otto Laporte Memorial Award of American Physical Society, TWAS Medal Lecture in Engineering Science and many more.

Title of the talk: Quantum Turbulence: Why should you care?

ICATP 2022, ISBN 978-81-952903-0-7

About the speaker
Prof. Rama Govindarajan is an Indian scientist specialized in the field of fluid dynamics. She is recipient of one of the prestigious award named Shanti Swarup Bhatnagar Award in 2007 for her contributions in Science and Technology.

Title of the talk: *Raindrops and other particles in vortices, and what they remember*

Abstract: There is a problem in cloud physics called the "droplet growth bottleneck", which is that raindrops grow much faster than condensation rates and gravitational collisions can explain. Turbulence in the cloud is supposed to bridge the gap. I will outline this problem, and show how the flow near one vortex can provide some answers. I will talk about the memory force.

About the speaker
Dr. Sreepriya Vedantam has a research experience in the area of Design and Scale-up of Chemical Process Equipment for Process Development, Process Intensification including flow processes using MRT, Multiphase flows with phase change, Computational and Experimental Fluid Dynamics, and Advanced Separation Techniques. She carries experience in CFD modeling of single and multi-phase flows including phase change involving laminar and turbulent flows, Model Integration, Compartmental Modeling at various scales.

Title of the talk: Hydrodynamics in modular multiphase reactors: A Performance Perspective

About the speaker
Dr. Anirudh Singh Rana has completed his PhD from University of Victoria in 2018. His research domain includes fluid dynamics, micro/nanofludics, finite volume methods, gas dynamics, non-equilibrium thermodynamics, continuum mechanics, transport phenomenon.

Title of the talk: Entropy beyond equilibrium: A curious case of polyatomic gases

Abstract: In the classical irreversible thermodynamics approach, the Navier-Stokes-Fourier (NSF) constitutive equations are obtained so as to satisfy the entropy inequality; assuming that the entropy flux is equal to the heat flux over the temperature. In this talk, I will present two approaches to the extended fluid dynamics models for polyatomic gases:
(1) A second-order constitutive equations for polyatomic gases; it takes the basis of CIT, but most importantly, allowing up to quadratic nonlinearities in the entropy flux, and
(2) The regularized 11 moment equations using an extended moment method.
Mathematical similarities between the proposed model and the classic Stokes-Laplace equations are exploited so as to construct analytic/semi-analytic solutions for the slow rarefied gas flow over different shapes; the model's prediction for the drag force is in excellent agreement with the experimental data over the whole range of the Knudsen number.

ICATP 2022, ISBN 978-81-952903-0-7

CHAPTER -1

STEADY CONVECTIVE FLOW OF A MONO-NANOFLUID ALONG A VERTICAL FLAT SURFACE SUBJECTED TO SINUSOIDAL TEMPERATURE VARIATIONS

Richa Saha[1*], Mahesha Narayana[2], P. G. Siddheshwar[1] and Smita S. Nagouda[1]
[1]Centre for Mathematical Needs, Department of Mathematics, CHRIST (Deemed to be University), Bangalore, India
[2]Department of Mathematics, The University of the West Indies, Kingston, Jamaica
E-mail* (richa.saha@res.christuniversity.in)

INTRODUCTION

This paper illustrates the thermo-convective flow of a water-copper mono-nanofluid over a vertical flat surface which is subjected to sinusoidal temperature variations. The effect of the pertinent parameters on the nature of the flows and the heat transfer has been discussed qualitatively. The Keller-Box scheme has been used to solve the resulting boundary value problem numerically. The dimensionless stream function, velocity and temperature curves have been illustrated. To study the nature of the flows, streamline and isotherm plots have also been compared, which reveal that the volume fraction and amplitude of surface variations play a pivotal role in enhancing heat transfer. The results also indicate that, raising the volume fraction leads to a reduction in the shear stress at the surface, while the rate of surface heat transfer gets augmented. On the contrary, the amplitude of the temperature variation serves to amplify both these properties.

MATERIALS AND METHODS

In order to study how the surface temperature variations affect the flow, the equations governing the boundary value problem are reduced to a non-similar system of equations (Rees (1999)), which are solved using the expressions for stream function and then, the Keller-Box scheme is applied (Keller (1978)).

RESULTS AND DISCUSSION

The surface shear stress, $f_{\eta\eta}(\xi,0)$ decreases significantly with an increase in N, which is responsible in the elevation of the rate of surface heat transfer, $\theta_\eta(\xi,0)$. In contrast, the effect of α is to amplify both $f_{\eta\eta}(\xi,0)$ and $\theta_\eta(\xi,0)$.

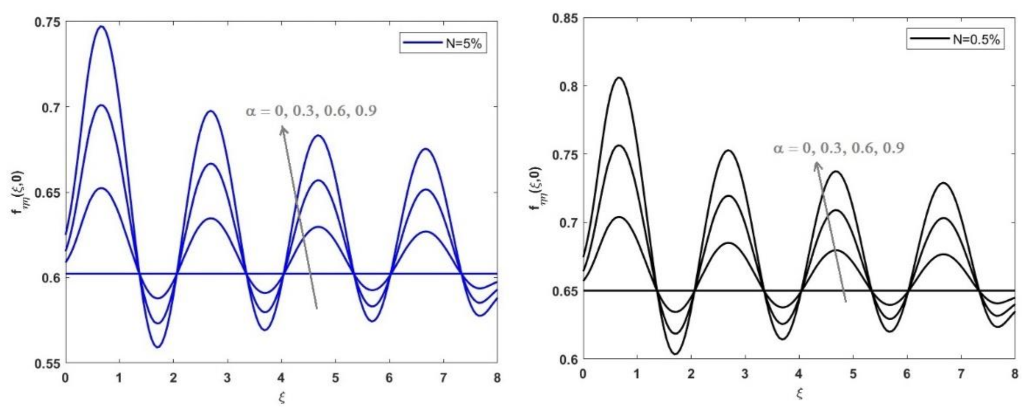

Figure 1. Variation in surface shear stress, $f_{\eta\eta}(\xi,0)$, with different volume fractions, N, and variation of the amplitude, α, of the surface temperature

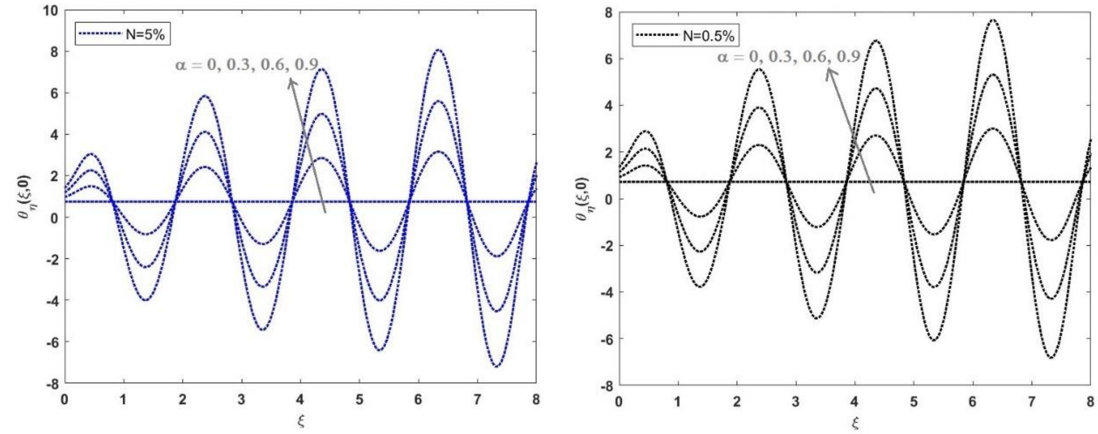

Figure 2. Variation of the rate of surface heat transfer, $\theta_\eta(\xi,0)$, with N and α

The isotherm plots clearly indicate an augmentation of the heat transfer with the collective and individual increases of N and α.

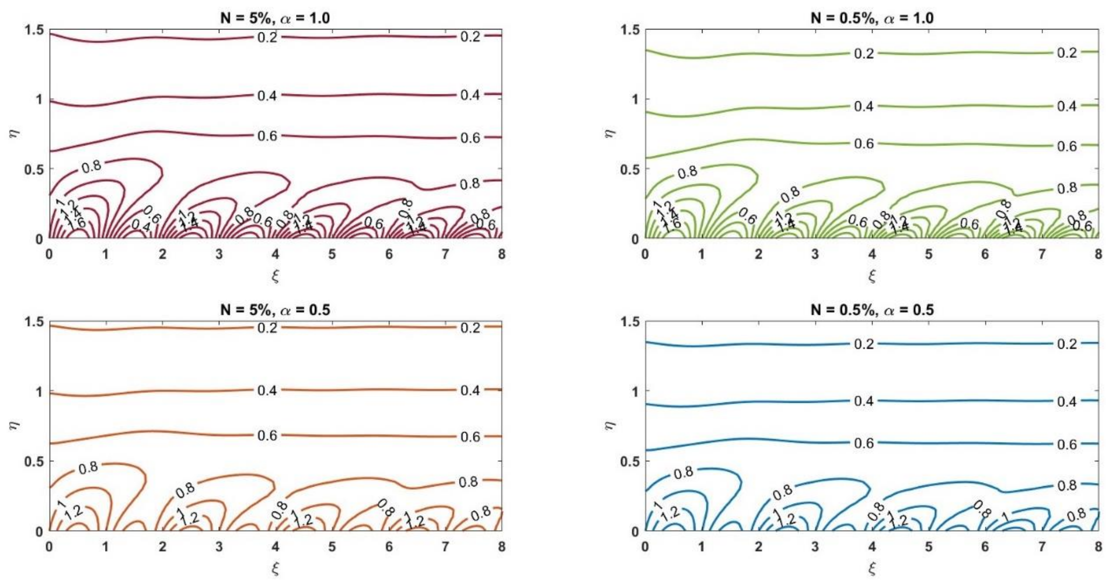

Figure 3. Isotherm contours for the sinusoidal temperature variation

CONCLUSION

One can conclude that increasing the volume fraction of the nanoparticles enhances the heat transfer but reduces the surface shear stress. Moreover, a sinusoidal temperature variation on the flat surface serves to further improve the heat transfer characteristics in such situations. The results obtained from this study have potential applications in the manufacturing of nanofluids, and in industries utilizing nanofluids for processes which require a significant boost in the heat transfer.

REFERENCES

Keller, H.B. 1978. Numerical methods in boundary-layer theory. Annu. Rev. Fluid Mech., 10: 417-433.

Rees, D.A.S., 1999. The effect of steady streamwise surface temperature variations on vertical free convection. Int. J. Heat Mass Transfer, 42(13): 2455-2464

CHAPTER -2

Hall and ion-slip currents in gyrating flow of tri-hybridized Casson nanofluid past a vertical plate with ramped motion, Newtonian heating, and chemical reaction

Ali, Asgar[1,*], Das, Sanatan[2], and Jana, RN[3]

[1] Department of Mathematics, Bajkul Milani Mahavidyalaya, Purba Medinipur 721 655, India
[2] Department of Mathematics, University of Gour Banga, Malda 732 103, India
[3]Department of Applied Mathematics, Vidyasagar University, Midnapore 721 102, India
[*]E-mail: asgaralimath@gmail.com (corresponding author)

INTRODUCTION

In order to generate a colloidal solution, distinct types of nanostructures (more than one) or hybridized nanocomposites are suspended in the pure liquid to develop a new category of nanofluids recognised as the hybrid nanofluids (HNF). The hybrid nanomaterials combine the physical and chemical properties of various materials at the same time, offering the properties in a homogeneous phase. Mastery in the domains of hydromagnetic flow of Casson tri-hybridrized nanofluid (THNF), taking Hall and ion-slip currents into account, is necessary for power generators, MHD accelerators, electric transforms, transmission lines, heating elements, refrigeration coils, etc. Recently, many researchers [Ali et al. (2021), Mahmud et al. (2022), Veera Krishna (2021a,b)] have investigated the influence of Hall and ion-slip currents on flow dynamics.

A thorough review of literature indicates that there are no researches regarding the impacts of Hall and ion-slip currents on a time-dependent gyrating flow of Casson tri-hybridrized nanofluid (THNF). In this study, Hall and ion-slip currents on a time-dependent gyrating flow of Casson tri-hybridrized nanofluid (THNF) past a vertically fluctuating plate with ramped motion, Newtonian heating and chemical reaction in a porous environment has been inspected. Tri-hybridized nanoparticles (copper-titania-alumina) are scattered into the blended base Casson liquid water-ethylene glycol mixture (vol.60–40 %). Heat transit is investigated as a physical consequence of thermal radiation. Darcy's law is used in the flow field to engage to the permeability of the porous material. In the beginning, the modelled problem is explained in terms of physical conditions and partial differential equations (PDEs). The resulting non-dimensional PDEs are solved analytically using the powerful Laplace transform technique. Several graphs and tables are plotted to visualise and explain the physical consequences of significant variables linked to flow features of industrial concern.

MATERIALS AND METHODS

The equations describing incompressible non-Newtonian Casson tri-hybridized nanofluid flow taking Hall and ion-slip currents into account are

$$\rho_{thnf}\left(\frac{\partial u}{\partial t}-2\Omega v\right)=\mu_{thnf}\left(1+\frac{1}{\beta}\right)\frac{\partial^2 u}{\partial z^2}-\sigma_{thnf}B_0^2\frac{u(1+\beta_e\beta_i)-v\beta_e}{(1+\beta_e\beta_i)^2+\beta_e^{\,2}}-\frac{\mu_{thnf}}{K^*}\left(1+\frac{1}{\beta}\right)u$$
$$+g(\rho\beta_T)_{thnf}\left(T-T_\infty\right)+g(\rho\beta_C)_{thnf}\left(C-C_\infty\right), \tag{1}$$

$$\rho_{thnf}\left(\frac{\partial v}{\partial t}+2\Omega u\right)=\mu_{thnf}\left(1+\frac{1}{\beta}\right)\frac{\partial^2 v}{\partial z^2}-\sigma_{thnf}B_0^2\frac{v(1+\beta_e\beta_i)+u\beta_e}{(1+\beta_e\beta_i)^2+\beta_e^{\,2}}-\frac{\mu_{thnf}}{K^*}\left(1+\frac{1}{\beta}\right)v, \tag{2}$$

$$(\rho c_p)_{thnf}\frac{\partial T}{\partial t}=k_{thnf}\frac{\partial^2 T}{\partial z^2}-\frac{\partial q_r}{\partial z}, \tag{3}$$

$$\frac{\partial C}{\partial t}=D_{thnf}\frac{\partial^2 C}{\partial z^2}-Kr^*\left(\mathrm{C}-\mathrm{C}_\infty\right), \tag{4}$$

The initial and boundary conditions for the fluid stream past the electrically non-conducting plate with ramped motion and Newtonian heating are

$$\begin{aligned}
&t\le 0, z>0: u=v=0, T=T_\infty, C=C_\infty,\\
&t>0, z=0: u=\begin{cases}u_0\dfrac{t}{t_0}, \text{ if } 0<t\le t_0\\ u_0, \text{ if } t>t_0\end{cases}, v=0, \frac{\partial T}{\partial z}=-h_T T, \frac{\partial C}{\partial z}=-h_C C,\\
&t>0: u\to 0, v\to 0, T\to T_\infty, C\to C_\infty \text{ as } \quad z\to\infty,
\end{aligned} \tag{5}$$

where t_0 is the characteristic time and $t_0=v_f/u_0^2$. The Laplace Transformation method is applied to the equations (1-5) after non-dimensionalized with suitable non-dimensional variables to obtain closed-form solutions. Several graphs and tables are plotted to visualise and explain the physical consequences of significant parameters to flow features of industrial concern.

RESULTS AND DISCUSSION

It is witnessed that the primary velocity gets a decrement while the absolute secondary velocity is energized for mounting gyrating parameter K^2 in both cases THNF and HNF. Greater estimations of K^2 imply higher gyrating effects and the fluids nearby the gyrating axis is propelled vertically outward directions due to the centrifugal force. The THNFs or HNFs are then substituted by the heated nanofluids transferring in the axial direction. Therefore, the secondary velocity profile in gyrating environment uplifts for elevating estimations of rotation. Coriolis force generates a flow in reverse direction. The consequences of magnetic field dominate both velocity components while Hall and ion-slip parameters explore reversal conduct on these components. A comparative inspection for tri-hybridized and hybridized nanofluids is carried out. It is witnessed that the THNFs temperature is higher compared to HNF. This behaviours of NFs or HNFs or MHNFs can be used in cooling system, for example, polymer processing industries.

CONCLUSION

The key outcomes of this research are succinctly mentioned as follows: (1) The effectiveness of Hall and ion-slip currents promote the velocity components but reversal conduct is detected for magnetic field, (2) The temperature for THNF is discerned to be significantly greater than HNF, (3) The obtained findings are of critical interest in chem-reactors, chemical and polymer industry segments, and nutrient manufacturing, (4) Future researches may examine the entropy development in the flow of ionic magnetic tri- hybridized nanolubricants with non-Newtonian fluid models..

ACKNOWLEDGMENT

The authors express their sincere thanks to the reviewers.

REFERENCES

Ali, A., Banerjee, S.M. and Das, S. 2021. Hall and ion slip current's impact on magneto-sodium alginate hybrid nanoliquid past a moving vertical plate with ramped heating, velocity slip and Darcy effects, Multidiscip. Model. Mater. Struct., 17(1): 65-101.

Mahmud, K., Mehmood, R., Rana, S., Al-Zubaidi, A. 2022. Flow of magnetic shear thinning nano fluid under zero mass flux and hall current. J. Mol. Liq., 352: 118732.

Veera Krishna, M. 2021a. Hall and ion slip effects on radiative MHD rotating flow of Jeffreys fluid past an infinite vertical flat porous surface with ramped wall velocity and temperature, Int. Commun. Heat Mass Transf., 126: 105399.

Veera Krishna, M. 2021b.Radiation-absorption, chemical reaction, Hall and ion slip impacts on magnetohydrodynamic free convective flow over semi-infinite moving absorbent surface, Chinese J. Chem. Eng., 34: 40-52.

ICATP 2022, ISBN 978-81-952903-0-7

CHAPTER -3

EFFECT OF FLOW CHANNEL CONFIGURATIONS ON THE COOLING PERFORMANCE OF LI-ION BATTERIES WITH BINARY FLUID

Zahid, H[1], Kumar, R[1]
[1]Deparment of Mechanical Engineering, Dr B R Ambedkar National Institute of Technology, Jalandhar, Punjab, 144011, India
hubban.zahid@gmail.com, rajank@nitj.ac.in.

INTRODUCTION

The potential for various types of energy storage has been greatly enhanced by the increased use of renewable energy sources in the energy sector today. Lithium-ion batteries are a leading contender in a wide range of storage applications, including electric vehicles (EVs) because of their lightweight and high energy density properties. However, despite their promising future, battery systems face significant challenges, such as safety issues, cost, a short cycle life, and temperature-related issues. The performance, longevity, and safety of Li-ion batteries are greatly affected by temperature. For these batteries, the optimal working temperature range is 15–35 °C (Liu et al., 2017). The major goal of the study is to prevent the thermal runaway condition by keeping the maximum temperature of the batteries within the safety limit and establishing temperature uniformity between cells. From 2020 to 2030, the market share of EVs is expected to expand by roughly 15 to 30 percent, with potential for development in the following decades (Zhang et al., 2015).

MATERIALS AND METHODS

15-S (series) configuration batteries (Li-ion cylindrical 18650 2200 mAh) are placed having two distributed channels connected to the container through a pump. Two outlets from the inlet and outlet were connected to the U-tube manometer to measure the pressure drop in the distributed channel. The schematics sketch of the experimental setups is shown in Fig. 1. A combination of 15 Li-ion batteries is arranged into a 3×5 matrix so that they all are connected in a 15-S combination inside a rectangular channel made from aluminum and have a thickness of 1 mm. Due to the load unit's limited power capacity in terms of voltage and ampere, this number of batteries was chosen. A power supply having specification (balanced charger 382275 60 V 10A DC supply) coupled to a multifunction high power load unit and a Li-ion battery management circuit board was used for the charging and discharging respectively, which is shown in Fig. 2, when they are in discharging condition. Fifteen K-type thermocouples were attached to the surface of the battery to measure the temperature. As a working fluid, we used a binary fluid which is a solution containing 20 % (volume percentage) Ethylene Glycol (EG) and 80 % of water. In each experimental reading average temperature was noted after 120 seconds, 300 seconds, 420 seconds, and 600 seconds at different discharges of 1.2 C, and 2.1 C, The pressure drop was estimated using a U-tube manometer.

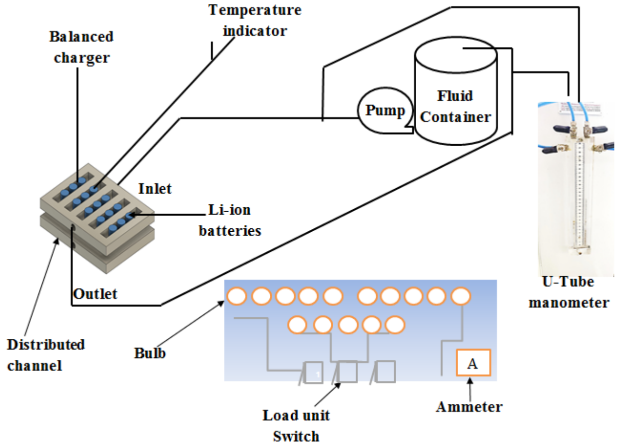

Figure 1. Schematics diagram of the experimental setup

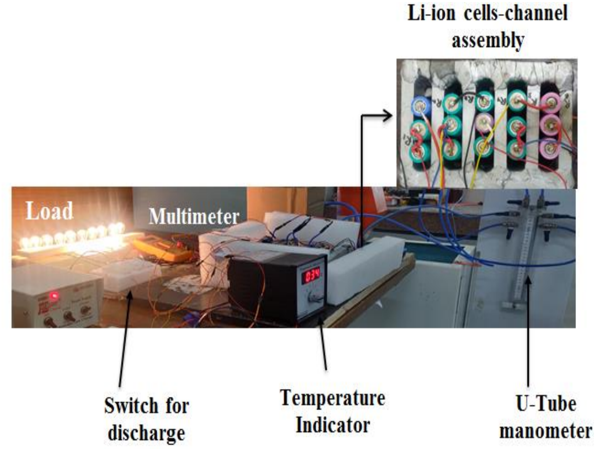

Figure 2. Experimental setups during discharging

RESULTS AND DISCUSSION

The main objective of the study is to maintain the maximum temperature of the batteries within the safety limit and to maintain temperature uniformity between the cell i.e. ± 5°C to avoid thermal runaway condition. The impact of different channel flow configurations on the cooling performance of the Li-ion battery is investigated at different discharging rates of 1.2 C and 2.1 C, which is compared with without cooling cases. The ambient temperature was noted as 28°C and the temperature of the working fluids was 20°C. As the discharging rate increases, the average temperature of the battery ($T_{avg,c}$) also increases at a rapid rate. The $T_{avg,c}$ is about 42°C for 1.2 C at 600 seconds in the case of without cooling as shown in Fig. 3, and with a further increase in the discharging rate, the $T_{avg,c}$ is about 49°C for 2.1 C at 600 seconds as shown in Fig. 4. It is concluded that the temperature of batteries inside the battery pack also increases with increasing discharging rate, which is nearly an unsafe temperature limit for that we use cooling of battery with the help of binary fluid. After a different interval of time and at different discharge rates, the working fluid also gains heat from the batteries through conduction as well as convection. The variation in $T_{avg,c}$ for different flow configurations at discharging rates of 1.2 C and 2.1 C is illustrated in Fig. 3 and Fig. 4 respectively.

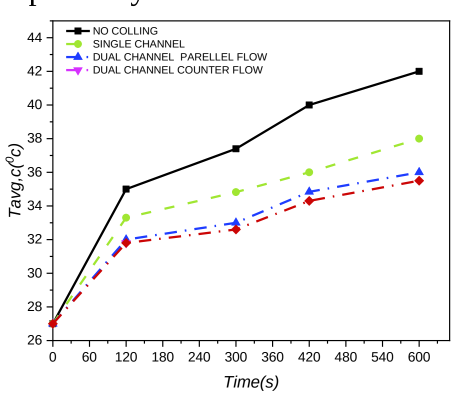

Figure 3. $T_{avg,c}$ v/s time at a discharge rate of 1.2 C

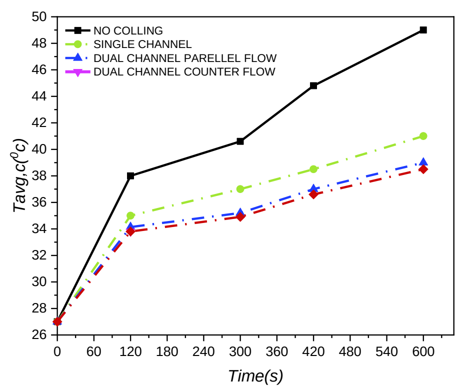

Figure 4. $T_{avg,c}$ v/s time at a discharge rate of 2.1 C

In a single channel, the cooling is low as compared to the other two configurations. In a single-channel, maximum drop in temperature is observed at 4°C and 8°C at a discharging rate of 1.2 C and 2.1 C respectively having a mass flow rate of 0.02235 kg/s. In a dual-channel where the flow is parallel, a drop in temperature is more and a cooling effect can be seen more effectively in this case maximum drop in temperature is observed as 6°C and 10°C. Whereas in the case of dual-channel having the counter-flow configuration, a maximum drop in temperature of about 7°C and 11°C is observed at a discharging rate of 1.2 C and 2.1 C respectively.

CONCLUSION

Among all the configurations, dual-channel having a counter-flow configuration gives the highest cooling efficiency of 14.20% and 22.50% at a discharge rate of 1.2 C and 2.1 C, respectively.

ACKNOWLEDGMENT

The first author is grateful to the Director, Dr. B R Ambedkar National Institute of Technology Jalandhar for providing facilities and support in carrying out the experiments.

REFERENCES

Liu, H., W. Zhongbao, H. Weidong and Z. Jiyun. 2017. Thermal issues about Li-ion batteries and recent progress in battery thermal management systems: A review. Energy Convers. Manag.,150: 304-330.

Zhang, T., C. Gao, Q. Gao, G. Wang, M. Liu, Y. Guo, C. Xiao and Y.Y. Yan, 2015. Status and development of electric vehicle integrated thermal management from BTM to HVAC. Appl. Therm. Eng., 88: 398–409.

CHAPTER -4

CONVECTION IN A CASSON FLUID LAYER WITH WEAK VERTICAL HARMONIC OSCILLATIONS

Sameena Tarannum[1], S. Keerthana[2], P. G. Siddheshwar[3], Ruwaidiah Idris[4]
[1]Assistant Professor, Department of Professional Studies, CHRIST (Deemed to be University), Bangalore, India
[2, 3]Centre for Mathematical Needs, Department of Mathematics, CHRIST (Deemed to be University), Bangalore, India
[4]Faculty of Ocean Engineering Technology and Informatics, Universiti Malaysia Terengganu, 21030 Kuala Nerus, Terengganu, Malaysia.
Corresponding author: sameena.tarannum@christuniversity.in

INTRODUCTION

The convection in a Casson fluid layer are performed in the presence of vertical harmonic vibrations for the linear and weakly nonlinear cases. In the linear analysis, expression is obtained for the Correction-Rayleigh-number arising due to the vibrations. The nonlinear analysis based on the Ginzburg-Landau equation is used to compute the Nusselt-number with repect to the Correction-Rayleigh-number. The mean-Nusselt-number is then obtained as function of the scaled-Rayleigh-number, the amplitude of modulation, the frequency, the Prandtl number, and the Casson parameter. The non-autonomous amplitude-equation is numerically evaluated by Runge-Kutta-Fehlberg45 method. From the study, it's examined that the influence of increasing the amplitude of modulation, lead to a delayed-onset situation and thereby to an enhanced-heat-transport situation. For small and large frequencies, the influence of increase in the frequency of oscillations is to decrease the Critical-Rayleigh-number. However, the mean-Nusselt-number decreases with increase in the frequency of oscillations only in the case of small frequencies. The influence of increase in the value of the Casson parameter lead to an advanced-onset and thereby to an augmented-heat-transfer in the system.

MATERIALS AND METHODS

In the linear analysis, expression is obtained for the Correction-Rayleigh-number arising due to the vibrations. The nonlinear analysis based on the Ginzburg-Landau equation is used to compute the Nusselt-number with repect to the Correction-Rayleigh-number. The non-autonomous amplitude-equation is numerically evaluated by the Runge-Kutta-Fehlberg45 method.

RESULTS AND DISCUSSION

From figure (1), we see the graph of the Correction-Rayleigh-number (R2C) versus the frequency (Ω), for various values of casson parameter (β) and it is inferred that as β increases, R2C decreases. Therefore, increase in the value of β is to advance the onset of convection.

Figure (2) is the graph of mean-Nusselt-number ($\overline{\mathrm{Nu}}$) versus Ω, for various values of β and it is inferred that as β increases, $\overline{\mathrm{Nu}}$ decreases resulting in diminished heat-transport. Also, we see from the

ICATP 2022, ISBN 978-81-952903-0-7

figure that, for small values of frequencies, $\overline{Nu}$ decreases with Ω. However, $\overline{Nu}$ increases for large values of Ω.

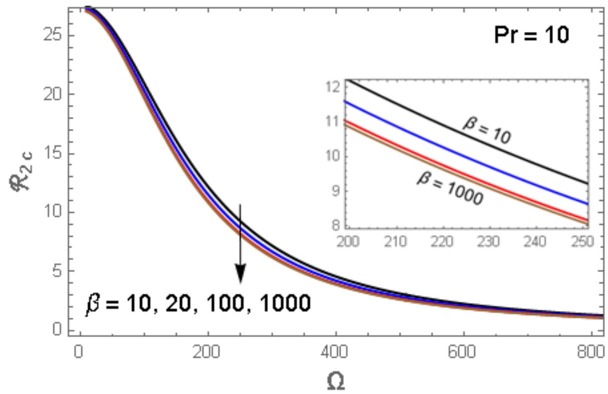

Figure 1: Plot of R2C versus Ω, for different values of β.

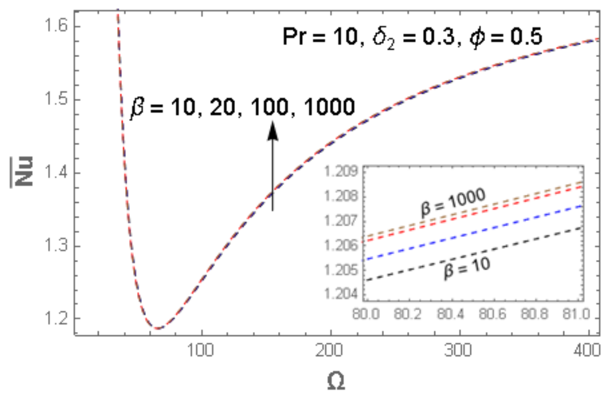

Figure 2: Plot of $\overline{Nu}$ versus Ω, for different values of β.

CONCLUSION

From this work, we conclude the following:

1. Increase in the values of the Casson parameter (or decrease in the yield-stress) give rise to advanced-onset and thereby to an augmented-heat-transfer in the system.
2. Increasing the value of Prandtl number is to decrease the heat-transport.
3. The influence of increase in the frequency of vertical harmonic oscillations is to decrease or increase the heat-transport based on the value of Ω. However, the influence of increasing Ω is to stabilize the system for all values of Ω.

ACKNOWLEDGMENT

We would like to acknowledge the support of CHRIST (Deemed to be University) and Universiti Malaysia Terengganu through the International Partnership Research Grant (IPRG).

REFERENCES

1. L. Rayleigh. 1916. On convection currents in a horizontal layer of fluid, when the higher temperature is on the underside. Philosophical Magazine, 32: 529-546.
2. P. G. Siddheshwar. 2010. A Series Solution for the Ginzburg-Landau Equation with a Time-Periodic Coefficient. Applied Mathematics, 3: 542-554.

CHAPTER -5

NUMERICAL INVESTIGATION OF HEAT TRANSFER CHARACTERISTICS OF CRYO-NANOFLUIDS

Dasari Bramhaiah[1], Smrutiranjan Nayak[1], Atul Bhattad[2], K. S. Patel [1*]
[1]Mechanical Engineering, National Institute of Technology Rourkela, Odisha, India
[2]Mechanical Engineering, Koneru Lakshamaiah Education Foundation, Guntur, A.P, India
[*]Email address: patelks@nitrkl.ac.in; kishpatel.mech@gmail.com; Ph. No.: +91 9945676486

INTRODUCTION

The use of cryogenic fluids is unavoidable to cool any material or equipment to the cryogenic level. However, the cooling capacity of cryogenic fluids without phase change are considerably low because of the small temperature difference and operating range of cryogenic fluids in their liquid state. Cryo-fluids with a phase change could increase heat carrying capacity to some extent, but handling such a system requires additional cooling circuits to bring back the fluid to a liquid state again. Moreover, the chances of leakage will also be high. This problem can be alleviated by adding nanoparticles, which will enhance the thermophysical properties of cryogenic fluids in their liquid state. The effects of nanoparticles in cryo-fluids have been explored limitedly in the past. In this direction, Dondapati et al. (2017) and Uppada et al. (2020) have investigated the effects of nanoparticles using the homogeneous computational model, which usually predicts inaccurate results for the high Reynolds number flows. Moreover, these studies also ignore the variation in thermophysical properties of base liquid nitrogen (LN_2) with temperature change, which is as high as ~70% for the flow viscosity between the temperature range of 64 K – 83 K and 2 bar pressure.

In the present study, a compact cylindrical tube, which is a building block of various heat exchangers, is analyzed computationally using the Ansys 18.1 solver. A cylinder of 7.8 mm in diameter and length of 873 mm is heated with a constant heat flux rate of 91300 W/m^2. The investigation focuses on changes in heat transfer properties and pressure losses of base LN_2 by mixing Al_2O_3, SiC, and TiO_2 nanoparticles at different volume concentrations. In this, the effects of variable thermophysical properties of LN_2 are also considered, and a comparative study is made between the homogeneous and discrete phase mixture computational models. Finally, the overall enhancement in the heat transfer properties and the pressure losses are investigated using the mixture computational model.

MATERIALS AND METHODS

The present work considers the variable thermophysical properties of base LN_2 with Al_2O_3, TiO_2, and SiC nanoparticles at 2 bar pressure. The properties of nanoparticles at a 77 K temperature are mentioned in Table 1. A two-phase mixture model that can handle the solid-liquid discrete phases separately and consider the drift velocities between them is employed to solve the accurately cryo-nanofluid system. The flow inside the pipe is fully turbulent ($Re \approx 64000$, based on the inlet velocity and pipe diameter), which has been resolved using the Realizable k-ε turbulence model with standard wall model.

ICATP 2022, ISBN 978-81-952903-0-7

Table 1. Thermophysical properties of nanoparticles at 77 K.

Nanoparticles	Density (Kg/m^3)	Specific heat (J/kg-k)	Thermal conductivity (W/m-k)
Al_2O_3	3970	60	157
TiO_2	4157	161.905	32.776
SiC	3160	52	4000

RESULTS AND DISCUSSION

At first, the validation of the computational setup is performed (Figure 1) using the reference results reported by Dondapati et al. (2017). As per the reference, the validation study employs the homogeneous computational model for the cryo-nanofluid simulations and considers the constant LN_2 thermophysical properties at 77 K. As can be seen, the computation results shown for the average temperature difference between the outlet and inlet planes closely agrees with the reference results with the maximum error of less than 2%. Further, Figure 2 shows the enhancement in heat transfer coefficient (HTC) of base LN_2 with the addition of three nanoparticles at different volume concentrations. The inlet velocity for this study is kept fixed at 2.5 m/s. The simulation employs a discrete phase mixture model, where the effects of variable thermophysical properties of base LN_2 with temperature are considered. As can be seen, SiC gives a maximum 2.7 times enhancement in HTC at 0.5% volume concentration, while the TiO_2-based cryo-nanofluids show the least enhancement of 17% as compared to the pure LN_2.

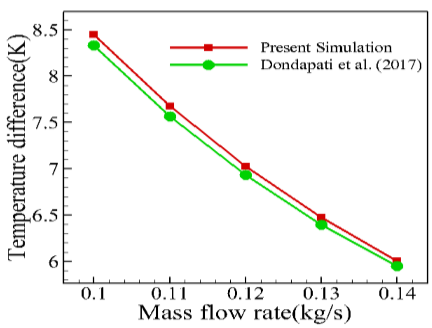

Figure 1. Temperature difference plot for pure LN_2 with different mass flow inlet.

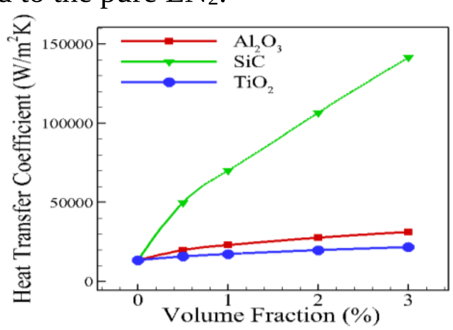

Figure 2. HTC profile at outlet section for all nanofluids with different volume concentration.

Figures 3 and 4 show the difference in temperature contours of pure LN_2 and SiC-based cryo-nanofluid. In all the cases, the maximum temperature inside the cylinder is bound within the limit of evaporation temperature of 84 K for LN_2 at 2 bar pressure. Moreover, the addition of nanoparticles reduces the difference between the wall and bulk fluid temperature, leading to the enhancement in HTC, as per Newton's law of cooling.

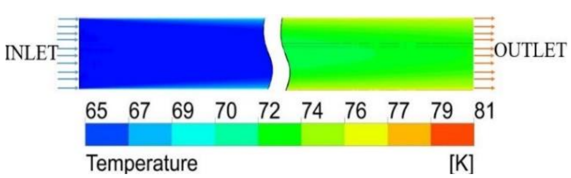

Figure 3. Temperature contour plot of pure LN_2 obtained for the flow inlet velocity of 2.5m/s.

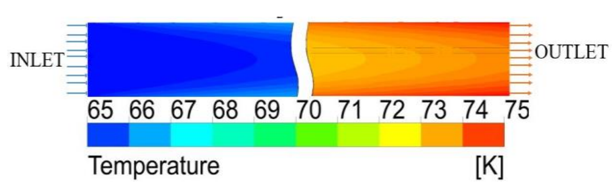

Figure 4. Temperature contour plot of LN_2+3%SiC obtained for the flow inlet velocity of 2.5m/s.

ICATP 2022, ISBN 978-81-952903-0-7

CONCLUSION

It has been observed that the addition of nanoparticles in the cryo-fluids increases the HTC of LN_2 by many folds. Moreover, it has also been observed that a little addition of SiC nanoparticles (0.5%) is sufficient to enhance the overall heat carrying capacity of base LN_2 cryo-fluids.

REFERENCES

Dondapati, R.S., Saini, V., Verma, K.N. and Usurumarti, P.R., 2017. Computational prediction of pressure drop and heat transfer with cryogen based nanofluids to be used in micro-heat exchangers. *International Journal of Mechanical Sciences*, *130*, pp.133-142.

Uppada, V.R. and Dondapati, R.S., 2020. Role of nanocryogenic fluids in optimizing the thermohydraulic characteristics of high temperature superconducting (HTS) cables with entropy generation minimization strategy. *Physica C: Superconductivity and its Applications*, *571*, p.1353620

ICATP 2022, ISBN 978-81-952903-0-7

CHAPTER -6

ANALYSIS OF SCOUR FORMATION AT BRIDGE ABUTMENTS USING COLLAR

Mullapudi Sri Lasya, Mulupuri Gnana Deepthi Keziya, B. Sandeep and Balakrishna Murthy V.
Department Of Mechanical Engineering, Velagapudi Ramakrishna Siddhartha Engineering College, Vijayawada, Andhra Pradesh.
Email: lassi.mullapudi15@gmail.com

1. INTRODUCTION

Scour at the bridge abutments is the major cause of the damage to the bridges. Scour is defined as the removal of dirt and debris from a bridge foundation due to fast-moving water. Collars used as a countermeasure which are integrated around the abutment, control this scour effect as it acts as a barrier by reducing the upward flow of fluid which decreases the negative pressure at the bottom. The effect of a collar as a countermeasure to reduce negative pressure at the bottom is determined using ANSYS software by simulation considering various parameters that include various sizes of collars 0.26m, 0.27m, 0.28m at various positions 0.5m, 0.75m, 1.25m, and 1.5m from the bed level. The simulation is carried out under a symmetric top surface to determine the negative pressure.

2. METHODOLOGY

A Parallelopiped fluid domain of 6m-2m-3m is created in which a slot for abutment with a width of 0.25m integrated with a collar is considered for the simulation analysis. The fluid domain has meshed and refined at high concentrated area. The side face and top face are considered symmetric and the side adjacent to the wall and the bottom level are considered as the wall. The collar integrated around the abutment with different sizes of 0.26m, 0.27m, 0.28m, positioned at various heights of 0.5m, 0.75m, 1.25m and 1.5m from the bed level is considered a wall-bound simulated for pressure analysis. The pressure at the bottom is analysed at different velocities for different parameters mentioned. From simulation results, it is observed that negative pressure at the bottom of the abutment reduces by increasing collar width and reducing collar height distance from the bed level.

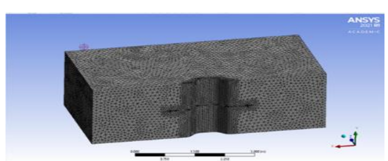

Fig 1. Collar around the abutment is meshed and refined.

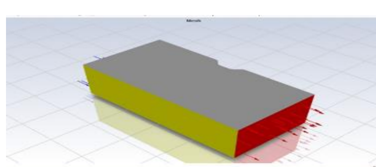

Fig 2. Fluid domain in setup.

3. RESULTS

The following table represents negative pressures at the bottom of the fluid domain at different velocities at 0.25m width of abutment with collars of 0.26m, 0.27m, 0.28m widths for the fluid domain of 6m-3m-2m dimensions.

Table 1. Determining negative pressures at bottom with collar at different widths.

Velocity(m/s)	Collar width 0.26m		Collar width 0.27m		Collar width 0.28m	
	Maximum Pressure (kPa)	Negative pressure (kPa)	Maximum Pressure (kPa)	Negative Pressure (kPa)	Maximum Pressure (kPa)	Negative Pressure (kPa)
1m/s	0.310	-0.830	0.312	-0.821	0.321	-0.814
2m/s	1.268	-3.375	1.269	-3.347	1.308	-3.305
3m/s	2.880	-7.887	2.884	-7.581	2.972	-7.508

The following tables represents negative pressures at the bottom of the domain at different velocities and at different collar heights from the bottom level (bed level) with collar of 0.28m and 0.27m width.

Table 2. Determining negative pressure when collar of 0.28m placed at different heights from the bottom.

Velocity	1m/s		2m/s		3m/s	
Height of collar	Maximum Pressure (kPa)	Negative Pressure (kPa)	Maximum Pressure (kPa)	Negative Pressure (kPa)	Maximum Pressure (kPa)	Negative Pressure (kPa)
1.5m	0.3127	-0.869	1.274	-3.528	2.891	-7.994
1.25m	0.3126	-0.862	1.274	-3.495	2.888	-7.930
0.75m	0.3217	-0.846	1.312	-3.474	2.984	-7.864
0.5m	0.3268	-0.844	1.331	-3.433	3.018	-7.744

Table 3. Determining negative pressure when collar of 0.27m placed at different heights from the bottom.

Velocity	1m/s		2m/s		3m/s	
Height of collar	Maximum Pressure (kPa)	Negative Pressure (kPa)	Maximum Pressure (kPa)	Negative Pressure (kPa)	Maximum Pressure (kPa)	Negative Pressure (kPa)
1.5m	0.3230	-0.928	1.303	-3.740	2.958	-8.470
1.25m	0.3293	-0.909	1.334	-3.695	3.018	-8.357
0.75m	0.3254	-0.879	1.355	-3.589	3.072	-8.130
0.5m	0.310	-0.852	1.287	-3.461	2.925	-7.880

4. CONCLUSIONS

- The size of collar width plays an important role in reducing the scour depth at the bottom of the abutment. Using collars of greater width around the abutments decreases the negative pressure at the bottom. They act as the barrier for the fluid flow and obstruct the wave formation to greater heights, which could increase the negative pressure responsible for the scouring effect.

- It is observed that the negative pressure is reduced at the abutments of collars at lower heights, i.e.,0.5m (decreased elevation) compared to collars located far away from the bottom level, i.e. (0.75m,1.25m,1.5m). Hence, it proved that the abutments with collars arranged at lesser elevation or near to the bed level form fewer height waves, thereby decreasing the negative pressure.

REFERENCES

1. Kayaturk S. Y., Kokpinar M. A., and Gogus M. (2004c). “Effect of collar on temporal development of scour around bridge abutments.” Proceedings., 2nd Int. Conf. on Scour and Erosion, Surbana, Meritus Mandarin, Singapore, pp. 180-186.

2. M. Gogus, A. E. Dogan (2010) “Effect of collars on scour reduction at bridge abutments” Proceedings of the 5th International Conference on Scour and Erosion. ASCE, San Franciso (2010), 10.1061/41147(392)100.

CHAPTER -7

Electrophoresis of Hydrophobic Rigid Colloids: Mathematical Approach

Paramita Mahapatra*[,1], Partha P. Gopmandal [1]
[1] Department of Mathematics, National Institute of Technology Durgapur, Durgapur-713209, India
* Corresponding Author: Email- pmscc412@gmail.com

INTRODUCTION:

The electrophoretic technique often used for the correct measurement of electric charge, more specifically the ζ-potential of the colloidal particles. The classical works on the electrophoresis of rigid colloids often consider the no slip boundary conditions along the surface of colloids. However, there are various environmental and functionalized nanoparticulates which possesses hydrodynamic slipping behavior along their surface [Kobayashi (2020)]. Thus, the measurement of surface potential using the classical theories of electrophoresis of rigid colloids [Henry (1931), Obrien and White (1978)] may give rise a significant discrepancy in the measured value of surface potential from its actual value. For hydrophilic colloids, the tangential component of fluid velocity vanishes along its surface. However, such an assumption is certainly invalid for hydrophobic rigid particles. For such cases we need to consider the Navier-slip boundary condition along the particle surface [Ohshima (2019)]. For hydrophobic particles, the electrohydrodynamic behavior is not only influenced by surface ζ-potential, but also by the nonzero slip length (Λ that characterizes the hydrophobic behavior of nanoparticulates. In the present study we are intended establish a tractable analytical theory for the electrophoretic mobility (electrophoretic velocity per unit field strength) expression for hydrophobic rigid colloid carrying low, moderate and high ζ-potentials in the extent of binary symmetric z: $z$electrolytes.

MATERIALS AND METHODS:

We consider here the motion of hydrophobic rigid colloids exposed under weak electric field. For such a case the deviation of electrolyte concertation, electrostatic potential, electrochemical potential, space charge density due to mobile electrolyte ions etc. ($n_i(r)$, $\psi(r)$ $\mu_i(r)$ and $\rho_e(r)$ from their respective equilibrium values are small. Here we use the linearization technique of O'Brien and White (1978) to derive the expression for mobility involving integrals valid for arbitrary surface potential. We further derive closed form analytical results for electrophoretic mobility valid for low potential limit. To derive the same, we have invoked Debye-Huckel linearization technique. Besides, we have also used the asymptotic analysis for the closed form analytic derivation of electrophoretic mobility, which is applicable for any value of ζ-potential and at large $\kappa a(\kappa a \geq ca.30)$. Here κ^{-1} and a are the Debye-layer thickness and radius of the particle, respectively.

RESULTS AND DISCUSSION:

Under low ζ-potential approximation, the mobility expression can be obtained as

$$\mu = \frac{\varepsilon_e \zeta}{\eta}\left\{\left(\frac{\Lambda}{a+2\Lambda}\right)\kappa a + \left(\frac{a+\Lambda}{a+2\Lambda}\right) + 2e^{\kappa a}E_5(\kappa a) - \left(\frac{5a}{a+2\Lambda}\right)e^{\kappa a}E_7(\kappa a)\right\} \tag{1}$$

where ε_e, η are dielectric permitivity and viscosity of electrolyte solution, respectively. The Debye-layer thickness κ^{-1} is defined as $\kappa^{-1} = (2z^2 e\, n^{\infty}/\varepsilon_e\, k_B T)^{1/2}$. The expression $E_i(\kappa a)$ in (1) refers the exponential integrals. Expression (1) is valid for weakly charged hydrophobic rigid colloids in the extent of binary symmetric z: $z$electrolytes. In Fig. 1a we have shown graphically the dependednce of electrophoretic mobility on the cocnetration of electrolytes considering $\Lambda = 0$ (hydrophilic) and $\Lambda = 0.01a$(hydrophobic). We observe a singnificant enhancement in mobility for hydrophobic particle and the difference in mobility for hydrophobic and hydrophilic particles increases with the rise in electrolyte concetration. We further derived the mobility expression for moderate to highly charged hydrophobic rigid colloids in the extent of *z:z* electrolytes applicable for large $\kappa a(\kappa a \geq ca.30)$, which is given below

ICATP 2022, ISBN 978-81-952903-0-7

$$\mu_E = sgn(\zeta)\frac{\varepsilon_e}{\eta}\left(\frac{a}{a+2\Lambda+3\Lambda F_2}\right)\left[\left(\frac{k_BT}{ze}\right)\frac{\kappa\Lambda\left\{e^{\bar{\zeta}/2}-e^{-\bar{\zeta}/2}+F_1\left(1-e^{-\bar{\zeta}/2}\right)\right\}}{(1+F_1)}+\left(\frac{a+2\Lambda}{a}\right)\left\{|\zeta|-\left(\frac{k_BT}{ze}\right)\left(\frac{2F_1}{1+F_1}\right)ln\left(\frac{1+e^{\bar{\zeta}/2}}{2}\right)\right\}-\left(\frac{k_BT}{ze}\right)\left\{\frac{6\Lambda m}{a(1+F_1)}\right\}\left(1-e^{\bar{\zeta}/2}\right)^2 ln\left(\frac{1+e^{-\bar{\zeta}/2}}{2}\right)\right] \quad (2)$$

where $\bar{\zeta} = \frac{ze\zeta}{k_BT}$, $sgn(\zeta) = +1$, if ζ is positive and -1, if ζ is negative, $F_1 = \frac{2}{\kappa a}(1+3m)\left(e^{\bar{\zeta}/2}-1\right)$ and $F_2 = \left(\frac{m}{1+F_1}\right)\left(1-e^{\bar{\zeta}/2}\right)^2 + \cancel{m}\left(1-e^{-\bar{\zeta}/2}\right)^2$. We have shown the dependency of electrophoretic mobility on scaled surface potential for various binary electrolyte solutions (Fig. 1b). A significant deviation of mobility of hydrophilic colloids to that of hydrophilic colloids is observed. In addition a local maximum in mobility occurs depending on the critical choice of scaled surface potential.

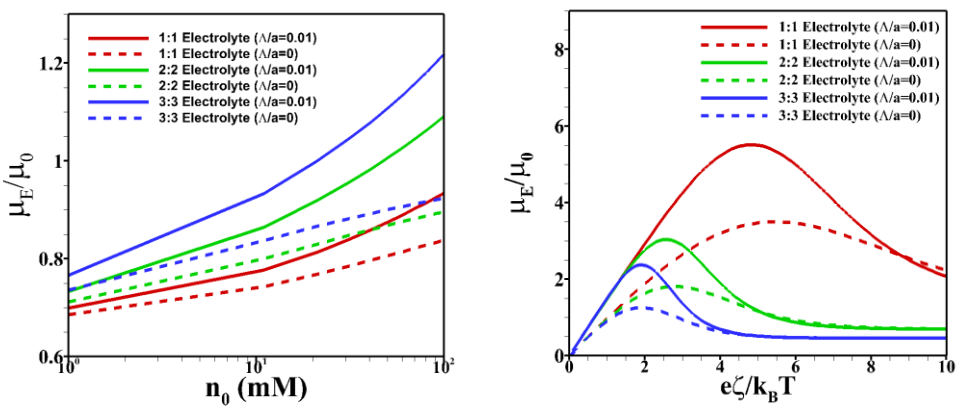

(a) (b)

Fig. 1. Scaled electrophoretic mobility μ_E/μ_0, $(\mu_0 = \varepsilon_e\,\zeta/\eta)$ as a function of (a) bulk electrolyte concentration n_0 with $\Lambda/a = 0$ and 0.01 and scaled zeta potential $e\zeta/k_B T = 1$; (b) scaled zeta potential $e\zeta/k_B T$ at fixed κa= 50 with scaled slipping length Λ/a= 0 and 0.01. The results in (a) are obtained from expression (1) and (b) obtained from the expression (2).

CONCLUSION: The existing theories of electrophoresis of hydrophilic colloids are revisited. Based on weak electric field and low charge assumption we derived the exponential form of electrophoretic mobility of hydrophobic rigid colloids. Besides, we have deduced a tractable analytical expression of electrophoretic mobility of moderate to highly charged hydrophobic colloids. The derived expressions will pave the way for refined calculation of electrostatic charged properties of the rigid nanoparticulates.

ACKNOWLEDGMENT: P.M. gratefully acknowledge CSIR for their financial support. P.P.G. gratefully acknowledge SERB for the financial support through a project grant (File No. MTR/2018/001021).

REFERENCES

[1] Kobayashi, M. 2020. An analysis on electrophoretic mobility of hydrophobic polystyrene particles with low surface charge density: effect of hydrodynamic slip. Colloid Polym Sci., 298:1313–1318.

[2] Henry, D. C. 1931. The Cataphoresis of Suspended Particles. Part I. The Equation of Cataphoresis Proc. R. Soc. Lond. A, 133:106-129.

[3] O'Brien, R. W., White, L. R. 1978. Electrophoretic mobility of a spherical colloidal particle. J. Chem. Soc., Faraday Trans. 2, 74:1607-1626.

[4] Ohshima, H. 2019. Electrokinetic phenomena in a dilute suspension of spherical solid colloidal particles with a hydrodynamically slipping surface in an aqueous electrolyte solution. Adv. Colloid Interface Sci., 272:101996.

CHAPTER -8

Novel brine based high density completion fluid for oilfield applications: Aging effect and rheology

Ramanand Singh[1*], R. Sharma[1], G. Ranga Rao[2],

[1]Design and Simulation Laboratory, Petroleum Engineering Section, Department of Ocean Engineering, IIT Madras, Chennai, India.

[2]Department of Chemistry, IIT Madras, Chennai, India.

[*]Corresponding Author: [1*]ramanand8038@gmail.com

1. Introduction

According to the American Institute of Petroleum, a completion fluid is solid free, and high density liquid used to complete a drilled oil/gas well (Ezzat et al., 1990). The effect of aging and rheology is an important parameter for the design and formulation of high density completion fluid (Singh et al., 2022). Rheological properties of the completion fluid are subjected to change during the exposure to reservoir formation pressure and temperature. The experimental rheological investigation is essential in real-time monitoring of the rheological changes during the aging of completion fluid while being subjected to different aging times (days).

2. Materials and Methods

We have formulated Magnesium Bromide based completion fluid in the aqueous medium. Magnesium Bromide ($MgBr_2$), having a purity of 99%. is manufactured by the NICE Chemicals Private Limited, India. We have explored the Bingham Plastic model (BP) rheological model for non-Newtonian fluids is:

$$\tau = \mu_p \gamma + \tau_y \qquad (1)$$

Where, τ is the shear stress in $lb_f/100\ ft^2$, γ is the shear rate per second, τ_y is the yield point in $lb_f/100\ ft^2$, and μ_p is the plastic viscosity in cP.

3. Results and Discussions

Our work is to investigate the rheological parameter of apparent viscosity, plastic viscosity, and yield point at the ambient conditions for the entire aging time period of 5 days. We have obtained a favorable apparent and plastic viscosity range (<10 cP). The yield point value is less than 5 $lb_f/100\ ft^2$. Figure 1 shows (a) an image of the 1st day aged completion fluid sample, and (b) An image of the 5th day aged completion fluid sample. We have observed a clear fluid system during the aging process. There are no solid settlements at the bottom of the sample during the entire five-day aging process. A clear and solid free completion fluid is

ICATP 2022, ISBN 978-81-952903-0-7

highly demanding for mitigating formation damage near the wellbore.

(a) (b)

Figure 1: (a) An image of the 1st day aged completion fluid sample, (b) An image of the 5th day aged completion fluid sample.

4. Conclusions

We have investigated the effect of aging and rheology of Magnesium bromide based completion fluid. We have formulated high density completion fluid of specific gravity of 1.617. We have observed that long-aged samples (5days) had showed less variation in rheological properties (<1 cP in apparent and plastic viscosity), density, and pH value. A stable and high density completion fluid is very helpful during the drilling and well completion process in offshore and complex reservoirs. Our work will help in improving the completion fluid design by investigating the aging, rheology, alkalinity, and density of the fluid.

5. References

API Recommended Practice 13B-1. 2003. Recommended Practice for Field Testing Water-Based Drilling Fluids. American Petroleum Institute, Washington, DC.

Ezzat, A.M., 1990. Paper presented at the Society of Petroleum Engineers Formation Damage Control Symposium, Lafayette, Louisiana. https://doi.org/10.2118/19434-MS

Singh, R., R. Sharma and G.R. Rao. 2022. Aging Effects on the Rheological Properties of Novel Magnesium Bromide Hexahydrate-Based Completion Fluids for Oil and Gas Reservoirs. Arab J Sci Eng. doi: https://doi.org/10.1007/s13369-022-06798-2

CHAPTER -9

Numerical Investigation of Hydrogen Blending on Methane Combustion in a Domestic Cook Stove Burner

Aravindan M[1], Praveen Kumar G[1], Thundil Karuppa Raj[2], Sakthivadivel D[2]
[1]CO_2 Research and Green Technologies Centre,
[2]School of Mechanical Engineering,
Vellore institute of Technology, Vellore 632017, Tamil Nadu
praveenkumar.g@vit.ac.in(corresponding author)

INTRODUCTION:

The use of fossil fuels has increased dramatically for a wide range of applications, from industry to domestic use. In recent years, the cost of fuels, particularly for cooking, has gradually increased due to inflation, pandemic and the depletion of fossil fuel sources. Blended fuels are an important alternative fuel source for efficient cooking because they use less conventional fuel, take less time to cook, and emit less pollution. In this study, an alternative clean fuel of Hydrogen is chosen for blending with Methane (H-M), because it can be produced from different domestic resources and emission of greenhouse gases also zero. In this present work, the combustion performance of commercial cooking burner (CCB) for blended fuels of hydrogen/methane ranging from 0 to 50% with constant mass flow rate of air and fuel is analysed by using Ansys CFD and solid works for modelling the geometry. The performance of blended fuels H-M clearly shows that as the hydrogen percentage increases, the flame temperature, velocities, and pressure increase, while CO and CO_2 emissions decrease.

MATERIALS AND METHODS:

The main objective of this study is to analyse the thermal efficiency of blended fuel H-M. In the non-premix combustion, the numerical study is conducted with four step process to analyse the blended fuel. The first step involves modelling a commercial burner in solid works with dimensions of 15mm in height and inner and outer diameters of 30mm and 80mm, respectively [1]. The number of holes in the centre of the burner is 30, and the outer side has 60 holes and 30 holes in the bottom and upper rows, respectively. Meshing is done in the second step using an unstructured grid made up of hexahedral, prism, and tetrahedral profiles. Considering the high grid quality, each element of mesh is 0.007 m after grid independence test to generate optimal fine element in the burner. Finally, the meshing model is simulated using "k-Ɛ turbulence model" and the results are obtained and analysed using the post processor section.

RESULTS AND DISCUSSION:

In this study the combustion performance and flow phenomena of CCB using H-M blend in different ratio mixture is examined. To verify the result of simulation, the flow patterns of combustions are compared with flame picture of CCB is perfectly matched. The hydrogen is mixed with methane in different fuel mass ratio (FMR) named as A to F, among the ratio $0.5H_2$ and $0.5CH_4$ mixture result is shown in Fig.1. The simulation result of combustion at midplane of CCB represented in terms of temperature, velocity, pressure are shown in Fig.1. The flame near the burner holes is highly stabilized due to influence of hydrogen on methane because it has high calorific value, highly flammable. So ignition can occur at low volumetric ratio it produces more heat during combustion so that temperature also increased. During 100% methane combustion in conventional burner, the maximum temperature is about 2166 K. For FMR of 0.1 to 0.5 the flame temperature is steadily increased from 2204 K to 2292 K as shown in Fig.2. At $0.5H_2$+0.5 CH_4, FMR is very flammable and lighter than air so the maximum pressure of 0.8639 Pa and the velocity of 1.06 m/s is attained.

ICATP 2022, ISBN 978-81-952903-0-7

Hence, the cooking time gets reduced compared to using of pure methane in CCB. If the hydrogen percentage exceeds more than 50% flash back will occur and cooking efficiency also decreased [1]

FMR Temperature & CO mass fraction Pressure & CO_2 mass fraction Velocity & NO mass fraction

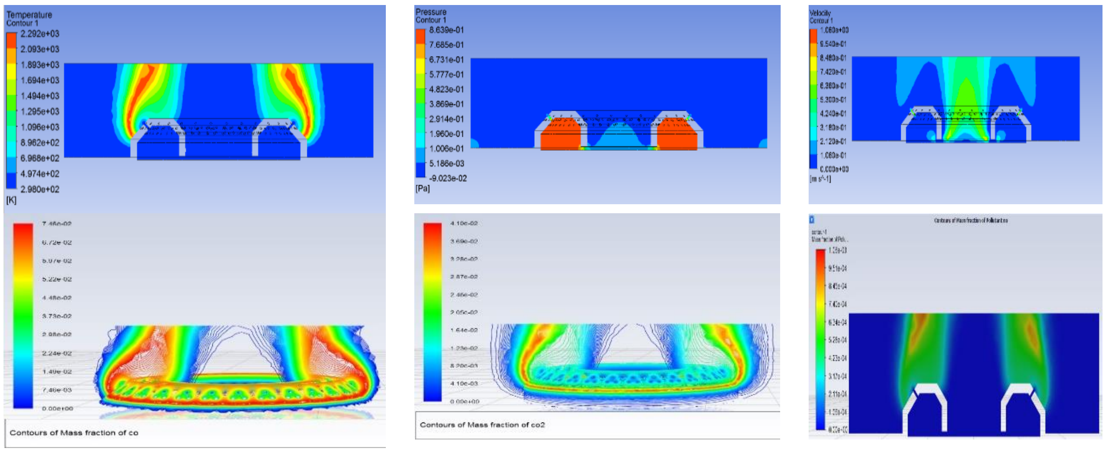

Figure 1. Comparison of temperature, pressure, velocity, CO, CO_2 and NO contours for variation of hydrogen with methane in 0.5:0.5

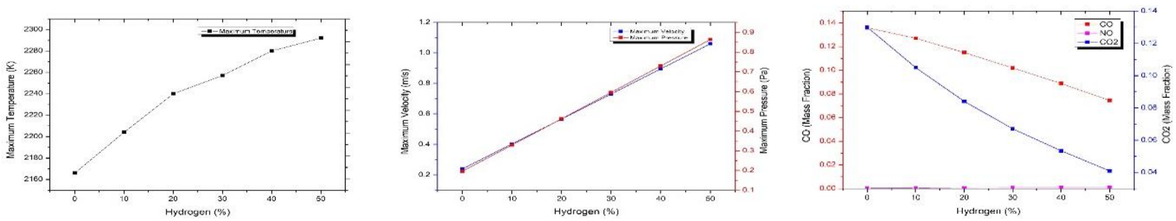

Figure 2. Effect of variation of hydrogen mixing ratio in maximum temperature, Pressure and velocity, CO, CO_2 and NO emission

CONCLUSION:

The effect of H-M blend, temperature, velocity, pressure and emissions for CCB are numerically investigated. It clearly indicates that the general emission levels of CCB are much higher than the blended fuels of H-M from 0 to 50%. In H-M blend in the ratio of 0.5:0.5 the temperature is increased to 5.8% and emission of CO and CO_2 decreased to 45.1% and 68.46% compared to CCB based on methane alone. The overall result shows that hydrogen blends with fuels provide high thermal efficiency, high pressure and velocity, and low emissions, which lead to improved cooking performance.

ACKNOWLEDGMENT:

The work is financially supported by the Department of Science and Techneology, Government of India under the Science for Equity Empowerment and Development Division (Grant No. DST/SEED/TSP/STI/2020/243).

REFERENCES:

1. Yan Zhao, Vincent McDonell and Scott samuelsen. 2019. Influence of hydrogen addition to pipeline natural gas on the combustion performance of a cooktop burner: International journal of hydrogen energy 44(2019) 12239-12253.
2. Livio de santoli, Romano Paiolo and Gianluigi lo basso. 2017. An overview on safety issues related to hydrogen and methane blend applications in domestic and industrial use. 72nd conference of the Italian thermal machines engineering associations, AT12017, Lecce, Italy

CHAPTER -10

ANALYSIS OF SCOUR FORMATION AT BRIDGE ABUTMENTS COMPARING DIFFERENT COUNTER MEASURES

Mulupuri Gnana Deepthi Keziya, Md. Anwar, M. Sai Kiran and Balakrishna Murthy V.
Department Of Mechanical Engineering, Velagapudi Ramakrishna Siddhartha Engineering College, Vijayawada, Andhra Pradesh.
Email: keziyaprakash@gmail.com

1. INTRODUCTION:

Scour is a rubbing action of water flowing on the bed against the banks. Collars when added to the abutments, acts as the barrier that obstruct the flow of the fluid in upward direction and reduce negative pressure. Sacrificial piers are the column-like construction which are made to stand against the flow around the constructions like piers and abutments that support the bridges. The main purpose of the sacrificial piers is to reduce the pressure exerted by the fluid flow on these constructions. The fluid domain of dimension 6m-2m-3m with abutment of 0.25m width is considered to understand negative pressure. Countermeasures including a collar of 0.28m width and sacrificial piers of 0.05m diameter are used around the abutment to prevent the scouring effect. These countermeasures incorporated around the abutment in the fluid domain to obtain negative pressure in open channel boundary condition to make it more real eliminating the assumptions. The effectiveness of reduction of negative pressure with use of these countermeasures is observed by pressure analysis from the simulation which helps to identify a better countermeasure.

2. METHODOLOGY:

A Fluid domain of 6m-2m-3m dimension is created in geometry along with countermeasures like a collar and sacrificial piers separately. The flow is subjected around the abutment using simulation analysis after meshing the domain. The side surface considered as side symmetry, the side along the abutment and bottom wall is considered as a wall. To be more specific and real, the top surface is assumed to be the free surface with open channel multi-phase boundary conditions to resemble the original water domain where the fluid can enter the top surface as well as the outlet. The pressure analysis is performed using simulation with a collar of 0.28m width and sacrificial piers of 0.05m diameter around the abutment. From the simulation results, Collar is identified as a better countermeasure to prevent the scour effect compared to sacrificial piers when simulated in real conditions.

3. RESULTS:

In the following tables, the fluid domain of dimension 6m-2m-3m is considered.

Velocity(m/s)	Fluid domain with abutment 0.25m width		Fluid domain with Collar 0.28m width	
	Maximum pressure kPa	Negative pressure kPa	Maximum pressure kPa	Negative pressure kPa
1	14.983	-15.033	25.196	-9.729
2	21.632	-21.240	44.956	-18.596

3	30.070	-29.396	51.924	-26.509

Table 1. Determining negative pressure for fluid domain with abutment: bare and with collar

Veloc-ity(m/s)	Maximum pressure kPa	Negative pressure kPa
1	30.58	-11.826
2	36.05	-20.228
3	43.909	-28.015

Table 2. Determining negative pressure for fluid domain with sacrificial piers

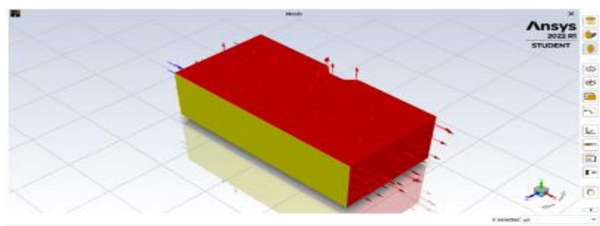

Fig 1. Fluid domain with collars for top free surface

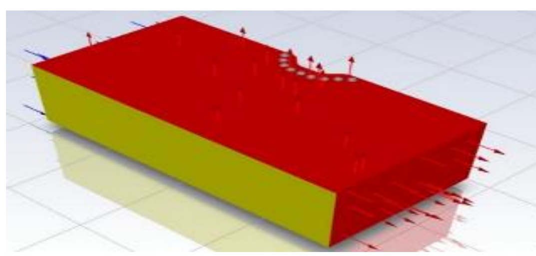

Fig 2. Fluid domain with sacrificial piers for top free surface piers

Veloc-ity(m/s)	Abutment	With collar	With Sacrificial piers
1	-15.033 kPa	-9.729 kPa	-11.826 kPa
2	-21.240 kPa	-18.596 kPa	-20.228 kPa
3	-29.396 kPa	-26.509 kPa	-28.015 kPa

Table 3. Comparing negative pressures for fluid domain with abutment, with collar and sacrificial

4. CONCLUSIONS

- Placing a collar around the abutment decreases the scour effect at the bottom of the abutment by reducing the negative pressure rather than leaving the abutment bare.
- Using sacrificial piers around the abutment is another effective method to decrease the scouring effect and negative pressure.
- The effect of collar around abutment on the reduction of the negative pressure is more than the effect of sacrificial piers around the abutment. In simple terms, the scour formation is less when collars are added to abutments than abutments with sacrificial piers.

5. REFERENCES

1. Kayatürk, S. Y and Gögüs M. 2006. Application of Sacrificial Piles to Control Scouring Around Bridge Piers. Henry.baw.de 347-350.
2. Mohammad Nazari-Sharabian, Aliasghar Nazari-Sharabian, Moses Karakouzian and Mehrdad Karami 2020. Sacrificial piers as countermeasures in river bridges a numerical study using a 3D flow. Civilejournal. Vol 6, No 6. DOI: 10.28991/cej-2020-03091531.

CHAPTER -11

COMPOUND FACIAL EMOTION RECOGNITION USING TWO STAGE COMPOUND FACIAL EMOTION PREDICTION- GAN

Sahaya Sugirtha Cindrella S, A[1], Dr.Jayashree R, B[2]

[1]College Science and Humanities, SRMIST
[2]College Science and Humanities, SRMIST
cindrellavinoth@gmail.com, jayashrr@srmist.edu.in

INTRODUCTION

Robotics and automation with artificial intelligence are becoming prevalent in our daily lives, and their possible existence will lead to the development of novel technologies. Therefore, if computers or robots are able to identify more specific human expressions throughout the interaction, observations of human-computer interaction (HCI) become more realistic. Modern facial expression detection technologies often concentrate on seven fundamental emotions: joy, surprise, fear, sadness, anger, disgust, and contempt. Furthermore, due to recent developments in the study of complex emotions, some efforts are being made to identify more precise and comprehensive facial emotion displays.

BASIC AND COMPOUND EMOTION RECOGNITION

This work organised a competition to identify complex emotions, which calls for proficient visual analysis as well as dealing with the identification of microemotions. The collection includes 31,250 faces from 115 participants, representing a range of emotions with roughly equal gender distribution. The competition took place at FG2020. Compared to the seven classical facial emotions, a compound facial emotion combines dominant and complimentary feelings such as "happily surprised" and "sadly surprised" (e.g., sadly, happy, disgust, and so on). To ensure improved extraction of picture features from the detected data set, the suggested method engages in dynamic confrontation training between the generator and discriminator elements of generative adversarial networks (GANs). Based on the concept of residual networks, the CFEP GAN generator is improved. To guarantee the good precision of the recognition and classification and enhance real-time performance, the image will be first decreased in size and afterwards processed. The CFEP GAN discriminator is trained while simultaneously receiving input from both the generated and real images.This paper cites the VGG-16 network as the backbone network structure for the discriminator network in the GAN [1].

RESULTS AND DISCUSSION

Face images are scaled to 224 x 224 x 3 and aligned using a linearization. Following feature extraction, the VGG-16 CNN is used. Cross-entropy loss is then utilised for optimization. When the estimated labels are exclusive, the cross-entropy loss performs as expected. The Emotion Net Challenges dataset’s labels, however, are connected (e.g., "happily surprised" and "sadly surprised," "happily-angry" and "surprisingly-angry"). Participants chose the middle loss function as a supplementary loss as a solution to this issue in order to lessen the impact of comparable labelling. The centre loss can simultaneously learn the

ICATP 2022, ISBN 978-81-952903-0-7

deep feature class centres for each class and persecute the gaps between both the feature representation class centres. This loss improves the model's ability to discriminate between identical and sample, which therefore boosts overall effectiveness.This experiment was able to find 105,200 photos with emotion classifications using the Emotion Net Challenges dataset. Table 1 displays the distribution of each emotion category. As is visible, there is a severe imbalance in the distribution of emotion categories. The happy category has been allocated to the majority of the photographs, whereas the input image in the other categories is extremely low and occasionally close to zero.

Table 1. Emotion vs. Images

Happy	Angrily Surprised	Angry	Neural	Sad
104521	389	400	250	578

The classification problem of the 50 classes given in Table 2 is used to treat the emotion recognition for the three top-ranked algorithms mentioned thus far.

Table 2. Misclassification of three Datasets

Dataset	Misclassification(test set)	Misclassification(Training set)
Emotion Net Challenges	**0.896**	**0.845**
RAF-DB	0.745	0.720
iCV-MEFFD	**0.875**	**0.862**

CONCLUSION

The Emotion Net Challenges dataset shows that it is exceedingly difficult to recognise compound emotions, allowing considerable scope for improvement. Analysis and comparison of CFEP GAN approaches from the FG 2020 workshop have indeed been done. As may be predicted, some compounded emotions are more challenging to identify. For model verification in the experimental section of the paper, the Emotion Net Challenges dataset is used, and the performance is evaluated with RAF-DB and the iCV-MEFFD dataset. The RAF-DB dataset offers the best outcome.

REFERENCES

1. C. F. Benitez-Quiroz, R. Srinivasan, Q. Feng, Y. Wang, & A .M. Martinez. (2017). EmotioNet challenge: Recognition of facial expressions of emotion in the wild. *Available:* *Https://Arxiv.Org/Abs/1703.01210*.
2. A. Martinez, & S. Du. (2012). A model of the perception of facial expressions of emotion by humans: Research overview and perspectives. *J. Mach. Learn. Res., Vol. 13, No. 1, Pp. 1589–1608, Jan. 2012.*, *13*(1), 1589–1608.
3. L. Zhu, Y. Chen, P. Ghamisi, & J. A. Benediktsson. (2018). *Generative adversarial networks for h image classification*. *56*(9), 5046–5063.
4. A. Bellocchi. (2015). Methods for sociological inquiry on emotion in educational settings. *Emotion Rev.*, *7*(2), 151–156.

ICATP 2022, ISBN 978-81-952903-0-7

CHAPTER -12

ANALYSIS OF ISOTROPIC SQUARE PLATE WITH A HOLE

Singh, D K[1], Agarwal, P[2], Varshney, M[3] and Nath, S[4]
[1, 4]Amity University, Patna
[2]MUIT University, Lucknow
[3]NIT Patna
E-mail (erdeepak.india@gmail.com)

INTRODUCTION

Plate structure have been very popular structural member since decades. The analysis of such structures are very important to investigate due to the involvement of various kind of static and dynamic loads. The response of plate structure vary with the variation of load. In the present study, the plate with a hole at the centre having different hole dimensions has been analyse subjected to static and hydrostatic loads. A number of literature are available on the analysis of plate structures and some of the important are presented in the next paragraph to show the importance of this study.

Jain and Mittal (2008) investigated isotropic, orthotropic and laminated composite plates with hole at the centre subjected to transverse static load using finite element method. Kishore et al. (2017) investigated the frequencies of rectangular plate with central hole having different boundary conditions. Kim and Park (2020) presented a theory to carry out free vibration analysis of a composite laminated rectangular plate with holes using Ritz method. Zhou et al. (2021) studied the stress modal analysis of L-shaped thin plates with holes. Zang et al. (2022) investigated functionally graded plates for static and free vibration analyses using isogeometric method. Based on the studies carried out so far, the aim of the present study is to investigate clamped and simply supported plates with square and circular holes subjected to uniformly distributed load (UDL) of 1 kPa and hydrostatic load (HSL).

METHODOLOGY

ANSYS Workbench, a finite element software, has been used for carrying out the analysis. The plates are modelled based on the minimum thickness criteria specified in IS: 800 (1984), i.e., 6 mm. A square plate with a square and circular holes with 1000 mm width and variable thicknesses (6 mm, 7 mm, 8 mm, 9 mm, and 10 mm) for clamped and simply supported boundry conditions is considered in the analysis. The geometry of the plates are shown in Fig. 1. The value of b_s and b_c is considered as 500 mm.

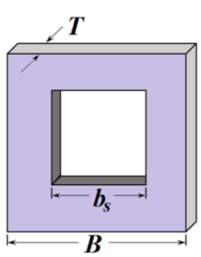

(a) Plate with square hole

B: width of plate,
T: thickness of plate,
b_s: width of square hole, and
b_c: width of circular hole

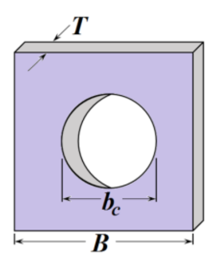

(b) Plate with square hole

Figure 1. Geometry of plates

RESULTS AND DISCUSSION

The results of maximum deflection and stress are evaluated on the plates with hole having different thicknesses for clamped and simply supported on all edges boundry conditions. The results of deflection and stress for clamped and simply supported edges are demonstrated in figures 2 and 3, respectively. The is dominance of HSL on deflection and stress can be observed easily from the figures, which is almost 4 times compared to UDL. Also, the values are more for plate with square hole.

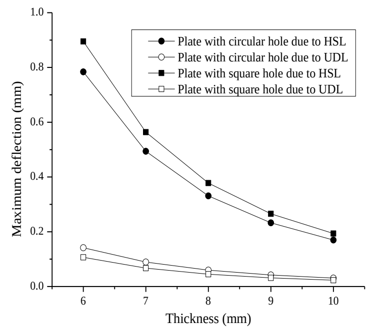

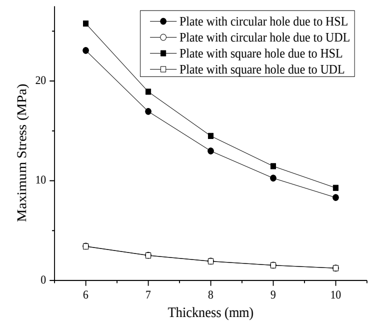

(a) Deflection **(b) Stress**

Figure 2. Clamped on all edges

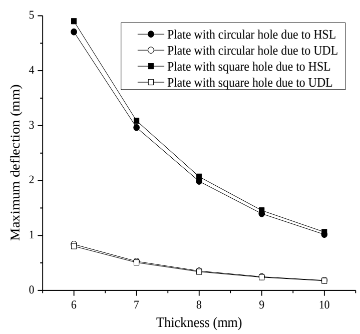

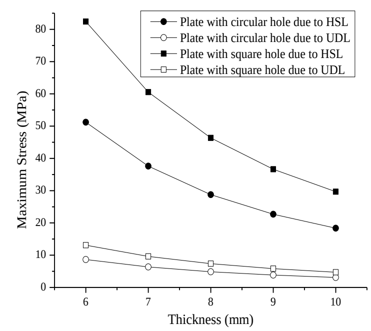

(a) Deflection **(b) Stress**

Figure 3. Simply supported on all edges

CONCLUSION

The following conclusions can be drawn from the present study:

1. The values of stress and deflection are more for simply supported plates compared to clamped plates.
2. The values are decreasing with the increment of the thickness of plate, and this is more significant when plates are subjected to HSL.
3. The difference in results are more when plates subjected to HSL. So, the investigation due to the influence of fluid is very important.

REFERENCES

IS: 800, General construction in steel - Code of practice, Bureau of Indian Standards, New Delhi, 1984.

ICATP 2022, ISBN 978-81-952903-0-7

Jain, N.K., Mittal, N.D. 2008. Finite element analysis for stress concentration and deflection in isotropic, orthotropic and laminated composite plates with central circular hole under transverse static loading. Mat. Sci. Eng.: A., 498: 115-124.

Kim, Y., Park, J. 2020. A theory for the free vibration of a laminated composite rectangular plate with holes in aerospace applications. Compos. Struct., 251: 112571.

Kishore, M.L.P., Bezawada, S., Reddy, B.C.R.K. 2017. Modal Analysis of Rectangular Plate with Central Hole Subjected to Various End Conditions. Mater. Today: Proc., 4: 1653-1661.

Zang, Q., Liu, J., Ye, W., Yang, F., Hao, C., Lin, G. 2022. Static and free vibration analyses of functionally graded plates based on an isogeometric scaled boundary finite element method. Compos. Struct., 288: 115398.

Zhou, Y., Zhang, Y., Zeng, W., Sun, Y. 2021. Fast modification-aimed stress modal analysis of thin plates with holes/notches. Eng. Struct. 238: 112248.

ICATP 2022, ISBN 978-81-952903-0-7

CHAPTERS-13

ACCURATE MAJORITY VERTEX COVERING NUMBER OF A GRAPH

I. Paulraj Jayasimman[1], T. Dhivya[2] and J. Joseline Manora[3]
[1,2] Department of Mathematics, AMET Deemed to be University, Kanathur, Chennai, India
[3]PG & Research Department of Mathematics, T.B.M.L College, Porayar, India Email
Email: [1] ipjayasimman@gmail.com

Abstract

A set of vertices $S \subseteq V(G)$ is a majority vertex cover if atleast half of the edges of G is incident with atleast one of the vertices in$S$. The majority vertex covering number $\alpha_{M(G)}$ of $G$is the minimum cardinality of majority vertex cover set$S$ of$G$. A majority vertex cover S of G is an accurate majority vertex cover if $V - S$ has no majority vertex cover of cardinality $|S|$. The accurate majority vertex covering number $\alpha_{aM(G)}$ is the minimum cardinality of an accurate majority vertex cover set of G . In this paper accurate majority vertex covering number obtained for complete, path, cycle, wheel, friendship graph, and bipartite graph. Also, $\alpha_{aM(G)}$ investigated for product of two graphs.

Keywords: Vertex covering number, Majority vertex covering number and accurate majority vertex cover number.

INTRODUCTION

In this article we use simple, undirected and non-trivial graphs. A set of vertices S which covers at least half of the edges is a majority vertex cover of G. The majority vertex covering number $\alpha_M(G)$ of G is the minimum number of vertices in a majority vertex cover. A majority vertex cover S of G is an accurate majority vertex cover if $V - S$ has no majority vertex cover of cardinality $|S|$. The accurate majority vertex covering number $\alpha_{aM(G)}$ is the minimum cardinality of an accurate majority vertex cover set of G

ACCURATE MAJORITY VERTEX COVERING NUMBER ($\alpha_M(G)$

Theorem 2.1: For any graph G is a path with n vertices the accurate majority vertex covering number $\alpha_{aM}(G)$is $\lceil\frac{n+1}{2}\rceil$.

Proof:

Let G be the path with $n \geq 3$vertices and $V(G) = \{v_1, v_2, v_3, \dots, v_n\}$, $|V(G)| = n$ and$|E(G)| = n - 1$. The maximum and minimum degree of G is $\Delta(G) = 2 \wedge \delta(G) = 1$ respectively. Let $S = \{v_1, v_2, v_3, v_4, \dots v_{\lceil\frac{n+1}{2}\rceil}\}$is a accurate majority vertex covering set and $\{v_1, v_2, v_3, v_4, \dots v_{\lceil\frac{n+1}{2}\rceil}\} \Longrightarrow |S| = \lceil\frac{n+1}{2}\rceil$, here $\lceil\frac{E(G)}{2}\rceil = \lceil\frac{n-1}{2}\rceil$ which is less then $\lceil\frac{n+1}{2}\rceil$. Therefore, S covers greater than $\lceil\frac{n}{2}\rceil$ edges. $|V - S| = n - \lceil\frac{n+1}{2}\rceil = \lfloor\frac{n-1}{2}\rfloor$. $|V - S| < S \vee$ Hence $\alpha_{aM}(G)$is $\lceil\frac{n}{2}\rceil + 1$.

Theorem 2.2: If the graph G is complete graph $K_m, m \geq 3$ then$\alpha_{aM}(G) = \lfloor\frac{p}{2}\rfloor + 1$.

Theorem 2.3: If a graph $G = K_{m,n}, m \leq n$ is complete bipartite graph then

$$\alpha_{aM}(G) = \begin{cases} n, if m < n \\ n+1, if m = n \end{cases}$$

Theorem 2.4: If any graph $G = C_n, n \geq 4$ is cycle graph then $\alpha_{aM}(G) = \lceil\frac{n-1}{2}\rceil + 1$

Conclusion :

In this article the accurate majority vertex covering number are determined for some classes of graphs such as path, cycle, complete, complete bipartite graph. Further finding the results for other standard graphs and product of two graphs. Also finding bounds for accurate majority vertex covering number of a graph.

REFERENCES

Basavanagoud B., Timmanaikar S (2018), "Further Results on Accurate Domination in Graphs", International Journal of Scientific Research in Mathematical and Statistical Sciences, Vol.5, Issue-6, December.

Cyman J., Henning M.A. and Topp J (2019), "On Accurate Domination in Graphs", Discussiones Mathematicae Graph Theory 39.

Harary F. ,(1969)., "Graph Theory", Addison-Wesley, Reading, Mass.

Haynes T.W., Hedetniemi S.T., and Slater P.J.(1998), "Fundamentals of Domination in Graphs", Marcel Dekker, New York,

Joseline Manora J. and Swaminathan V (2006), "Majority Dominating sets", J A R J; Vol.3, No.2, pp.75-82,.

Kulli V.R. (2010)., "Theory of Domination in graphs", Vishwa International Publications, Gulbagara, India.

Kulli V.R. and Kattimani M.B. (2012), "Accurate Domination in Graphs", In V.R.Kulli, ed., Advances in Domination Theory-I, Vishwa International Publications, Gulbagara, India.

Kulli V.R and Kattimani M.B (2013), "Global Accurate Domination in Graphs", Int. J.Sci. Res. Pub. 3, 1-3

Nordhaus E.A. and. Gaddum J.W, (1956) "On Complementary Graphs", Amer. Math. Monthly 63, 175-177.

ICATP 2022, ISBN 978-81-952903-0-7

CHAPTER -14

ACCURATE MAJORITY DOMINATION IN GRAPHS

T. Dhivya, A[1], I. Paulraj Jayasimman,B[2], and J. Joseline Manora, C[3]
[1]Assistant Professor, Department of Mathematics
AMET Deemed to be University, Kanathur, Chennai, India
[2]Associate Professor, Department of Mathematics
AMET Deemed to be University, Kanathur, Chennai, India
[3]PG & Research Department of Mathematics, T.B.M.L College, Porayar, India

E-mail (dhivyasmile94@gmail.com)

ABSTRACT

A Majority dominating set D_M of a graph $G = (V, E)$ is an majority accurate dominating set(MAD), if $V - D_M$ has no majority dominating set of cardinality $|D_M|$. The accurate majority domination number $\gamma_{am}(G)$ is the minimum cardinality of an accurate majority dominating set. In this paper introduced new parameter accurate majority domination number and also determined the accurate majority domination number for cycle and complete bipartite graphs.

KEYWORDS: Domination number, Majority domination number, Accurate domination number

INTRODUCTION

Definition 2 [1]

A set $S \subseteq V(G)$ is called a majority dominating set if atleast half of the vertices either in S or adjacent to the vertices S. The minimum cardinality of a majority dominating set is called majority domination number $\gamma_M(G)$.

Definition 3 [3]

A dominating set D of a graph $G = (V, E)$ is an accurate dominating set, if $V - D$ has no dominating set of cardinality $|D|$. The accurate majority domination number $\gamma_\propto(G)$ is the minimum cardinality of an accurate dominating set.

METHOD

A Majority dominating set D_M of a graph $G = (V, E)$ is an majority accurate dominating set, if $V - D_M$ has no majority dominating set of cardinality $|D_M|$. The accurate majority domination number $\gamma_{am}(G)$ is the minimum cardinality of an accurate majority dominating set

RESULTS

Theorem 1

For the graph $= C_p$, $\gamma_{am}(G) = \left\lceil \frac{p}{2} \right\rceil - 3$.

Proof

Let $D_M = \left\{v_1, v_2, \dots, v_{\left\lceil \frac{p}{2} \right\rceil - 3}\right\}$ be the majority accurate dominating set. The set D_M covers $\geq \left\lceil \frac{p}{2} \right\rceil$ vertices. Therefore $\gamma_{am}(G) = \left\lceil \frac{p}{2} \right\rceil - 3$.

Theorem 2

If the graph $G = K_{m,n}$, $m < n$ then

$$\gamma_{am}(G) = \begin{cases} \left\lceil \frac{n}{2} \right\rceil + 3\left\lceil \frac{m}{2} \right\rceil & if \;\; n \;\; is\ odd \\ \left\lceil \frac{n}{2} \right\rceil + \left(3\left\lceil \frac{m}{2} \right\rceil + 1\right) & if \;\; n \;\; is \;\; even \end{cases}$$

Proof

Let $G = K_{m,n}$ be the vertex set $V(G) \subseteq (V_1(G), V_2(G))$.

$V_1(G) = \{a_1, a_2, a_3, \dots, a_m\}$ & $V_2(G) = \{b_1, b_2, b_3, \dots, b_n\}$.

Case (i) $\boldsymbol{n \;\; is\ odd}$

Let $D_M = \left\{a_1, a_2, a_3, \dots, a_{3\left\lceil \frac{m}{2} \right\rceil}, b_1, b_2, b_3, \dots, b_{\left\lceil \frac{n}{2} \right\rceil}\right\}$ be the accurate majority dominating set. The set D_M covers $\geq \left\lceil \frac{p}{2} \right\rceil$ vertices. Therefore $\gamma_{am}(G) = \left\lceil \frac{n}{2} \right\rceil + 3\left\lceil \frac{m}{2} \right\rceil$.

Case (ii) $\boldsymbol{n \;\; is\ even}$

Let $D_M = \left\{a_1, a_2, a_3, \dots, a_{3\left\lceil \frac{m}{2} \right\rceil + 1}, b_1, b_2, b_3, \dots, b_{\left\lceil \frac{n}{2} \right\rceil}\right\}$ be the accurate majority dominating set. The set D_M covers $\geq \left\lceil \frac{p}{2} \right\rceil$ vertices. Therefore $\gamma_{am}(G) = \left\lceil \frac{n}{2} \right\rceil + \left(3\left\lceil \frac{m}{2} \right\rceil + 1\right)$.

CONCLUSION

The researcher has introduced the new parameter accurate majority domination of a graph and also accurate majority domination number determined for cycle and complete bipartite graph.

ACKNOWLEDGMENT

The authors wish to thank AMET Deemed to be university for its support and encouragement.

REFERENCES

[1] Joseline Manora, J and Swaminathan, V. 2006. Majority Dominating Sets.*J A R J*.3(2) :75-82.

[2] Kulli, V.R and Sigarkanti, S.C. 1991. Inverse Domination in Graphs. Nat.Acad.Sci.Lett. 14:473-475.

[3] Kulli, V.R and Kattimani, M.B. 2012. Accurate Domination in Graphs. Advances in Graph Theory, I. 1-8.

[3] Kulli, V.R and Janakiram, B. 1997. The Maximal Domination Number of a Graph. Graph Theory Notes of New York Academy of Sciences. 33: 11-13.

[4] Kulli, V.R. and Soner, N.D.1997. Complementary Edge Domination in Graphs. *Indian* J.Pure Appl.Math.28:917-920.

[5] Kulli, V.R and Kattimani, M.B. 2000. A note on Maximal Domination Number of a Graph. Graph Theory Notes of New York Academy of Sciences. 39: 35-36.

CHAPTER -15

Effects Of Dust Particles On Dust Acoustic Solitary Waves (DASWs) Propagating In Inhomogeneous Magnetized Dusty Plasmas (MDPs) With Dust Charge Fluctuations

Hirak Jyoti Dehingia[1], and P. N. Deka[2]
Department of Mathematics, Dibrugarh University, Assam, India
hirakjyotidehingia11@gmail.com (corresponding author)

INTRODUCTION

Dusty plasmas (DPs) are one of the fundamental ingredients of the universe. It is a mixture of plasma particles and dust charges. DP consists of plasma and both dust. Due to the inclusion of dust particles in plasma, the plasma becomes more complex in its behaviors. So, such plasmas are also termed as "complex plasmas." DP plays a very significant role in space and astrophysical environments and during the modifications of plasma processing. Nishida (1984), Rao (1990), and Lakshmi (1994), have observed that the modifications in plasma processing occur due to the existence of dust particles in the plasma system. Dorranian (2012) has also observed that solitary waves are formed due to the balance in nonlinearity and dispersion effects in the plasma system. Malik (2013), Merlino (2014), and Emamuddin *et al.* (2014) have studied DASW in various physical situations. Some authors have studied DASW in the presence of isothermal electrons and ions with Boltzmannean distribution and negatively charged dust grains. Malik *et al.* (1998) studied DASWs and the effect of the magnetic field in inhomogeneous plasma associated with negative potential and in the presence of ions, electrons, and charged dust particles. Recently, Pakzad *et al.* (2022) have investigated the properties of DASW associated with negatively charged dust, ions, and superthermal electrons for inhomogeneous unmagnetized plasmas. In this paper, we have studied the effect of dust grains in DASWs propagating in weakly inhomogeneous MDP.

GOVERNING EQUATIONS, DERIVATION OF m-ZK EQUATION

In this problem, we have considered a MDP constituting of ions, electrons, and dust grains with charge fluctuations. We have considered the following set of nonlinear governing equations to represent our plasma model is as follows:

$$\frac{\partial n_d}{\partial t} + \vec{\nabla}.(n_d \vec{v}_d) = 0 \tag{1}$$

$$\frac{\partial \vec{v}_d}{\partial t} + (\vec{v}_d.\vec{\nabla})\vec{v}_d = \gamma \vec{\nabla}\phi - \delta(\vec{v}_d \times B_0 \vec{x}) = 0 \tag{2}$$

$$\nabla^2 \phi - n_e - q n_d + n_i = 0 \tag{3}$$

$$n_e = n_{e0} e^{\alpha k \phi} \tag{4}$$

$$n_i = n_{i0} e^{-\alpha \phi} \tag{5}$$

To study the effect of dust charges on DASWs propagating in inhomogeneous plasmas, we have considered the following appropriate stretched coordinates to employ the Reductive Perturbation Theory (RPT) as follows:

$$\xi = \epsilon^{\frac{1}{2}}(x - Mt),\ \eta = \epsilon^{\frac{1}{2}} y,\ \lambda = \epsilon^{\frac{1}{2}} z,\ \tau = \epsilon^{\frac{3}{2}} x \tag{6}$$

Using the RPT and the appropriate stretched coordinate's eq.(6), we have obtained the modified Zakharov Kuznetsov (m-ZK) equation as follows:

$$\frac{\partial \phi_1}{\partial \tau} + P\phi_1 \frac{\partial \phi_1}{\partial \xi} + Q \frac{\partial^3 \phi_1}{\partial \xi^3} + R \frac{\partial S \phi_1}{\partial \xi} = 0 \tag{7}$$

ICATP 2022, ISBN 978-81-952903-0-7

The above eq. (7) is the m-ZK equation. The solution of the m-ZK equation indicates the solutions for the DAWs in weakly inhomogeneous MDPs. The solitary wave solution indicates the effects of the various parameters on the DAWs.

$$\Rightarrow \phi_1 = A_m\, sech^2 \beta A \tag{8}$$

Where the terms $A, B, P, Q, R, S, T, X, \beta, A_m, W$ have their usual meaning. The term A_m , W represents amplitude and width of the DASW represented by eq. (8) .

RESULTS AND DISCUSSION

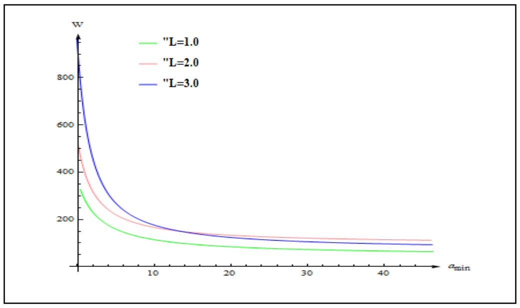

Figure 1. A_m vs $a_{(\min)}$ plot for $L = 1,2,3$

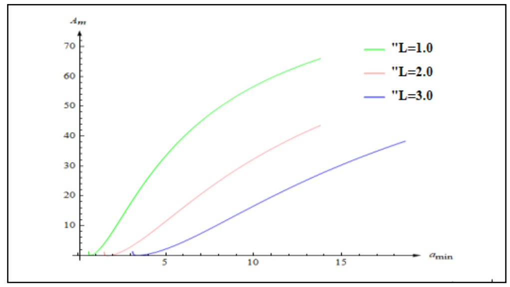

Figure 2. W vs $a_{(\min)}$ plot for $L = 1,2,3$

The amplitude A_m and width W of DASW varies with the various choices of the parameters L, k, r and $a_{(\min)}$. We have obtained the numerical results to describe the dependency of both A_m and W on the above parameters. Here, we have presented only two figures to illustrate the amplitude and width of DASW. More figures can be drawn to describe the effects of dust on the amplitude and width of the solitary waves. Here both the figures indicate how A_m and W of DASW increase/decrease with the increase of various choices of L. But for a specific value of L, the amplitude/width of the DASW decreases/ increases with increase in dust size $a_{(\min)}$.

CONCLUSION

In this manuscript, we have studied the effect of dust grains in DASWs propagating in weakly inhomogeneous MDPs. We have considered a system of MDP in the presence of ions, electrons, and dust charges with charge fluctuations. Here, the RPT is applied to obtain the m-ZK equation. The solution of the m-ZK equation describes the effects of dust charges on the various choice parameters for the DASWs in weakly inhomogeneous magnetized plasmas. It is clear from both Fig. 1 and Fig. 2 that the positive values of $a_{(\min)}$ the DASW will produce rarefactive solitons. Here, both A_m and W depend on the angle of wave propagations, magnitude, and direction of the external magnetic fields (MFs). Thus, we can conclude that MF and dust grains significantly impact describing the characteristics of DASWs.

REFERENCES

1. Nishida Y, Nagasawa T. Excitation of ion-acoustic rarefactive solitons in a two-electron-temperature plasma. Phys Fluids. 1986; 29:345.
2. Rao NN, Shukla PK, Yu MY. Dust-acoustic waves in dusty plasmas. Planet Space Sci. 1990; 38:543–546.
3. Lakshmi SV, Bharuthram R. Arbitrary amplitude rarefactive dust-acoustic solitons. Planet. Space Sci. 1994; 42: 875–881.
4. Dorranian D, Sabetkar A. Dust acoustic solitary waves in a dusty plasma with two kinds of nonthermal ions at different temperatures. Phys Plasmas. 2012; 19:013702.
5. Malik R, Malik HK. Compressive solitons in a moving e-p plasma under the effect of dust grains and an external magnetic field. J Theory Appl. Phys. 2013; 7:65.
6. Merlino RL. 25 years of dust acoustic waves. J Plasma Phys. 2014; 80:773–786.
7. Emamuddin M, Masud MM, Mamun AA. Dust-acoustic solitary waves in a magnetized dusty plasmas with nonthermal ions and two-temperature nonextensive electrons. Astrophys Space Sci. 2014; 349:821–828.

8. Malik HK, Tripathi KD, Sharma SK. Dust acoustic solitons in a magnetized dusty plasma. J Plasma Phys. 1998; 60:265–273.
9. H.R. Pakzad, and D. Nobahar, Dust-ion acoustic solitons in superthermal dusty plasmas, New Astronomy, 2022, 93:10175.

ICATP 2022, ISBN 978-81-952903-0-7

CHAPTER -16

NANOFLUID FROM A HEATED VERTICAL PLATE IN SLIP CONDITION

Papri Bhattacharjee[1],
[1] Department of Mathematics, Gauhati University, Assam-781014, India
E-mail: papri201514@gmail.com

INTRODUCTION

This paper presented the analytical study of a two-dimensional constant unidirectional incompressible flow of a nanofluid across a vertical flat plate that has been convectively heated for different slip conditions. Before being solved numerically, the governing equations are non-dimensionalized and transformed into a two-point boundary value problem with linked nonlinear ODE in similarity variables. Numerical Runge-Kutta-Fehlberg 4th–5th order algorithms have been used to solve the resulting equations with the corresponding boundary conditions. So according to our analysis, if the convective heat transfer coefficient is directly proportional to x-1/4, where x is the axial distance from the plate's leading edge, the problem can be solved. In the figures, the effects of parameters like momentum slip and convective heat transfer have been shown and discussed. The study has a solid argument due to comparisons between the current numerical solution and the achieved results. The data for various values of the convective heat transfer parameters are presented in tabular form for the skin friction factor, reduced Nusselt number, and reduced Sherwood number.

METHODOLOGY

We analyse the flow of a nanofluid in a two-dimensional laminar boundary layer over a solid, vertical flat plate that has undergone convective heating. By convection from a hot fluid at a temperature $T_f(\bar{x})$ that provides a heat transfer coefficient $h_f(\bar{x})$, the left surface of the plate is heated. The temperature of the right surface of the plate is T_w . The nanoparticle fraction at the wall is C_∞. The field variables are the velocity vector $\bar{v}$, the temperature T and, the nanoparticle volume fraction is C. It is assumed that $T_f > T_w > T_\infty$ and all the physical properties are constant except the density in the body force term in the momentum equation. The four field equations are stated in terms of dimensional forms and the Oberbeck-Boussinesq approximation is used. [Kuznetsova & Nield (2010)]

$$\bar{\nabla}.\bar{v} = 0 \qquad (1)$$

$$\rho_{nf}\left(\frac{\partial \bar{v}}{\partial \bar{t}} + \bar{v}\bar{\nabla}\bar{v}\right) = -\bar{\nabla}p + \mu_{nf}\bar{\nabla}^2\bar{v} + \left[C\rho_p + (1-C)\left\{\rho_{nf}\left(1-\beta(T-T_\infty)\right)\right\}\right]g \qquad (2)$$

$$\left(\rho C_p\right)_{nf}\left(\frac{\partial T}{\partial \bar{t}} + \bar{v}\bar{\nabla}T\right) = k_{nf}\nabla^2 T + \left(\rho C_p\right)_p\left[D_B\nabla C.\nabla T + \left(\frac{D_T}{T_\infty}\right)\nabla T.\nabla T\right] \qquad (3)$$

$$\frac{\partial C}{\partial \bar{t}} + \bar{v}\bar{\nabla}C = D_B\bar{\nabla}^2 C + \frac{D_T}{T_\infty}\bar{\nabla}^2 T \qquad (4)$$

We can linearize the momentum equation and write equ (2) as long as the nanoparticle concentration is adequately diluted and the reference pressure is selected appropriately. [Kandasamy et.al. (2011)] Then neglect the small order terms. On introducing dimensionless variables with suitable similarity transformations of governing equation to a coupled non-linear ODEs with boundary conditions.

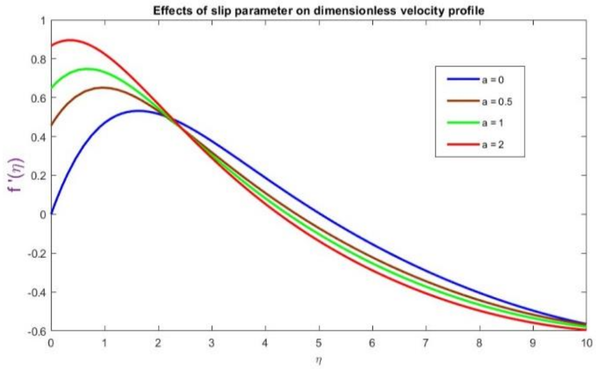

RESULTS AND DISCUSSION

Figure 1 shows the impact of linear momentum slip on the dimensionally-invariant horizontal velocity profiles. Slip, it has been observed, causes the velocity to rise close to the plate and decrease away from it. Once again, as slip parameter increases, there is less penetration through the fluid domain, which reduces the hydrodynamic boundary layer.

CONCLUSION

With an increase in the momentum slip parameter, the temperature, the dimensionless axial velocity, and the volume fraction of nanoparticles all decrease. Convective heat transfer parameter raises the skin friction factor, reduced Nusselt and Sherwood number, and skin friction decreases with slip parameter and reduced Sherwood number decreases with thermophoresis parameter. On the graphs, it is easy to see how numerous dimensionless values vary in relation to the momentum slip parameter and convective heat transfer parameter.

ACKNOWLEDGMENT

Author thanks the Almighty, reviewers and Prof. Shyamanta Chakraborty

REFERENCES

1. Abdul Aziz, 2010. Hydrodynamic and thermal slip flow boundary layers over a flat plate with constant heat flux boundary condition, Commun Nonlinear Sci Numer Simulat, Elsevier, 15(2010), 573-580. https://doi.org/10.1016/j.cnsns.2009.04.026
2. MD.J. Uddin, I. Pop and A.I.MD. Ismail, 2012. Free convection boundary layer flow of a nanofluid from a convectively heated vertical plate with linear momentum slip boundary condition, Sains Malaysiana, 41(11) (2012):1475-1482
3. Kandasamy, R., Loganathan, P. and Puvi Arasu, P. 2011. Scaling group transformation for MHD boundary layer flow of a nanofluid past a vertical stretching surface in the presence of suction/injection, Nuclear Engineering and Design, 241(6):2053-2059.
4. Kuznetsov, A.V. and Nield, D.A. 2010a. Natural convective boundary layer flow of a nanofluid past a vertical plate. International Journal of Thermal Science, 49:243-247.
5. Sohail Nadeem, Salman Akhtar, Nadeem Abbas, 2020. Heat transfer of Maxwell base fluid flow of nanomaterial with MHD over a vertical moving surface, Alexandria Engineering Journal, Elsevier, (2020)59, 1847-1856. https://doi.org/10.1016/j.aej.2020.05.008

CHAPTER -17

STUDY OF MIXED CONVECTION FLOW OF HYBRID NANOFLUID WITHIN A NON-DARCY POROUS MEDIUM

[1]Snehalata Jena, [2]Manoj Kumar Mishra
[1]Vellore Institute of Technology, Amaravati, Andhra Pradesh
[2]Vellore Institute of Technology, Amaravati, Andhra Pradesh
E-mail: manoj.m@vitap.ac.in

ABSTRACT

In the present research paper, the mixed convection flow of a hybrid nanofluid within a non-Darcy porous medium is numerically investigated. The governing partial differential equations derived from the flow situation are transformed into an ordinary differential equation using some suitable similarity variable. Then the non-dimensional ordinary differential equations are solved by using MATLAB inbuilt software package BVP4C. The effect of various flow controlling parameters like the non-Darcy porous parameter and mixed convection parameter on the flow field is displayed graphically. The quantity of physical interest like the Nusselt number and the skin friction coefficients are represented in tabular form. The investigation revealed that the velocity of hybrid nanofluid increase with the rise of non-Darcy porous parameters, But the temperature profile decreases with the increase of non-Darcy porous parameters, and increases with the rise of mixed convection parameter.

CHAPTER -18

STARTING FLOW OF TWO IMMISCIBLE FLUIDS IN A POROUS SPACED CHANNEL WITH MAGNETIC FIELD

Komal Goyal, Suripeddi Srinivas

Department of Mathematics, School of Advanced Sciences,
VIT-AP University, Inavolu, Vijayawada, 522237, India.

Email: srinusuripeddi@hotmail.com, komal.21phd7085@vitap.ac.in

Abstract

This study is concerned with starting flow of immiscible fluids in porous space owing to a rapid pressure differential in the presence of a transverse magnetic field. The flow is divided into two regions, region1(upper layer) and region2(lower layer) and they are of variable widths. The required eigenvalues and eigenfunctions, along with the orthogonality, are developed. The analytic solution took on an infinite series structure due to the time-dependent initial transient component of the velocity. Analytical expressions for fluid velocity, volumetric flow rate, and shear stress are evaluated for pertinent parameters. We take cases when channels are filled with air over water and oil over water for analyzing the results. Channel with air over water illustrates that the upper layer is filled with air and the lower layer is filled with water. Similarly, a channel with oil over water illustrates that the upper layer is filled with oil and the lower layer is filled with water. The effect of hartmann number and time on velocity profiles has been seen in this study for variable fluid widths in both cases. It is observed that the starting flow velocity slows down with the increase of the hartmann number and porosity parameter. The effect of hartmann number and porosity parameter on volumetric flow rate, for oil over water case, are shown graphically. Shear stress on the lower and upper walls of the channel has been presented in the tabular form.

CHAPTER -19

THERMAL NON-EQUILIBRIUM EFFECTS DUE TO COMBUSTION ON DARCY-BÉNARD CONVECTION

Reena Nandal, P. G. Siddheshwar
Centre for Mathematical Needs, Department of Mathematics,
Christ (Deemed to be University), Bengaluru - 560029, INDIA
E-mail: reena.nandal@christuniversity.in

INTRODUCTION

The problem of convection in the presence of combustion has been studied for different media and boundary conditions and is a well documented problem in the literature (Frank-Kamenetskii (1938), Gatica et al. (1987), Malashetty et al. (1994), Belk and Volpert (2004)). Many studies assumed that the reacting fluid and the porous matrix are in thermal equilibrium. Continuous reaction processes create a significant temperature gradient between the porous matrix and the fluid in it and the local thermal equilibrium cannot be a valid assumption. In view of this, in this paper, we focus on chemical reaction-driven convection in a porous medium with LTNE undergoing combustion in a way that the energy equation subscribes to the Frank-Kamenetskii formulation.

MATERIALS AND METHODS

The dimensionless form of the governing equations and boundary conditions considered are:

$$\nabla \cdot \mathbf{q} = 0, \tag{1}$$

$$\mathbf{q} = -\nabla P + \left(\frac{Kd\left(\rho c\right)_f \rho_0}{\varepsilon k_f \mu_f} g - Ra_D^{FK} \theta \right) \hat{k}, \tag{2}$$

$$\frac{\partial \theta}{\partial t} + \left(\mathbf{q} \cdot \nabla\right)\theta = \nabla^2 \theta - H\left(\theta - \phi\right) + FK \exp\left(\theta\right), \tag{3}$$

$$\Lambda \frac{\partial \phi}{\partial t} = \nabla^2 \phi + H\left(\theta - \phi\right). \tag{4}$$

$$\mathbf{q} = \theta = \phi = 0 \qquad at \qquad z = 0,1. \tag{5}$$

Methodology: The boundary condition in so far as z is considered is the periodic one pertaining to longitudinal rolls. Normal mode analysis is used obtain the critical Frank-Kamenetskii-Darcy-Rayleigh number$\left(Ra_{Dc}^{FK}\right)$. The following BEVP is obtained from the analysis:

$$\left(4D^2 - a^2\right)W + a^2 \sqrt{Ra_D^{FK}}\, \Theta = 0, \tag{6}$$

$$\sqrt{Ra_D^{FK}}\, D\theta_b W + \left(4D^2 - a^2\right)\Theta - H\left(\Theta - \Phi\right) + FK \exp\left(\theta_b\right)\Theta = 0, \tag{7}$$

$$\left(4D^2 - a^2\right)\Phi + H\gamma\left(\Theta - \Phi\right) = 0. \tag{8}$$

$$W = \Theta = \Phi = 0 \qquad at \qquad z = -1,1. \tag{9}$$

RESULTS AND DISCUSSION

We commence our discussion with plots of the basic state temperature profiles of the solid and fluid phases, θ_b and ϕ_b, versus z for different values of FK (Frank-Kamenetskii number) and fixed values of other parameters. From the figure 1, it is clear that even for small values of FK the two temperature profiles, θ_b and ϕ_b, cannot be the same. The presence of a chemical reacting fluid in the porous medium creates a local thermal non-equilibrium within the system, and one cannot reach LTE limits, and with an increase in value of FK.

Variation of Ra_{Dc}^{FK} with H for $FK = 0.1, 1$ and for different values of porosity-modified conductivity ratio (γ) is presented in figure 2. An increase in the value of FK leads to advanced-onset of convection.

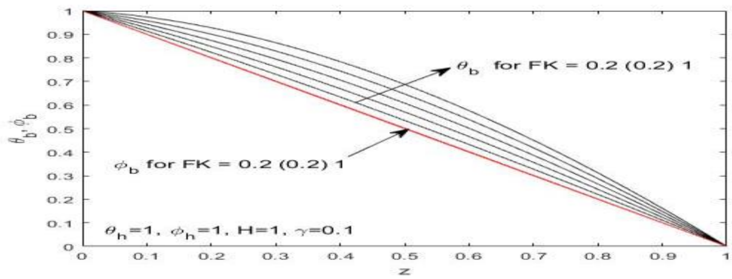

Figure 2 Basic temperature profiles of ϕ_b and θ_b for different values of FK.

Figure 2 also shows that as the inter-phase heat transfer parameter (H) approaches large values, leads to delayed convection. In the case of increasing values of γ, we see accelerated convection (see figure 3). From Figures 2 and 3, one further observe that the curves for Ra_{Dc}^{FK} with H and γ are plotted up to a specific value of H and γ. This is because the system shows extreme behavior in terms of Ra_{Dc}^{FK}, beyond a particular value of H and γ and nothing much can be said about the system stability.

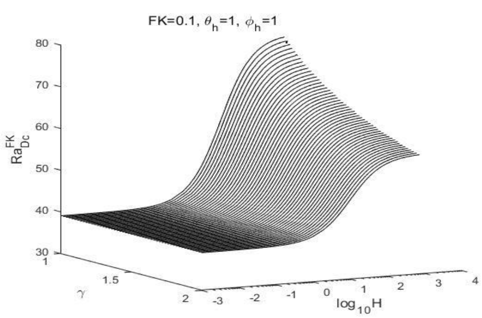

Figure 2: Variation in Ra_{Dc}^{FK} with $\log_{10} H$ and γ.

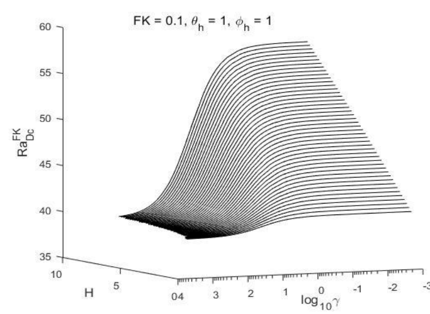

Figure 3: Variation in Ra_{Dc}^{FK} with $\log_{10} \gamma$ and H.

CONCLUSION

Based on the obtained results, we conclude that a chemically reacting fluid leads to an LTNE situation in the basic state, and one cannot approach the LTE from it. The increase in the value of the Frank-Kamenetskii number and porosity-modified conductivity ratio leads to advanced-convection while an increase in the value of the inter-phase heat transfer parameter delayed convection.

REFERENCES

1. Belk M., and Volpert, V. 2004. Modeling of heat explosion with convection. Chaos, 14, 263–273.
2. Frank-Kamenetskii, D.A. 1938. Towards temperature distributions in a reaction vessel and the stationary theory of thermal explosion. Doklady Akademii Nauk SSSR. 18.
3. Gatica, J.E., Viljoen, H., and Hlavacek, V. 1987. Stability analysis of chemical reaction and free convection in porous media. Int. Commun. Heat Mass Transfer 14, 391–403.
4. Malashetty, M.S., Cheng, P., and Chao, B.H. 1994. Convective instability in a horizontal porous layer saturated with a chemically reacting fluid, Int. J. Heat Mass Transf., 37, 2901-2908.

CHAPTER -20

ONSET OF MAXWELL-CATTANEO DOUBLE DIFFUSIVE CONVECTION IN ROTATING FLUID SATURATED ANISOTROPIC POROUS LAYER

Atul K. Srivastava[1], Monal Bharty[2] and Hrishikesh Mahato[3]

[1,2,3]Department of Mathematics, School of Natural Sciences, Central University of Jharkhand, Ranchi, Jharkhand, 825305, India.

†Corresponding Author Email: priyabharty58@gmail.com

INTRODUCTION

The onset of Maxwell-Cattaneo double diffusive convection in an infinite horizontal anisotropic porous layer under rotation effect is examined in limiting cases. Evaluation of temperature and salinity is regulated by parabolic advection diffusion equation, which assumes classical fickian diffusion for both heat and salt. The stability criteria for rotation effect on Maxwell-Cattaneo double diffusive convection is studied using linear stability analysis. Critical Rayleigh number is calculated for for both stationary and oscillatory convection. For oscillatory convection two cases has been discussed. (1) Maxwell-Cattaneo coefficient for salinity (C_S)=0. (2) Maxwell-Cattaneo coefficient for temperature (C_T)=0. In both the cases, C_S=0 without rotation and C_T=0 without rotation , the impact of C_T, C_S, mechanical anisotropic parameter (ξ) and solutal Rayleigh number (Ra_S) are also presented in detail in the manuscript. The effect of C_T (when C_S=0) and C_S(when C_T=0) is presented graphically on (a, Ra_T) plane where a is horizontal wave number. We have focused on the scenario where C_T and C_S is less than equals to 1.

MATERIALS AND METHODS

We consider double-diffusive convection in a horizontal porous layer of an incompressible Maxwell-Cattaneo fluid with the influence of rotation effect confined between two parallel horizontal plane. The origin is picked in the lower boundary of a Cartesian frame of reference. To account for the influence of density fluctuation, the oberbeck-boussinesq approximation is used. The stability criteria for rotation effect on Maxwell-Cattaneo double diffusive convection is studied using linear stability analysis.

RESULTS AND DISCUSSION

The impact of C_T (when C_S=0) on the system's stability in depicted in Fig 1. With a rise in C_T, the minimum of Rayleigh number (Ra_S) drops, suggesting that the influence of C_T is to make the system unstable. The fact that C_T is directly proportional to thermal diffusivity explains it.

The impact of C_S on the system's stability is depicted in Fig 2. The minimum of Rayleigh number decreases with increase in C_S (when C_T=0), indicating that increasing C_S undermines stability of the system. Since C_S is directly proportional to salutal diffusivity, a drop in bouyancy indicates a decrease in Rayleigh number, hence an increase in solutal diffusivity predicts a fall in Rayleigh number.

ICATP 2022, ISBN 978-81-952903-0-7

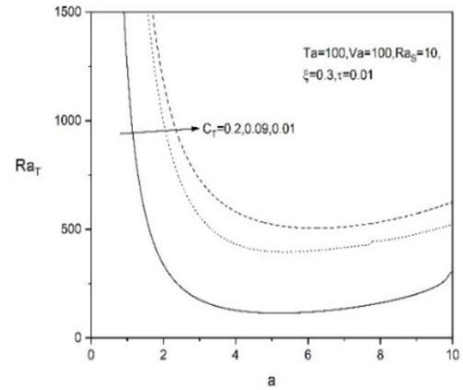

Fig 1: **Oscillatory Neutral curve for different values of C_T when C_S=0.**

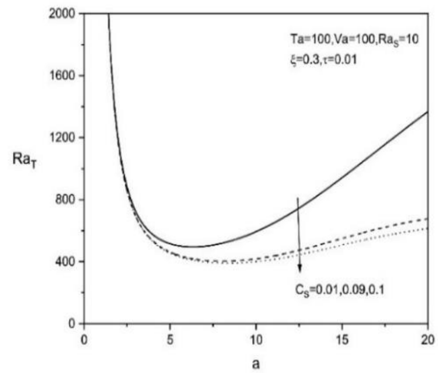

Fig 2: Oscillatory Neutral curve for different values of C_S when C_T=0

CONCLUSION

Using linear stability analysis, we attempted to investigate the stability criteria for rotation effect on Maxwell-Cattaneo double diffusive convection.

- For oscillatory convection, the onset criterion has been calculated analytically.
- On increasing the value of C_T (when C_S=0) and C_S (when C_T=0) Rayleigh number drops to its minimum, thus it advances the onset of oscillatory convection. It is because both C_T and C_S is proportional to thermal and solutal diffusivity respectively.

ACKNOWLEDGMENT

Author Monal Bharty, sincerely thanks Central University of Jharkhand for providing financial support in the form of a research fellowship.

REFERENCES

Barletta A, Zanchini E. 1997. Unsteady heat conduction by internal-energy waves in solids. Phys. Rev. B ; 55: 14208-14213.

Chandrasekhar, S. 1953. The instability of a layer of fluid heated below and subject to Coriolis forces, Proc. R. Soc. A; 217: 306-327.

Hughes D.W., Proctor M.R.E and Eltayeb I.A. 2021. Maxwell–Cattaneo double-diffusive convection: limiting cases. J. Fluid Mech ; vol. 927.

Malashetty M.S., and Heera R. 2007. The Effect of Rotation on the Onset of Double Diffusive Convection in a Horizontal Anisotropic Porous Layer. Transp. Porous Media; 74(1): 105-127.

DOUBLE-DIFFUSIVE CONVECTION IN DARCY POROUS LAYER UNDER INCLINED TEMPERATURE GRADIENT INCORPORATING THE SORET EFFECT

Kapil Dev, Om P Suthar
Department of Mathematics, Malaviya National Institute of Technology, Jaipur-302017, Rajasthan, India
E-Mail- 2019rma9046@mnit.ac.in

A horizontal component may exist along with the vertical temperature gradient in a physical problem. Convective instability in a porous medium saturated by a fluid due to an inclined temperature gradient is relevant in studying geothermal activities, gas reservoirs, underground transport of pollutants, and crystal growth, as reported by Manole and Lage [2]. Heat capacities constituting the earth's crust and sedimentary materials of different permeabilities cause non-uniform heating of the lower layers resulting in horizontal and vertical temperature gradients. Firstly, Weber [3] studied the convection problem in a porous medium with an inclined temperature gradient. This paper investigates the Soret effect and the effect of an inclined temperature gradient on double-diffusive convective motion in a horizontal Darcy porous layer. Under the appropriate assumptions, the governing equations for the perturbation quantities may be written as

$$\nabla \cdot \boldsymbol{q} = 0, \tag{1}$$

$$0 = -\nabla p - \boldsymbol{q} - RsC\hat{\boldsymbol{e}}_{\boldsymbol{z}} + Ra\theta\hat{\boldsymbol{e}}_{\boldsymbol{z}}, \tag{2}$$

$$\frac{\partial\theta}{\partial t} - \frac{R_H}{Ra}u + U(z)\frac{\partial\theta}{\partial x} + \frac{dF}{dz}w + (\boldsymbol{q}\cdot\nabla)\theta = \nabla^2\theta, \tag{3}$$

$$\frac{\epsilon}{\zeta}\frac{\partial C}{\partial t} + \left(U(z)\frac{\partial C}{\partial x} + \frac{dC_b}{dz}w + (\boldsymbol{q}\cdot\nabla)C\right) = \frac{1}{Le}\nabla^2 C + Sr\nabla^2\theta, \tag{4}$$

subject to the boundary conditions

$$w = 0, \quad \theta = 0, \quad C = 0 \quad \text{at} \quad z = 0, \quad 1, \tag{5}$$

where, the steady solution of the problem is $U(z) = R_H\left(z - \frac{1}{2}\right)$, $F(z) = 1 - z + \frac{R_H^2(1-z)z(1-2z)}{12Ra}$, $C_b(z) = z + \frac{LeR_H^2Sr(1-z)z(1-2z)}{12Ra}$. The above system of equations has the concentration, vertical thermal Rayleigh numbers, Lewis number, Soret coefficient and the horizontal component of thermal Rayleigh number defined respectively as:

$$Rs = \frac{\rho_0\beta_C gKd\Delta C}{\mu\alpha_m}, \quad Ra = \frac{\rho_0 g\beta_T Kd\Delta T}{\mu\alpha_m}, \quad Le = \frac{\alpha_m}{D}, \quad Sr = \frac{D_T\Delta T}{\alpha_m\Delta C}, \quad R_H = \frac{\rho_0 g\beta_T Kd^2\beta}{\mu\alpha_m}.$$

Following the normal mode analysis, linearized governing equations from Eqns (1)-(4) are

$$-(D^2 - a^2)W + a^2 Rs\Phi - a^2 Ra\Theta = 0, \tag{6}$$

$$(D^2 - a^2 - ia_xU - \omega)\Theta - WDF + \frac{ia_xR_H}{a^2Ra}DW = 0, \tag{7}$$

$$\left(\frac{1}{Le}(D^2 - a^2) - \frac{\epsilon}{\zeta}\omega\right)\Phi + Sr(D^2 - a^2)\Theta - (ia_xU\Phi + WDC_b) = 0, \tag{8}$$

subject to the boundary conditions $W = 0$, $\Theta = 0$, $\Phi = 0$ at $z = 0,1$. Using the Galerkin method, the above six-order system has been solved to obtain the Rayleigh number as an eigenvalue. We have numerically observed that the stationary longitudinal mode is the preferred convection mode. Further, to obtain nonlinear stability bounds, we define an energy functional in terms of norm squares of perturbations in the stability measure $L^2(V)$, where V is the spatial periodic cell in the layer, given by $V = \Omega \times [0,1]$, and Ω represents the general tile in the plane $[x, y]$ [1]. Then the defined energy will decay to zero with time, subject to a maximization problem for which provide the Euler-Lagrange equations are

$$-2\lambda_2(D^2 - a^2)W - (\lambda_2 Ra - DF)a^2\Theta + (\lambda_2 Rs + \lambda_1 DC_b)a^2\Phi = 0, \tag{9}$$

ICATP 2022, ISBN 978-81-952903-0-7

$$2(D^2-a^2)\Theta+(\lambda_2 Ra-DF)W+\frac{R_H^2}{2\lambda_2 Ra^2}\Theta+\lambda_1 Sr(D^2-a^2)\Phi=0, \tag{10}$$

$$2\frac{\lambda_1}{Le}(D^2-a^2)\Phi-(\lambda_1 DC_b+\lambda_2 Rs)W+\lambda_1 Sr(D^2-a^2)\Theta=0, \tag{11}$$

subject to the same boundary conditions $W=0,\ \ \Theta=0,\ \ \Phi=0$ at $z=0{,}1$. The critical Rayleigh number Ra_E, which is given by $Ra_E=\min_a \max_{\lambda_1,\lambda_2} Ra(a,\lambda_1,\lambda_2)$ that can now be obtained by solving the six-order eigenvalue problem (Eqns (9)-(11)) using the Galerkin method.

Table 1: Critical Rayleigh number with R_H

$Rs=1, Sr=0.02, Le=7$									
R_H	Ra_L	a_L	Ra_E	a_E	R_H	Ra_L	a_L	Ra_E	a_E
0	32.33	3.14	32.33	3.14	80	157.42	6.75	69.94	2.03
20	42.67	3.14	37.32	2.95	100	135.54	8.89	65.16	6.65
40	72.42	3.22	48.79	2.56	115.32	-	-	0.00	8.25
60	118.05	3.68	60.69	2.23	133.27	0.000	10.89	-	-

Figure 1: Graphical representation of table 1

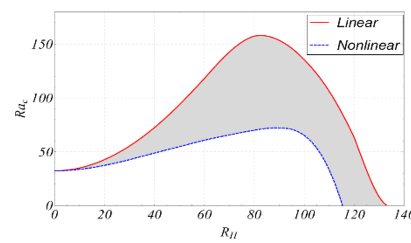

Conclusively, we can say that the energy stability bounds do not coincide with the linear stability bounds, which indicates the possibility of subcritical instability in the present study. Further, it is observed from the table that the subcritical region increases with an increase in the horizontal thermal Rayleigh number (R_H). The horizontal component R_H alone can induce the convection as the critical value of Ra is zero when R_H= 133.2789 for linear theory and R_H = 115.3297 for energy method. These values of R_H may change with the change of non-dimensional parameters (Rs, Le, Sr). Further, we observed that the critical vertical Rayleigh number (Ra) gets the maximum value for a corresponding value of the horizontal Rayleigh number (R_H) and then decreases for further increase in R_H. This observation is analogous to the results reported in the literature [4].

References

[1] Subrahmanyan Chandrasekhar. 2013. Hydrodynamic and hydromagnetic stability. Courier Corporation.
[2] Manole D.M. and Lage J.L. 1995. Numerical simulation of supercritical hadley circulation, within a porous layer, induced by inclined temperature gradients. International journal of heat and mass transfer, 38(14):2583–2593.
[3] Weber J.E.1974. Convection in a porous medium with horizontal and vertical temperature gradients. International Journal of Heat and Mass Transfer, 17(2):241–248.
[4] Nield, D. A. 1991. Convection in a porous medium with inclined temperature gradient, International journal of heat and mass transfer 34 (1) 87–92.

CHAPTER -22

RAYLEIGH-BÉNARD CONVECTION IN A HYBRID-NANOFLUID SUBJECTED TO GENERAL BOUNDARY CONDITION

Heena Firdose[1], P. G. Siddheshwar1[1] Ruwaidiah Idris[2]
1 Center for Mathematical Needs, Department of Mathematics, CHRIST (Deemed to be University), Bangalore - 560029, India.
2 Special Interest Group Modelling and Data Analytics Faculty of Ocean Engineering Technology and Informatics Universiti Malaysia Terengganu, 21030 Kuala Nerus Terengganu, Malaysia.
E-mail : heena.firdose@res.christuniversity.in

INTRODUCTION

A hybrid-nanofluid (hnf) is a type of nanofluid (nf) where two binary mixture of nanoparticles is dispersed in a single base fluid. A dilute concentration of nanoparticles is maintained in order to avoid agglomeration of nanoparticles (Suresh et al. (2011)). Kanchana et al (2019) studied Rayleigh-Benard convection(RBC) in hnf with boundaries that can be attained physically (rigid isothermal boundaries). A comparative study between water-alumina nf and water-copper-alumina hnf was done where it was reported that the hnf advanced the onset of convection.

MATHEMATICAL FORMULATION:

Using the single-phase model the following equations govern the RBC problem:

$$\nabla.\boldsymbol{V} = 0, \tag{1}$$

$$\rho_{hnf}\frac{\partial \boldsymbol{V}}{\partial t} = -\nabla p + \mu_{hnf}\nabla^2\boldsymbol{V} + \rho_{hnf}\boldsymbol{g}, \tag{2}$$

$$\frac{\partial \theta}{\partial t} + (\boldsymbol{V}.\nabla)\theta = \alpha_{hnf}\nabla^2\theta, \tag{3}$$

where, $\boldsymbol{V}$ is the velocity vector, ρ is the density, p is the pressure, μ is dynamic coefficient of viscosity, θ is the temperature, $\Delta\theta$ is the temperature difference between the horizontal walls, t is dimensional time, $\boldsymbol{g}$ is the acceleration due to gravity, α is the thermal-diffusivity, β is the coefficient of thermal-expansion. The subscript hnf stands for hybrid nanofluid.

The boundary conditions on the rough boundaries considered in the study are:

$$v = 0, \quad \frac{\partial u}{\partial y} = +\frac{\gamma_l u}{\sqrt{K_l}}, \quad +(k_{hnf})_m\frac{\partial \theta}{\partial y} = H_l\left(\theta - \theta_0 - \frac{\Delta\theta}{2}\right), \quad at \quad y = 0, \tag{4}$$

$$v = 0, \quad \frac{\partial u}{\partial y} = -\frac{\gamma_u u}{\sqrt{K_u}}, \quad -(k_{hnf})_m\frac{\partial \theta}{\partial y} = H_u\left(\theta - \theta_0 + \frac{\Delta\theta}{2}\right), \quad at \quad y = d, \tag{5}$$

where, γ_l, γ_u are dimensionless parameters that characterise the permeable properties of porous-matrix (pm), H_l, H_u are the heat transfer coefficients of horizontal walls respectively, $(k_{hnf})_m = \Phi\, k_{hnf} + (1-\Phi)\, k_s$ is the thermal-conductivity of the hnf-saturated pm, Φ and k_s are the porosity and the thermal conductivity of the pm respectively.

ICATP 2022, ISBN 978-81-952903-0-7

RESULTS AND DISCUSSION

The RBC problem in hybrid nanofluids using general boundary condition is solved by adopting a combination of single-term Galerkin technique and Maclaurin series. The boundary condition have been modelled in such a way that a slip-Darcy number (Ds_l, Ds_u) and a Biot number (Bi_l, Bi_u) arises in each of the horizontal wall. From the Figures 1, 2 it *can be* observed that the slip-Darcy-number and Biot-number have satbilising effects on the onset of convection. It can be concluded that slip-Darcy number bridges the gap between stress-free (F) and rigid (R) boundaries, likewise Biot number bridges the gap between adiabatic (A) and isothermal (I) boundaries.

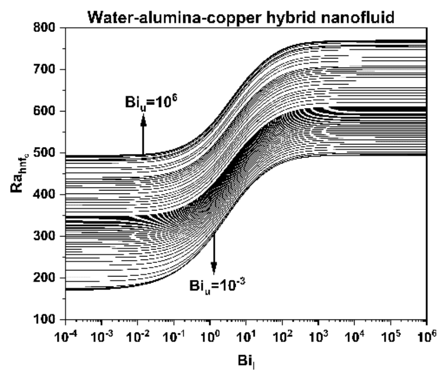

Figure 3 **Variation of critical Rayleigh-number with respect to Biot-number for $Ds_l = Ds_u = 1$.**

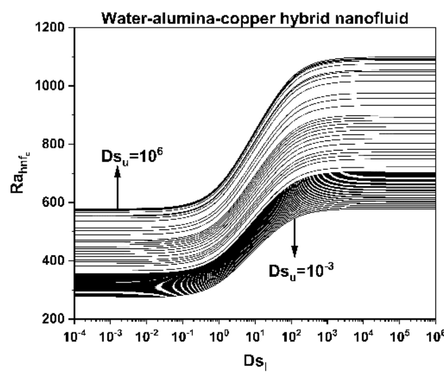

Figure 4 **Variation of critical Rayleigh-number with respect to slip-Darcy-number for $Bi_l = Bi_u = 1$.**

To validate the present study sixteen limiting cases of critical Rayleigh number (r) for different boundary combinations have been documented in Table 1.

Table 1 Critical Rayleigh number for sixteen combinations of boundaries

FF-II	FR-II	RR-II	FF-AA	RF-AA	RR-AA	FF-AI	RR-AI	RF-AI	RF-IA
657.627	1100.72	1707.81	120.136	320.238	720.374	384.349	1285.32	812.836	666.395

CONCLUSION

The following are the main findings of the present study:

$$(r_c)^{water} > (r_c)^{water-alumina} > (r_c)^{water-copper} > (r_c)^{water-alumina-copper},$$
$$\left(r_{hnf_c}\right)^{isothermal} > \left(r_{hnf_c}\right)^{general\ boundaries} > \left(r_{hnf_c}\right)^{adiabatic},$$
$$\left(r_{hnf_c}\right)^{rigid} > \left(r_{hnf_c}\right)^{general\ boundaries} > \left(r_{hnf_c}\right)^{stress-free}.$$

REFERENCES

1. Suresh, S., Venkitaraj, K.P., Selvakumar, P. and Chandrasekar, M., 2011. Synthesis of $Al_2O_3 - Cu$/water hybrid nanofluids using two step method and its thermo physical properties. *Colloids and Surfaces A: Physicochemical and Engineering Aspects*, *388*(1-3), pp.41-48.
2. Kanchana, C., Siddheshwar, P.G. and Zhao, Y., 2019. A study of Rayleigh–Bénard convection in hybrid nanoliquids with physically realistic boundaries. *The European Physical Journal Special Topics*, *228*(12), pp.2511-2530.

ICATP 2022, ISBN 978-81-952903-0-7

CHAPTER -23

EFFECT OF ROTATION ON THE ONSET OF CONVECTION IN MAGNETIC NANOFLUIDS WITH MAGNETIC FIELD DEPENDENT VISCOSITY

Monika Arora[1] and Kamalpreet Kaur[1*]
[1]Department of Mathematics, School of Chemical Engineering and Physical Sciences, Lovely Professional University, Phagwara-144411, Punjab, India
monikaarora1879@gmail.com, *kaurkamalpreet189@gmail.com

INTRODUCTION

The requirement of highly coherent heat transfer system in modern industrial world has led to the development of specific category of nanofluids widely known as "magnetic nanofluids" (MNFs). Accountability of Taylor number T_A which exhibits the effect of rotation on the onset of convection is very much considerable. Various studies have been performed to see the effect of the same by varying one or the other parameters. This study investigates the effect of $T_A$on the onset of convection in water based $MNF(W_{MNF})$ and ester based $MNF(E_{MNF})$.

FORMULATION AND METHOD

An infinite horizontal layer of an incompressible MNF of thickness d heated from below having a variable viscosity $\mu_1 = \mu(1 + \delta.B)$ is considered (Arora *et al.* (2016)) and system is supposed to rotate along z-axis with angular velocity $\Omega = (0,0,\Omega)$. The model involves three important slip mechanisms: Brownian motion, Thermophoresis and Magnetophoresis. The governing equations for the system are considered as given in Mahajan *et al.* (2014) and Arora *et al.* (2016). Graphical analysis is performed through linear stability method to check the effect of $T_A$on the onset of convection by varying different non-dimensional parameters. The eigen value problem obtained in the process is solved by Chebyshev pseudospectral method for W_{MNF} and E_{MNF}.

RESULTS AND DISCUSSION

Linear stability analysis is done for W_{MNF} and $E_{MNF}$to see the effect of rotation which is exhibited by T_A through neutral stability curves (NSCs) (see Fig 1 and Fig 2). The stabilizing effect of $T_A$is witnessed on the system since Ra_c increases as $T_A$increases.

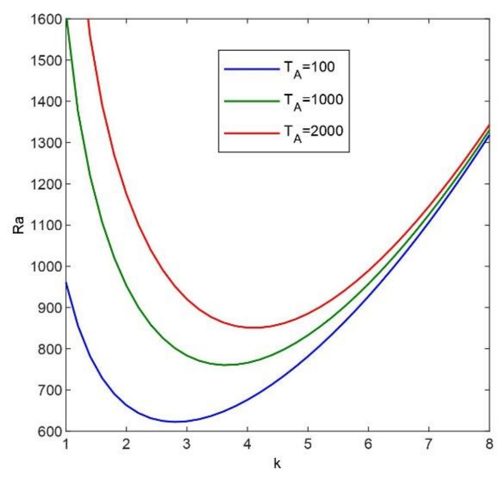

Fig 1: NSCs for different values of $T_A$for E_{MNF}

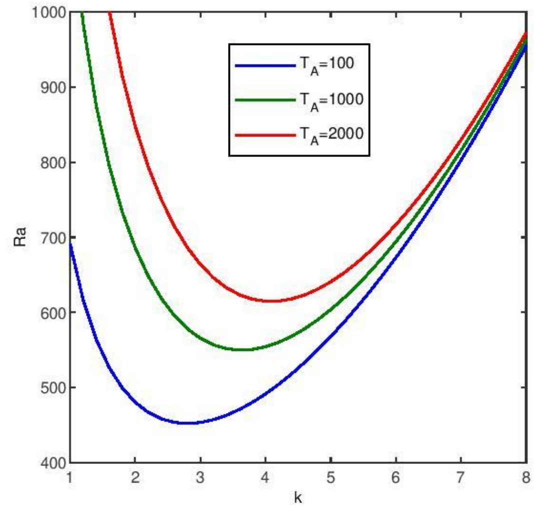

Fig 2: NSCs for different values of T_A for W_{MNF}

CONCLUSION

The effect of rotation on the onset of convection has been investigated in MNF with magnetic field dependent viscosity using linear stability theory. Stabilizing effect of T_A has been observed since on quantitative ground Ra_c and T_A follow the same trend.

REFERENCES

Arora, A., Singh, R. and Panda, M.K., 2016, Effects of magnetic-field-dependent viscosity at onset of convection in magnetic nanofluids, J. Eng. Math., 101: 201-217.

Choi, S., 1995, Enhancing Thermal Conductivity of Fluids with Nanoparticles, ASME-Publications-Fed, 231: 99-106.

Mahajan, A., Sharma, M.K. and Sunil, 2014, Convection in Rotating Magnetic Nanofluids in Porous Media, J. Nanofluids, 3: 350-360.

Nanjundappa, C., Shivakumara, I. and Srikumar, K., 2009, Effect of MFD viscosity on the onset of ferromagnetic fluid layer heated from below and cooled from above with constant heat flux, Meas. Sci. Rev., 9: 75-80.

Nanjundappa, C.E., Shivakumara, I.S and Lee, J., 2015, Effect of coriolis force on Bénard-Marangoni convection in a rotating ferrofluid layer with MFD viscosity, Microgarvity Sci. Technol., 27: 27-37.

CHAPTER -24

CONTROL OF CHAOS IN A RAYLEIGH-BENARD CONVECTION FOR A WEAKLY ELECTRICALLY CONDUCTING LIQUID

Noor Arshika, S[1], Ruwaidiah, Idris[2], and Sameena, Tarannum[3]
[1]Centre for Mathematical Needs, Department of Mathematics, CHRIST (Deemed to be University), Hosur road, Bengaluru, 560029, Karnataka, India
[2]Faculty of Ocean Engineering Technology and Informatics, Universiti Malaysia Terengganu, Kuala Nerus, 21030, Terengganu, Malaysia
[3]Department of Professional Studies, CHRIST (Deemed to be University), Hosur road, Bengaluru, 560029, Karnataka, India.
noor.arshika@res.christuniversity.in

INTRODUCTION

The paper aims to study the Rayleigh-Bénard convection problem bounded by rigid isothermal boundaries, in the presence of a vertical magnetic field. A minimal Fourier-Galerkin expansion is proposed accordingly. Using the multiscale method, the analytically intractable Lorenz model is reduced to a tractable Ginzburg-Landau equation. The results of these boundaries are extracted using the Chandrasekhar even eigen function and its corresponding even eigen value. The steady state equations of the Lorenz model provides a solution for the finite amplitude convection. The rigour of the convective instability, intensity of heat transfer and chaos in the system is analyzed and captured via graphs.

MATERIALS AND METHODS

The solution of the problem is studied using a linear and nonlinear analysis with the help of a minimal Fourier-Galerkin expansion. Using multiscale method, we arrive at a Ginzburg-Landau equation, which is used to study the heat transport. A Lorenz model resembling like that of the classical Lorenz model is obtained to study its dynamical behavior.

RESULTS AND DISCUSSION

In this research work, we analyze the behaviour of the dynamical system subjected to a vertical magnetic field in a weakly electrically conducting liquid bounded by the rigid isothermal boundaries. This can be viscualized in the physical confiuration in Figure 1. Insights on the convective instablity, heat transport phenomena and chaotic nature have been compiled in this section and are as follows: The effect of increasing magnetic field is to delay the onset of convection (see Table 1.) and chaotic motion; and to increase the heat transport. Trajectories revolve around their critical points giving rise to chaos in the system (see Figure 2(a)). A clear distinction between the regular convective motion, periodic and/or chaotic motion is traced using the bifurcation diagram in Figure 2(b).

Table 1. Values of the critical Rayleigh number for different values of Chandrasekhar number.

CHANDRASEKHAR NUMBER	CRITICAL RAYLEIGH NUMBER	WAVE NUMBER
0	1728.38	3.09
3	1865.36	3.10
5	1956.64	3.11

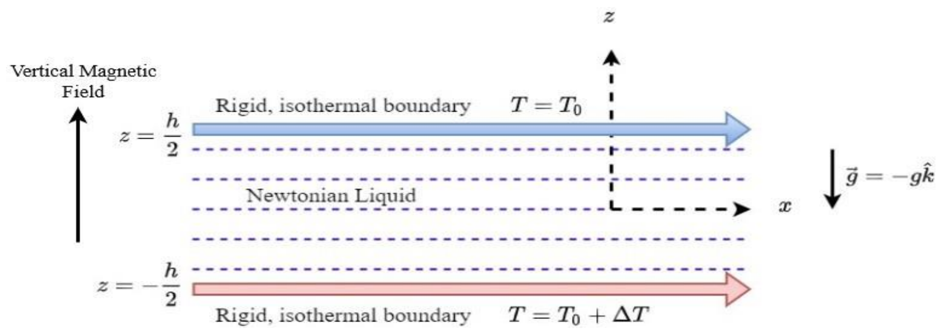

Figure 1. Sketch of a Rayleigh-Bénard convection problem bounded by rigid isotherma boundaries and subjected to a vertical magnetic field

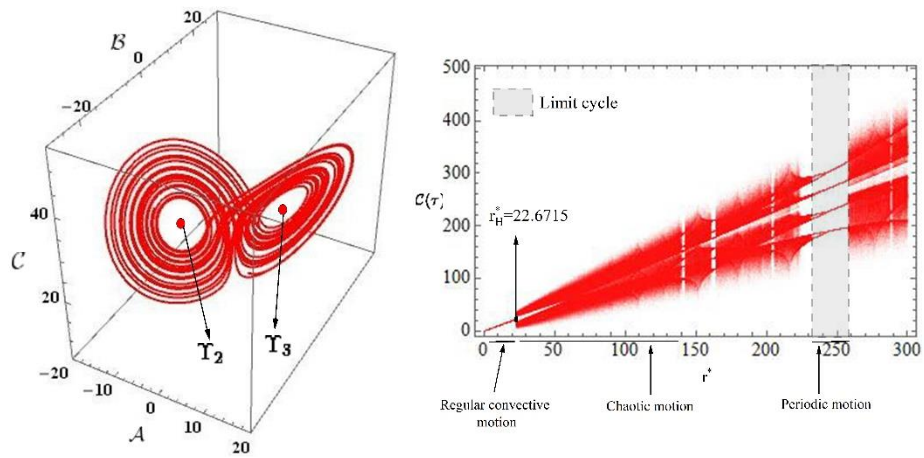

(a) **(b)**

Figure 2. (a) Phase space plot showing the chaotic nature of the Lorenz system revolving around its critical points (b) Bifurcation diagram predicting the Hopf-Rayleigh number and displaying the regular convective, chaotic and periodic nature of the Lorenz system

CONCLUSION

A weakly electrically conducting liquid subjected to a vertical magnetic field and bounded by the rigid isothermal boundaries is studied analytically in this paper. We aim to demonstrate the heat transport and study the dynamics of the Lorenz system. The effect of increasing magnetic field is to delay the onset of convection and chaotic motion; and to increase the heat transport. Chaos in the system can be witnessed by the chaotic movement of the trajectories without intersecting one another. Using the bifurcation diagram it is possible to clearly distinguish the dynamics of the system.

ACKNOWLEDGMENT

Authors would like to thank Dr. P.G. Siddheshwar, CHRIST(Deemed to be University), for his valuable inputs in the paper.

REFERENCES

1. Chandrasekhar, S. 1961. Hydrodynamic and Hydromagnetic stability. New York: Oxford University Press.
2. Lorenz, E. 1963. Deterministic nonperiodic flow. J. Atmos. Sci., 20: 130-141.
3. Sparrow, C. 1982. The Lorenz equations: bifurcations, chaos, and strange attractors., New York: Springer Verlag.
4. Siddheshwar, P.G., Shivakumar, B.N., Zhao, Y and Kanchana, C. 2020. Rayleigh-Bénard convection in a Newtonian liquid bounded by rigid isothermal boundaries. Appl. Math. Comput., 371: 124942.

CHAPTER -25

STABILITY ANALYSIS FOR THERMOHALINE CONVECTION IN A COUPLE-STRESS FLUID

Shalu Choudhary[1], Reeta Devi [2*], Amit Mahajan[3], Sunil[4]

[1] Department of Mathematics, Uttaranchal University, Dehradun, Uttarakhand, India
[2] Department of Mathematics, Govt. Degree College, Dharamshala, District Kangra (H.P.), India
[3] Department of Applied Sciences, National Institute of Technology Delhi, India
[4] Department of Mathematics & Scientific Computing, National Institute of Technology Hamirpur, India
[*] E-mail: reetamaths6@gmail.com (Reeta Devi)

INTRODUCTION

The stability of a layer of steady, viscous, incompressible thermohaline couple-stress liquid is investigated. The linear and nonlinear thresholds at the onset of convection are found to be same. The couple stresses and solute gradient both have the stabilizing impact on the system. Among the models proposed for the distinct behavior of non-Newtonian fluids, the one proposed by Stokes (1966) on couple stresses in fluids has relevance in theory of lubrication, synovial fluid present in synovial joints, liquid crystals, animal blood. Global nonlinear results are obtained in Sunil et al. (2011) for a layer of couple stress liquid. The corresponding problem in porous media is analysed by Choudhary and Sunil (2019).

MATERIALS AND METHODS

A horizontal layer of couple stress fluid with fixed viscosity heated and soluted from below for a free free conducting boundary system is considered. The temperature and concentration at lower and upper surfaces are fixed with gravitational force acting vertically downward. The governing equations for analysing onset in a thermohaline couple-stress liquid are (by using the Boussinesq approximation, Chandrasekhar (1961)):

$$\nabla\cdot\vec{q}_s=0, \tag{1}$$

$$\rho_r\left(\frac{\partial}{\partial t}+\vec{q}_s\cdot\nabla\right)\vec{q}_s=-\nabla p_1+\rho_r\left[1-\alpha\left(T-T_{av}\right)+\alpha'\left(C-C_{av}\right)\right]\vec{g}+\left(\mu-\mu'\nabla^2\right)\nabla^2\vec{q}_s, \tag{2}$$

$$\frac{\partial T}{\partial t}+\vec{q}_s\cdot\nabla T=\kappa\nabla^2 T, \tag{3}$$

$$\frac{\partial C}{\partial t}+\vec{q}_s\cdot\nabla C=\kappa'\nabla^2 C. \tag{4}$$

Here, ρ_r is the reference fluid density, $\vec{q}_s$ is the fluid velocity, $\vec{g}$ is gravity, t denotes time, p_1 is the fluid pressure, μ is the viscosity, μ' is the visco-elasticity coefficient, κ is the thermal diffusivity, κ' is the solute diffusivity, α and α' are thermal and solute expansion coefficients.

To the above set of equations, we apply perturbations, normal mode techniques for linear analysis and then the energy method for nonlinear analysis. The critical values of Rayleigh number for both the cases (linear as well as non linear) are calculated and found to coincide.

OUTCOMES

The values of the wave number (x_c) and thermal Rayleigh number (R_c) turned out to be dependent on couple stress parameter (F_1) and solute gradient (S_1). Figure 1 shows the behaviour of critical values of thermal Rayleigh number with varying solute gradient for considered values of couple stress parameter.

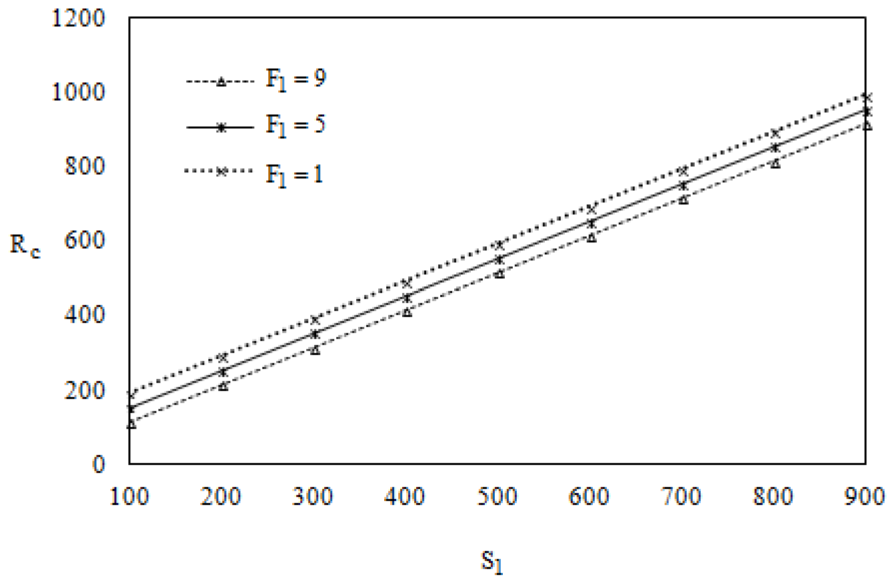

Figure 1: The variation in Rayleigh number R_c versus solute parameter S_1.

From this figure, the stabilizing nature of couple stresses as well as solute gradient is observed.

CONCLUSIONS

The critical values of Rayleigh numbers obtained using linearised theory and by energy technique of nonlinear theory are same. The coincidence of the two theories allows linear theory to capture the whole physics of the model. The onset of convection is advanced due to presence of solute. The critical Rayleigh number values for couple stress parameter shows stabilizing nature of the parameter.

REFERENCE

1. Chandrasekhar S. 1961. Hydrodynamic & Hydromagnetic Stability. Dover, New York.
2. Choudhary S. & Sunil. 2019. Global stability for double-diffusive convection in a couple-stress fluid saturating a porous medium. Studia Geotechnica et Mechanica, 41:13-20.
3. Sunil, Devi R. & Mahajan A.. 2011. Global stability for thermal convection in a couple-stress fluid. International Communication in Heat and Mass Transfer, 38:938-942.
4. Stokes V. K. 1966. Couple stresses in fluids. Physics of Fluids, 9:1709-1715.

ICATP 2022, ISBN 978-81-952903-0-7

CHAPTER -26

HYDRODYNAMIC NATURAL CONVECTION ACROSS A SEMI-INFINITE VERTICAL POROUS PLATE WITH CHEMICAL REACTION

Rajdeep Bordoloi[1], Mridusmita Bormudoi[2], Lukendra Kakati[3]

[1]Department of Mathematics, Gauhati University, Guwahati, Assam
[2]Department of Mathematics, Gauhati University, Guwahati, Assam
[3]Department of Mathematics, Lanka Mahavidyalaya, Lanka, Assam
E-mail (rajdeepbordoloi24@gmail.com)

INTRODUCTION

This study uses the Cogley *et al.* (1968) model to examine how the thermal radiation and chemical reaction affect the free convective viscous incompressible optically thin fluid. The core interest of this scrutiny is that the current problem involves a flow through a porous media of the Brickman type while a first-order chemical reaction is occurring. In order to find the solutions to the governing equations, the asymptotic series expansion approach is used. The current study could have an impact on a number of engineering procedures, including the manufacture of paper, the making of glass, etc.

MATERIALS AND METHODS

We consider a viscous, unsteady, two-dimensional flow of an incompressible radiating fluid with mass transfer past a semi-infinite vertical porous plate. The plate is along the X-axis and the Y-axis perpendicular to it with the Z-axis along the width of the plate. The plate is at temperature $\bar{T}_w$ and concentration $\bar{C}_w$ (at the wall) and far from the plate, we have the temperature at T_∞ and concentration at C_∞ (free stream). The semi-infinite nature of the plate makes the flow variable a function of $\bar{y}$ and $\bar{t}$ only. To solve the non-dimensional governing equations, we take into account the ensuing asymptotic form:

$$\left.\begin{aligned} u(y,t) &= u_0(y) + \varepsilon e^{i\omega t} u_1(y) + O(\varepsilon^2) \\ \theta(y,t) &= \theta_0(y) + \varepsilon e^{i\omega t} \theta_1(y) + O(\varepsilon^2) \\ \phi(y,t) &= \phi_0(y) + \varepsilon e^{i\omega t} \phi_1(y) + O(\varepsilon^2) \end{aligned}\right\}$$

Using the perturbation technique, the final solutions for the velocity, concentration, and temperature are obtained as

$$u = (\psi_3 + \psi_4)e^{-\xi_5 y} - \psi_3 e^{-\xi_1 y} - \psi_4 e^{-\xi_3 y} + \varepsilon e^{i\omega t}[(\psi_5 + \psi_6 + \psi_7)e^{-\xi_6 y} - \psi_5 e^{-\xi_1 y} - \psi_6 e^{-\xi_2 y} - \psi_7 e^{-\xi_3 y}]$$

$$\phi = e^{-\xi_3 y} + \psi_2 \varepsilon e^{i\omega t}(e^{-\xi_3 y} - e^{-\xi_4 y})$$

$$\theta = e^{-\xi_1 y} + \varepsilon e^{i\omega t}[(1-\psi_1)e^{-\xi_2 y} + \psi_1 e^{-\xi_1 y}]$$

RESULTS AND DISCUSSION

The effects of many parameters, such as the radiation parameter Q, Schmidt number Sc, thermal Grashof number Gr, chemical reaction K, etc., are examined graphically to gain a physical understanding of the problem. Figure 1 demonstrates how fluid velocity rises as Gr values rise. As a result, the fluid's velocity increases due to the force of thermal buoyancy. Figure 2 shows that the magnitude of the temperature decreases noticeably as the positive values of the radiation parameter Q increase. Figure 3 depicts how the chemical reaction parameter K affects the concentration profile. It is observed that when the effect of chemical reaction increases, the species concentration significantly falls.

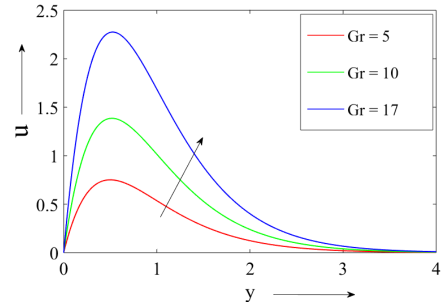

Figure 1. Velocity layout for thermal Grashof number Gr, when Pr=0.71, Sc=0.7.

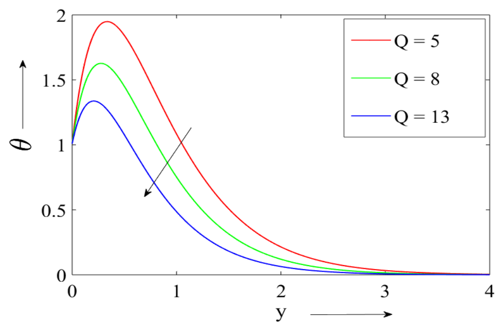

Figure 2. Temperature layout for radiation parameter Q, when Pr=0.71, Sc=0.7.

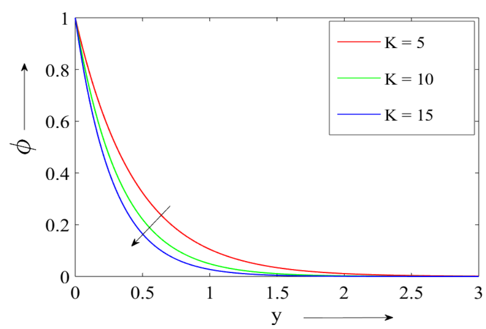

Figure 3. Concentratione layout for chemical reaction parameter K, when Pr=0.71, Sc=0.7.

CONCLUSION

We come to the conclusion that fluid velocity rises in the existence of thermal buoyancy force. Under the influence of the radiation parameter, the fluid's temperature decreases significantly. Due to the enhanced chemical reaction parameters and Schmidt number, a considerable decrease in fluid concentration is seen. For increased radiation, viscous drag at the plate diminishes.

REFERENCES

Cogley, A.C.L., Vincenti, W.G. and Gilles, E.S. 1968. Differential approximation for radiative heat transfer in a nongrey gas near equilibrium, *American Institute of Aeronautics and Astronautics*, 6: 551-553.

CHAPTER -27

Heat Transfer of not miscible micropolar nanofluid stuffed between viscous nanofluid

Umavathi, J.C[1], and Sutkar P.S[2]
Department of Mathematics, Gulbarga University, Gulbarga-585 106, Karnataka, INDIA
Department of Mathematics, NES Science College, Nanded-431605, Maharashtra, INDIA
drumavathi@rediffmail.com

INTRODUCTION

Eringen [1-2] introduced the micropolar fluid theory, which is one of the superior fluid theories for representation of the deformation of materials. Micropolar fluid is used to study the performance of novel lubricants [3-4], flow of polymeric fluids or colloidal suspensions [5], liquid crystals [6,7], supplemental suspensions, animal and human blood , turbulent shear flow etc. The flow of two not miscible fluids in a parallel plate channel was studied by Laharsabi and Shai [8], who assumed that the thermal equilibrium and velocity at the contact were constant. Nanofluids are known as super-coolants, since they ingest heat more efficiently than regular fluids, allowing systems to be smaller and more efficient [9,10]. Umavathi et al.[11,12] analyzed the properties of nanofluids for a viscous permeable, conducting, Newtonian/non-Newtonian fluid through various geometries. An analysis of the micropolar nanofluid stuffed between purely viscous nanofluid in the upper and lower regions is presented here.

MATERIAL AND METHODS

We consider a steady, completely formed, micropolar nanofluid flow flowing inside a definite horizontal channel bounded by $0 \le y \le h$ as given by [13]. This flow is described by a two-fluid model along a central micropolar nanofluid $(0 \le y \le h)$ and viscous Newtonian nanofluid of thickness h on the periphery layers $(-h \le y \le 0)$ and $(h \le y \le 2h)$ of same width. The formulations for one-dimensional, steady, linear velocity, temperature and microrotation velocity in nondimensional form are

Region-I

$$\frac{d^2 u_1}{dy^2} - mp = 0 \tag{1}$$

$$\frac{d^2\theta_1}{dy^2} + \left(\frac{Ec\,\Pr Cr}{m}\right)\left(\frac{du_1}{dy}\right)^2 = 0 \tag{2}$$

Region-II

$$(1+K)\frac{d^2 u_2}{dy^2} + K\frac{dN}{dy} - mp = 0 \tag{3}$$

$$\left(1+\frac{K}{2}\right)\frac{d^2 N}{dy^2} - 2KN - K\frac{du_2}{dy} = 0 \tag{4}$$

$$\frac{d^2\theta_2}{dy^2} + \frac{Ec\,\Pr Cr}{m}\left(\frac{du_2}{dy}\right)^2 = 0 \tag{5}$$

Region-III

$$\frac{d^2u_3}{dy^2}-mp=0 \tag{6}$$

$$\frac{d^2\theta_3}{dy^2}+\frac{Ec\Pr Cr}{m}\left(\frac{du_3}{dy}\right)^2=0 \tag{7}$$

Above eqns. are solved using the following boundary and interface conditions

$$u_1(2)=0,\ u_1(1)=u_2(1),\ u_3(0)=u_2(0),\ u_3(-1)=0,$$

$$\frac{du_1}{dy}=(1+k)\left(\frac{du_2}{dy}\right)+kN \text{ at } y=1,\ (1+k)\frac{du_2}{dy}+kN=\frac{du_3}{dy} \text{ at } y=0 \tag{8}$$

$$\frac{dN}{dy}=0 \text{ at } y=1\ ,\quad \frac{dN}{dy}=0 \text{ at } y=0$$

$$\theta_1(2)=1,\ \theta_1(1)=\theta_2(1),\ \theta_2(0)=\theta_3(0),\ \theta_3(-1)=0,$$

$$\frac{d\theta_1}{dy}=\frac{d\theta_2}{dy} \text{ at } y=1,\ \frac{d\theta_2}{dy}=\frac{d\theta_3}{dy} \text{ at } y=0 \tag{9}$$

Using authentic boundary and interface conditions, (8) and (9), the solution of equations (1) –(7) are obtained for the non dimensional linear velocities $u_i(i=1,2,3)$, the microrotation velocity N, and temperature $\theta_i(i=1,2,3)$ for three regions. -

RESULTS AND DISCUSSION

An exact analytical solution for the micropolar nanofluid saturated with nanofluid sandwitched between viscous nanofluid layers is studied. The non-dimensional governing equations (1)-(7) as well as boundary and interfacial conditions (8)-(9) are linked ordinary differential equation and hence exact solution are obtained. With the help of these elucidation numerical values are estimated for specific values of the controlling constants, and are commenced in tables and graphs respectively. Computations are carried out using pure water as the base fluid inside that $\Pr=6.06$ and alumina as nanoparticles [14]. The calculations are made for the values of $Ec=0.5, p=-2.0, \phi=0.01, K=2.0$ expect the varying parameters.

CONCLUSION

In the present study micropolar nanofluid sandwiched between pure viscous nanofluids was analyzed. The closed one solutions are computed. The linear velocity and temperature decreases with solid volume fraction ϕ and material parameter. The material parameter increases micropolar velocity in magnitude and solid volume fraction ϕ reduces the microrotation velocity. Eckert number helps to bust the energy. The cell rotational velocity reduces the velocity and also the microrotation velocity. The presence of nanoparticles like silver, copper, copper oxide and graphite oxide do not influence the linear velocity and temperature.

REFERENCES

1. Eringen, A.C., 1964.Simple microfluids. Int. J. Eng.Sci. 2: 205-217.
2. Eringen, A.C.,1966. Theory of micropolar fluids. J. Math. Mechanics, 16: 1-18.
3. Khonsari, M. M., Brew, D. 1989. On the performance of finite journal bearing lubricated with micropolar fluid. ASLE Tribiology Trans. 32: 155-160.
4. Khonsari, M. M., 1990. On the self-excited whirl orbits of a journal in a sleeve bearing lubricated with micropolar fluids. Acta Mech. 81: 235-244.
5. Hadimoto, B., Tokioka, T. 1969. Two dimensional shear flows of linear micropolar fluids. Int. J. Eng. Sci. 7 : 515-522.

6. Lee, J.D., Eringen, A.C.,1971. Boundary effect of orientation of nematic liquid crystals. J. Chem. Phys. 55: 4509-4512.
7. Lockwood, F., Benchaitra, M., Friberg, S.,1987. Study of polyotropic liquid crystals in viscometric flow and clastohydrodynamic contact. ASLE Tribiology Trans. 30: 539-548.
8. Loharsbi, J. Sahai, V.1988. Magnetohydrodynamic heat transfer in two-phase between parallel plates. Applied scientific Research, 45:53-66.
9. Umavathi, J.C., Manjula, M.H., Pop, I., Liu, I.C.2007. Flow and heat transfer of couple stress viscous fluids in a vertical channel. International journal of Applied Mechanics and Engineering. 12:537-555.
10. Ozturk, S., Hassan, A.Y., Ugaz, V.M. 2010. Intrfacial complexation explains anomalous diffusion in nanofluids, Nano Lett. 10: 665-671.
11. Mohammad, H.A., Al-aswadi, A.A., Shuaib, N.H., Saidur,R. 2011. Convective heat Transfer and fluid flow over a step using nanofluids: a Review, Renew. Sustain. Energy Rev. 15: 2921-2939.
12. Umavathi, J.C., Odelu Ojjela., Vajravelu, K. .2017.Numerical analysis of natural convective flow and heat transfer of nanofluids in a vertical rectangular duct using Darcy-Forchheimer-Brinkman model.IJTS, vol. 11:511-524.
13. Umavathi, J.C., Hakan F. Oztop.2021. Investigation of MHD and applied electrical field effects in a conduit cramed with nanofluids. Int. Comm. in Heat and Mass Transfer, vol. 121: 105097-1105097-16.
14. Bourantas, G.C., Loukopoulos, V. C.,2014. MHD natural-convection flow in an inclined square enclosure filled with a micropolar nanofluid. Int J. of Heat and mass Transfer, 79, 930-944.

DISPERSION OF HEAVY PARTICLES IN A STEADY COUETTE FLOW

Subham Dhar[1,*], Nanda Poddar[1], and Kajal Kumar Mondal[1]
[1] Department of Mathematics, Cooch Behar Panchanan Barma University, Cooch Behar, West Bengal, India-736101
*E-mail: dharsuvam94@gmail.com

INTRODUCTION

The transport of solute in Couette flow has various applications in food, polymer processing and lubrication. From the practical point of view, the heavy particles (i.e., heavier solutes with settling velocity) may be present in the crude oil or raw food. The transport of solute material in steady and oscillatory Couette flow was extensively studied by numerous researchers with considering boundary absorption (Barik and Dalal, 2017, 2019), sorption and phase exchange kinetics (Ng, 2006). The dispersion of heavy particle was studied in turbulent open channel flow (Mondal and Mazumder, 2005), wetland flow (Dhar et al, 2021; Poddar et al. 2021), laminar ice-covered channel flow (Dhar et al. 2022), but, the dispersion of heavy particle in Couette flow paid low attention.

From the industrial point of view, the vertical distribution of heavy particle is highly significant and so the present research enlightens on the vertical concentration distribution in a steady Couette flow. It is shown that, how the heavy particles move through the flow under the movement of the upper plate. Mei's homogenization technique with three time scale is used to obtain the solution of convection-diffusion equation. It is found that concentration of the particles falls downward and deposited near the lower plate as the settling velocity increases. The vertical concentration variation rate for the Couette flow is also disturbed with the introduction of small values of settling velocity.

MATERIALS AND METHODS

A laminar Couette flow for an incompressible, viscous fluid flowing between two infinite parallel plates of separation height h is considered. The $\bar{x}$ and $\bar{y}$ axes are taken along the longitudinal and vertical direction respectively. The upper plate $\bar{y} = h$ is moving with speed U and the lower plate $\bar{y} = 0$ is stationary (see Figure 1). The dimensionless velocity profile for Couette flow becomes:

$$u = \frac{\bar{u}}{U} = \frac{\bar{y}}{h} = y.$$

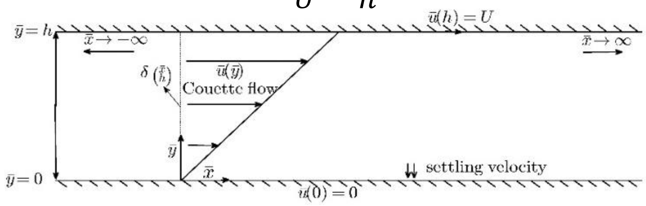

Figure 1. Physical situation of Couette flow with moving upper plate and steady lower plate.

When a heavy particle with settling velocity $\bar{\omega}$ and constant molecular diffusivity D is released into the above mentioned Couette flow, it is satisfied the mass transport equation and its dimensionless form is given by:

$$\frac{\partial C}{\partial t} - \epsilon\omega\frac{\partial C}{\partial y} + \epsilon u Pe\frac{\partial C}{\partial x} = \epsilon^2\frac{\partial^2 C}{\partial x^2} + \frac{\partial^2 C}{\partial y^2}$$

and the initial and boundary condition is given by $C(x, y, t)|_{t=0} = \Delta\left(\frac{x}{\epsilon}\right)$ and $\left[\frac{\partial C}{\partial y} + \epsilon\omega C\right]_{y=0,1} = 0.$

Here $\epsilon = \frac{h}{L}(\ll 1)$ is the perturbation parameter. The dimensionless terms are introduced as

$$t = \frac{\bar{t}}{h^2/D}, \omega = \frac{\overline{\omega} L}{D}, x = \frac{\bar{x}}{L}, y = \frac{\bar{y}}{h}, Pe = \frac{Uh}{D}$$

To solve the mass transport equation associated with initial and boundary condition, an asymptotic expansion of concentration and three time scales are adopted. The three time scales are given by diffusion time along vertical, convection time along longitudinal and diffusion time along longitudinal direction respectively.

RESULTS AND DISCUSSION

The dispersion coefficient and two dimensional real and mean concentration distribution of heavy particle is obtained for Couette flow using the multiple scale homogenization method. The effective dispersivity is equal with the steady dispersion coefficient of Barik and Dalal (2019). Figure 1a shows that as the tracer material become heavier, its concentration increases near the stationary lower plate. On the other hand, concentration decreases from the moving upper plate. A symmetric behavior is observed in vertical variation rate at different time form Figure 1b. It is seen from Figure 1c that, an important asymmetry is reveal in the vertical variation rate when the solute changes its state to heavy particle. Not only that, the bimodal variation rate profile becomes unimodal with the enhancement se4ttling velocity. The iso-concentration contour of heavy particle for different values of settling velocity is shown in Figure 2. The iso-concentration contour lines tilted towards the lower plate. The concentration of the particle moves from the upper plate to the lower plate and conglomerated near the lower plate as the particles becomes heavier.

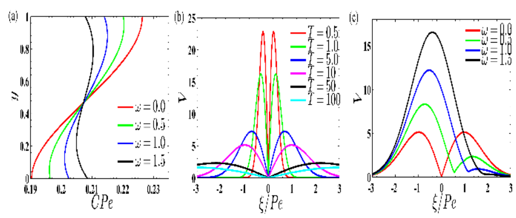

Figure 1. (a) Vertical concentration distribution (b) Vertical variation rate for different time (c) Verticla variation rate for different settling velocity

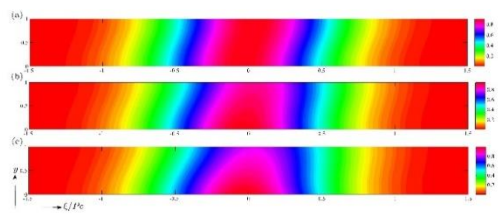

Figure 2. Iso-concentration contours for the values of (a) $\boldsymbol{\omega = 0.0}$ (b) $\boldsymbol{\omega = 1}$ (c) $\boldsymbol{\omega = 2}$.

CONCLUSION

In the present work homogenization technique is used for three time scale to solve the convection diffusion equation for heavy particle in a Couette flow. Some significant conclusions are: (i) the concentration of heavier particle deposited near the lower plate, (ii) a transition point in vertical concentration distribution is found for various settling velocity, (iii) the centroid of the particles cloud moves along the upstream direction as it becomes heavier, (iv) the strength of the concentration enhances as settling velocity increases, (v) The model may be useful to understand food, polymer processing and lubrication.

ACKNOWLEDGMENT

The first author is thankful to Council of Scientific and Industrial Research for financial support.

REFERENCES

Barik, S. and D. C. Dalal. 2019. Multi-scale analysis for concentration distribution in an oscillatory Couette flow. Proc. R. Soc. A: Math. Phys. Eng. 475: 20180483.

Barik, S. and D. C. Dalal. 2017. Multi-scale analysis for concentration distribution in an oscillatory Couette flow. Acta Mech. 228: 2391-2412.

Dhar, S., N. Poddar, R. R. Kairi, B. S. Mazumder and K. K. Mondal. 2021. Numerical study ondispersion of fine settling particles in a depth dominated wetland flow. Commun. Nonlinear Sci. Numer. Simulat. 96: 105707.

Ng, C. O. and Y. C. Bai. 2005. Dispersion in oscillatory Couette flow with sorptive boundaries. Acta Mech. 178: 65-84.

Poddar, N., S. Das, S. Dhar and K. K. Mondal. 2021. Semi-analytical study on environmental dispersion of settling partciles ina width independent wetland flow. Environ. Fluid Mech. 21: 1069-1090.

CHAPTER -29

Computational Analysis of Unsteady Flow of Non-Newtonian Casson Fluid in a 2-D Square Cavity: Fluid Flow Characteristics in Presence of an Obstacle

Dalmalka Praveen Kumar[1], Yadagiri Rameshwar [2]
[1,2]Dept. of Mathematics, University of college of science, Osmania University, Hyd-07, Telengana.
E-mail: dalmalkapraveen@gmail.com [1], rameshwar@osmania.ac.in [2]

1.INTRODUCTION

One of the major problems in the thermos-fluids is the natural and forced convection flow and heat transfer in the presence of internal obstacles of several shapes and disposition and with several aspect ratios for both obstacles inside and of cavity along with or without varying of shapes and many other extensions.

Due to the simplicity of the LDC setup, it has been investigated quite extensively and serves as a benchmark to test numerical methods, manifold code development, and many fluid mechanical phenomena[4]. Physics involved in LDC flow has relevance to vivid applications: lake dynamics, heat exchangers,roll-coasting, galvanization, material processing.The increasing use of non-Newtonion fluids has contributed to practical and fundamental prominence to scientific applications in nonlinear science, flow properties polymer solutions, composite and biological materials, foodstuffs, etc.,[2]. Most of the findings in the literature are that the cavity is filled with a Newtonian. Few of them studied cavity filled with non-Newtonian Casson fluid flow, there are no findings on the installed obstacles in LDC with changing AR of obstacles by Fractional step method on straggered grid conjunction with ORK5 sheme for time integtation and stable,optimal SOR for poission equation.

2.MATERIALS AND METHODS:

The physical model shown in figure 1 consist of square cavity with the height of L.Essential assumptions:The domain is filled with the Casson fluid ,non-Newtonian fluid is in thermal equalibrium & 2-D flow is laminar,incompressible , unsteady. Mass force and slip (between the fluid and the wall are not considered) ,the square obstacle installed at the center is of width l aspect ratio is AR=l/L.

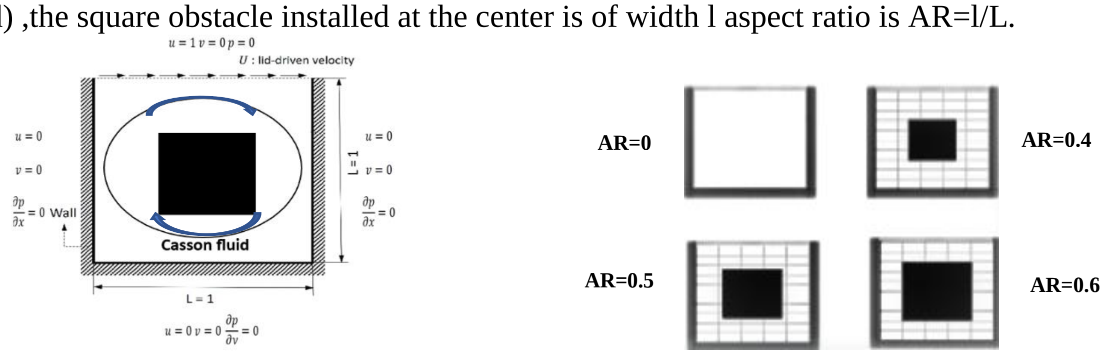

Fig.1 Schematic of LDC flow internal obstacle of AR=0,0.2,0.4,0.5,0.6 (at right) with boundary conditions.

The governing equations of continuity, momentum in dimenstional form:

$$\nabla \cdot \boldsymbol{U} = 0 \tag{1}$$

$$\rho\frac{D\boldsymbol{U}}{Dt} = -\nabla p + div(\tau) \tag{2}$$

where **U** = (u(x,y,t), v(x,y,t), 0) is the velocity of fluid, ρ is the density, p is the isotropic pressure, ∇ is

ICATP 2022, ISBN 978-81-952903-0-7

gradient operator,div is divergence operator, $\frac{D()}{Dt} = \frac{\partial()}{\partial t} + \mathbf{U}\cdot\nabla(\ )$ is the advective derivative,$e_{i,j}$ is (i,j)th component of deformation rate e and τ is extra stress tensor written as ,incompressible fluid follows casson phenomenological consitutive model,equation [3]:

$$\tau_{i,j} = 2\left(\mu_a + (e_{i,j})\left[\left(\frac{p_y}{\sqrt{2\pi_c}}\right)^{\frac{1}{n}}\right]^n\right) \tag{3}$$

Where μ_a is plastic viscosity,critical value depend on the non-Newtonian model of $\pi\left(i.e., \pi = e_{i,j}\, e_{i,j}\right)$. p_y is yield stress (of fluid). We chose n = 1 (for plasitic fluid), τ given in eq. (3) written as [3]:

$$\tau = -\mathrm{p}I + \left(1 + \frac{1}{\alpha}\right)\ [\nabla\mathbf{U} + (\nabla\mathbf{U})^{t}] \tag{4}$$

where $\alpha = (\mu_a \sqrt{(2\pi_c)})/p_y$, is the Casson fluid parameter. If $\alpha \to \infty$ then we get Newtonian fluid flow eqn.Make use of . (1), **U**, *and* $e_{i,j}$ in (1) and (2) and then Nondiminsionalised variables: velocity, length, time and pressure by the viscous scales $\frac{\nu}{L}$, L, $\frac{L^2}{\nu}$ and $\frac{\rho\nu^2}{L^2}$, resp., where L is the length of the sliding lid, ν is the kinematic viscosity and Re = UL/ν where U is velocity magnity of sliding lid.we also get nondimensionalised and bounadry conditions as shown in fig.1.

Then obtain non-dimenional, the mass eq. (1) and momentum conservation equations (2),(3) reduced to

$$\frac{\partial(\boldsymbol{u_i})}{\partial \boldsymbol{t}} = \mathbf{0}\ \boldsymbol{and}\ \frac{\partial(\boldsymbol{u_i})}{\partial \boldsymbol{t}} + \frac{\partial(\boldsymbol{u_i u_j})}{\partial \boldsymbol{x_j}} = -\frac{\partial(\boldsymbol{P})}{\partial \boldsymbol{x_i}} + \left(\mathbf{1} + \frac{\mathbf{1}}{\boldsymbol{\alpha}}\right)\left(\frac{\mathbf{1}}{\boldsymbol{Re}}\right)\frac{\partial^2(\boldsymbol{u_i})}{\partial \boldsymbol{x_i}\partial \boldsymbol{x_j}}, \qquad (\mathbf{5})\&(\mathbf{6})\ \boldsymbol{resp.}$$

The eqn.(5),(6) solved by fractional step method (FSM) jointly with Optimized five-stage Runge-Kutta (ORK5) for time integration, successive over relaxation method (SOR) for pressure eqn.in FVM. Solved in 3 stages:1) Stage: explicitly solve an auxiliary velocity without pressure term.

2)Stage: implicitly solve pressure is evaluated through Pressure poisson eqn. by the help of step1. 3)Stage: explicitly solve final required velocity field is evaluated by the help of step1and 2.

3. RESULTS AND DISCUSSION

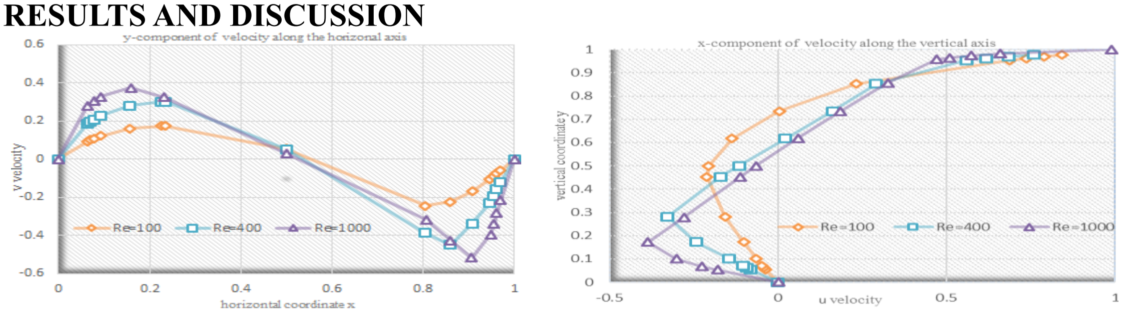

Fig.2 velocity profile:Comparison of of y-component (at left) , x-component (at right) of velocity with Ghai et al. experimental data as α → ∞.

AR=0,α→ ∞ AR=0.4,α=0.2 AR=0.5, α =0.2 AR=0.6, α =0.2 AR=0.4, ,α =0.93 AR=0.5, α =0.93 AR=0.6,α=.93

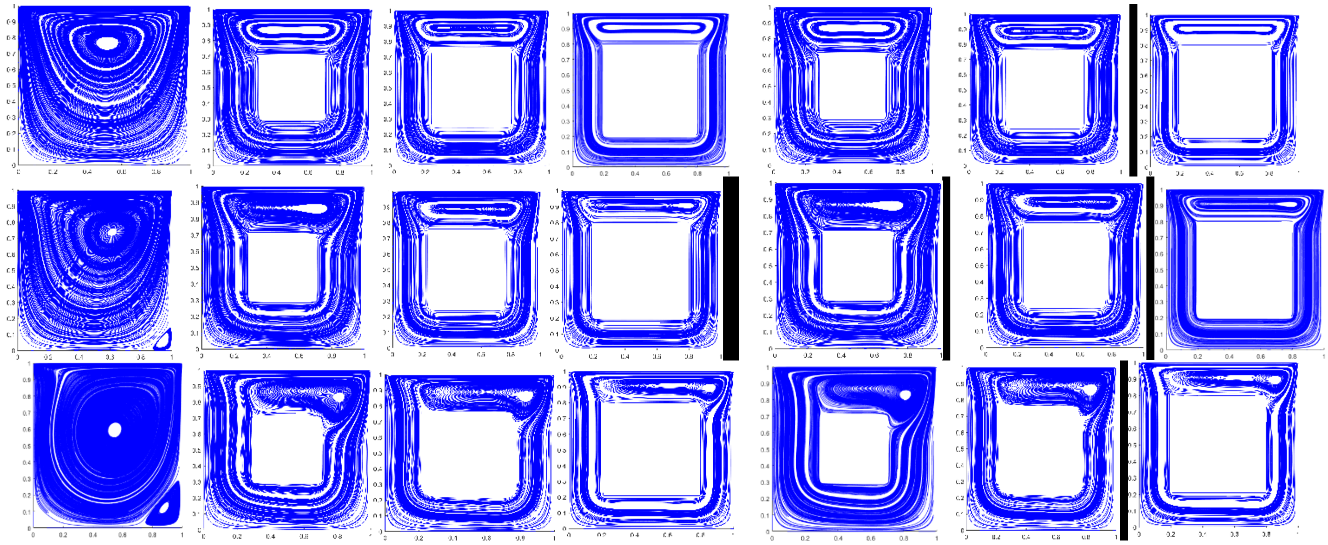

Fig.3:Streamline pattern with four ARs for two α values. 1st,2nd,3rd rows images for Re=10, 100 and 500. resp.

CONCLUSION

Numerical results show that fractional step method by FVM can accurately simulate the LDC problem of non-Newtonian Casson fluids (which are intricate than Newtonian fluids) in obstacle at centre.

a) we observed the size of the generated vortex increases as Reynolds number increases leading to effect in increase in magnitude of velocity, vorticity on top of obstacle and the secondary vortices at bottom right disappeared significantly in all taken non-zero AR compared to no obstacle(AR=0) figure b)Low Reynolds number chosen such that it demands in improved and complete mixing on the account of massive generated vortex as a regard to the AR of obstacle increases lead to flow region becomes compact in turn velocity increases to obey continuity. c) the Casson fluid parameter α has influence in strength of the vorticity with different AR, around the cavity observed dominant vorticity.

REFERENCES

[1] Kuhlmann, Hendrik (2018), The Lid-Driven Cavity,10.1007/978-3-319-91494-78.

[2] Chhabra, R.P., Richardson,J.F. (1999) Non-Newtonian Flow in Process Industries. Fundamentals and engineering applications ,Butterworth-Heinemann, Oxford.

[3] Nakamura M, Sawada T. (1988), Numerical study on the flow of a non-Newtonian fluid through an axisymmetric stenosis. ASME J Biomechanical Eng;110:137–143.

[4] Shankar P. N, and M. D. Deshpande (2000) Fluid mechanics in the driven cavity. Annual Review of Fluid Mechanics; 32: 93-136.

CHAPTER -30

Sixth and seventh-order derivative-free parameter-based iterative method for solving nonlinear equations

Kasmita Devi[1], Prashanth Maroju[2]
[1]Department of Mathematics, School of Advanced Sciences, VIT AP University, Amaravati, Andhra Pradesh
[2]Department of Mathematics, School of Advanced Sciences, VIT AP University, Amaravati, Andhra Pradesh

Abstract
In this article, we propose a two-second derivative-free parameter-based continuation method for solving nonlinear equations. According to Kung-Traub conjecture, both the suggested methods are optimal. Furthermore, two essential theorems which show the order of convergence and asymptotic error constant along with the theoretical and computational aspects of the proposed strategy are closely researched. The order of convergence of the proposed method is six for $\alpha = 0$ and seven for $\alpha = 1$. The performance and effectiveness of the proposed optimal methods are compared with their closest competitors on a concrete variety of nonlinear equations with the help of Mathematica-7, by using its high precision compatibility. Ultimately, based on the results, it is concluded that our proposed methods are found to be more effective than the similar robust methods of the same order.

ICATP 2022, ISBN 978-81-952903-0-7

CHAPTER -31

MARANGONI BOUNDARY LAYER FLOW AND HEAT TRANSFER OF NANOFLUID WITH MASS TRANSPIRATION: DARCY-BRINKMAN MODEL

T. Anusha[1], U. S. Mahabaleshwar[2*]
[1,2]Department of Mathematics, Shivagangotri, Davangere University, Davangere, India
[1]E-mail: anushat.math@gmail.com, [*]E-mail: usm@davangereuniversity.ac.in

Abstract

The current work considers the 2-dimensional incompressible flow and heat transfer over porous medium with mass transpiration and Marangoni boundary condition. The graphene nanoparticles are mixed in water base fluid to enhance the thermal conductivity of the fluid. It can acts as heater upon increase of its solid volume fraction, Eckert number, injection and can act as cooler upon increase of suction. The governing equations of the defined flow forms a system of partial differential equations (PDEs) and those are then transformed into system of ordinary differential equations (ODEs) upon applying the suitable similarity transformations. The solutions for velocity profile and temperature distribution are found from obtained system of ODEs. The results are analyzed through plotting graphs and effect of different parameters such as Marangoni number, inverse Darcy number, Brinkman ratio, Prandtl number and Eckert number is analyzed. The work of Marangoni boundary layer flow has many industrial applications in paints, glues, crystal growth in space etc.

Keywords: Brinkman ratio, Eckert number, Graphene, Marangoni number, porous media.

CHAPTER -32

A STUDY OF TERNARY HYBRID NANOFLUID FLOW DUE TO POROUS STRETCHING/ SHRINKING SHEET WITH MASS TRANSPIRATION AND THERMAL RADIATION

A.B. Vishalakshi[1], U.S. Mahabaleshwar[2]

[1]Department of Mathematics, Shivagangotri, Davangere University, Davangere 577007, India Email: vishalavishu691@gmail.com
[2]Department of Mathematics, Shivagangotri, Davangere University, Davangere 577007, India Email: u.s.m@davangereuniversity.ac.in

Abstract

Ternary hybrid nanofluid flow with transfer of heat under the impact of transpiration and radiation is studied in the present analysis. The PDES of the current work is mapped by using a similarity variable to convert into ODEs form. The volume fractions of the ternary hybrid nanofluid is used in the entire calculation to achieve better results. The momentum equation is investigated exactly to yield the value of domain. The impact of thermal radiation and is considered under energy equation and solved analytically with solution domain to yield the temperature profile. The impact of parameters namely, thermal radiation, heat source or sink parameter and porous medium parameter can be analysed with the help of graphical arrangements. The current work is considered under many industrial applications.

Key words: Ternary hybrid nanofluid; mass transpiration; porous medium; thermal radiation, stretching/shrinking sheet.

CHAPTER -33

A Single Server Queue with Second Optional Service and Working Breakdown

B. Somasundaram[1], A. Kavin Sagana Mary[2], R. Lokesh[3] and S. Karpagam[4]

Department of Mathematics, Vel Tech Rangarajan Dr Sagunthala R&D Institute of Science and Technology

somu.b92@gmail.com[1] kavinmary28@gmail.com[2] rlokesh1020@gmail.com[3] karpagammaths19@gmail.com[4]

In this study, a single server queuing system with second optional service and working breakdown is investigated. We assume that the batch of customers arrive to the system according to a compound Poisson process and service follows general distribution. The concept "working breakdown" refers to a system failure that can happen to a server at any time when it is in operation. These queueing systems have been utilized in a wide range of industries, including banking, various machine categories, flexible manufacturing, e-commerce, supply-chain systems, computer systems, and telecommunications.

Yen et al. [4] discussed the optimization analysis of the N-policy $M/G/1$ queue with working breakdown. Ammar et al. [1] developed and analysed preemptive priority retrial queuing system with disaster services and working breakdowns. Yang et al. [3] presented a optimization of two-server queue with multiple vacations and working breakdowns. The concept of working breakdowns was introduced by Kalidass and Kasturi [2].

Mathematical Description

Customers enter the system in batches of varying sizes according to compound Poisson process, and they are served one by one at a time on a 'first come - first served' basis. The first essential service is required by all arriving customers, and its distribution function and density function are $B_1(x)$ and$b_1(x)$ respectively. When a customer's first essential service is completely finished, they may opt for the second optional service with probability p in which their optional service will immediately start. Otherwise, with probability 1-p they may decide to exit the system, in which case a new customer (if any) is picked for their first essential service from the head of the queue. The optional service is also assumed to follow the general distribution, $B_2(x)$ and $b_2(x)$. When servicing a customer at first stage or second stage, the system may get breakdown and the breakdown times are supposed to occur under Poisson process with parameter α. After breakdown, instead of stopping the service completely, the server will complete the current service at slower rate. After the completion of current service at a slower rate, the server is sent to repair. Meanwhile after the repair, when the server returns to the system and if there are no customers in the system, the server remains in the

ICATP 2022, ISBN 978-81-952903-0-7

idle state and waits for the customers to arrive. Some of the numerical results and graphical representations were also presented.

Numerical Results

According to Figure 1, as the breakdown rate (α) has risen, the idle time (I) begins to fall, the expected queue size (L_q) tends to rise, and the expected waiting time of the customers in the queue (W_q) also tends to rise.

Figure 3: Expected queue lengths size, Expected waiting time, Idle time of customers verses breakdown rate

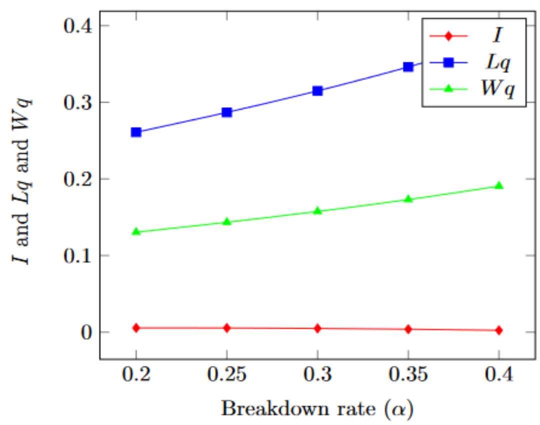

References

[1]. Ammar, S. and Rajadurai, P.(2019). Performance Analysis of preemptive priority retrial queueing system with Disaster under Working Breakdown Services. *Symmetry*, 11(3): 419 - 425.

[2]. Kalidass, K. and Kasturi, R.(2012). A queue with Working Breakdowns. *Computers and Industrial Engineering,* 63(4):779 - 783

[3]. Yang, D., Chen, Y. and Wu, C.(2019). Modelling and optimisation of a two-server queue with multiple vacations and working breakdowns. *International Journal of Production Research*, 58(10):1-13.

[4] Yen, T., Wang, K. and Chen, J.(2020). Optimization Analysis of the N Policy M/G/1 Queue with Working Breakdowns. *Symmetry*, 12(4): 583 – 594.

CHAPTER -34

OPTIMIZATION OF PROCESS PARAMETERS OF Al-6061 CASTINGS PRODUCED BY MICROWAVE ENERGY TECHNIQUE

Md Modassar Anwar[1], Mr. Girendra Bhati[2*], Mr. Vaibhav Gangwar[2]

[1] Research Scholar, Greater Noida Institute of Technology, Greater Noida, Gautam Buddha Nagar, U.P.201310, India

[2] Assistant Professor, Greater Noida Institute of Technology, Greater Noida, Gautam Buddha Nagar, U.P.201310, India

* Corresponding Author: Phone No.: +91-9910819291; Email: girendrabhatime@gmail.com

ABSTRACT

In this paper, microwave energy has been used to heat the Al 6061 metal to produce the casting products with more dimensional accuracy and surface finish. The applicator used for the melting, having 2.45 GHz microwaves at 600 W to 900 W. Three most significant process parameters with different levels have been selected as power, susceptor material and heating time. Optimization of process parameters indicated that the maximum value of hardness has been achieved at 750W power, stone charcoal susceptor and 180 minutes heating time. The optical microstructures have been studied for the most harder casting specimens.

Keywords: Microwave Casting Technique; Al-6061 alloy, Hardness strength, Microstructure Study

1. INTRODUCTION

The research we are working on is Al-6061/SiC charcoal using the microwave casting technique. We know about some materials and reinforcement like aluminum; silicon carbide and charcoal matrix composites. Which is used in automotive industries due to its tensile strength, more strength to weight ratio, more wear resistance, elevated temperature hardness, and more stiffness. Microwave energy can be effectively used for metal processing. In microwave processing, the fundamental of heating is the opposite of the traditional heating process. In the conventional heating process, the heat is conducted from the surface them to the inner core of the metal. So, heating is uniform throughout the material[1-8].

2. MATERIALS AND METHODS

Aluminum alloy 6061 has been selected as the pouring metal because of it has brilliant mechanical properties and great pliability, high strength, hardness, and great protection from exhaustion displayed in Figure.1. The support's silicon carbide properties of the composites like tractable way of behaving, influence strength, and flexural conduct were concentrated as an element of filler stacking displayed upgrades in the mechanical outcomes [9-10]. In this technique of microwave, the melting of Al-6061 has been takes place inside the apparatus that has microwave hybrid heating process with charge of subsector material. In in-situ casting process, the molten material has been solidified inside the microwave oven and in ex-situ molten has been placed outside the oven during solidification process [11]. The microwave casting process performed the experiment activated charcoal and, on that Al-6061 alloy and silicon block has been taken. [12].

Figure 1. Al-6061 alloy **Figure 2. Silicon block** **Figure 3. Microwave casting setup**

Figure 4. Microwave casting experimentation with specimen

5. RESULTS AND DISCUSSION

5.1 Hardness Test

The hardness measurements on Al-6061/SiC hybrid composite are taken using Brinell hardness testing machine as per the ASTM E10-08 standard at 100 kgf load on samples having different reinforcement particles of SiC with stone charcoal powder. The hardness value is found to increase with increased wt% of silicon carbide reinforcement. The show table 3 average value of hardness is 33.66 [1]

Table 3. Test data summery for Hardness

Experiment Run	Power	Susceptor	Heating Time	Trial 1	Trial 2	Trial 3	Hardness	S/N Ratio
1	6	WC	120	46.19	47.20	48.21	47.7	33.5867
2	6	SiC	180	58.09	59.10	60.11	59.2	35.4596
3	6	SC	240	36.08	37.16	38.20	37.5	31.4899
4	7	WC	180	47.33	48.35	49.10	48.9	33.7986
5	7	SiC	240	46.06	47.07	48.08	47.2	33.4807
6	7	SC	120	57.31	58.30	59.29	58.9	35.4053
7	9	WC	240	47.09	48.08	49.07	48.2	33.6699
8	9	SiC	120	37.16	38.15	39.14	38.4	31.6979
9	9	SC	180	55.20	56.31	57.29	56.9	35.1038
Average								**33.7436**

5.2 Taguchi Design

Analysis of Variance

Source	**DF**	**Adj SS**	**Adj MS**	**F-Value**	**P-Value**
Power (W)	2	26.99	13.493	0.09	0.006
Susceptor	2	15.64	7.822	0.05	0.050
Heating Time (min)	2	175.91	87.954	0.03	0.027
Error	2	295.58	147.792		
Total	8	514.12			

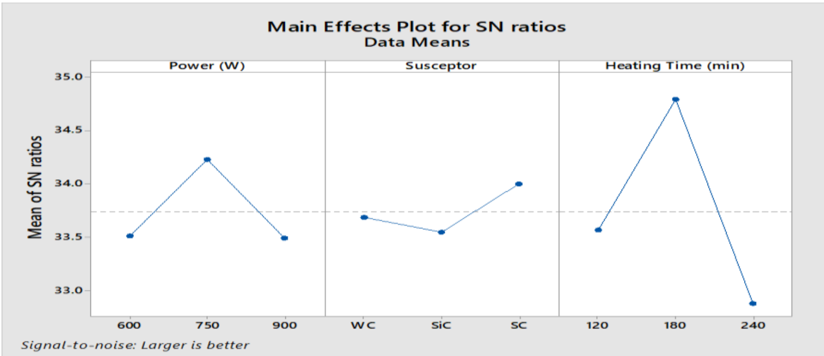

Figure 5. Main effects plot for SN ratios

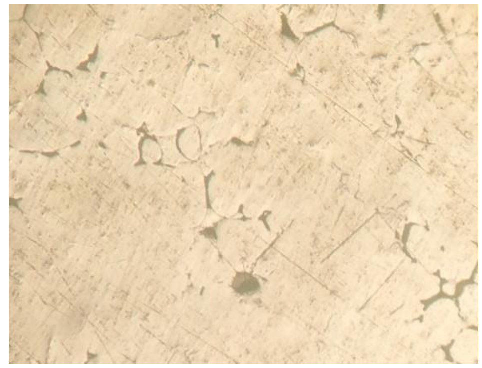

Figure 6. Optical microscope test

5.2 Optical Microscope Test

In the research optical micrograph of Al-6061 castings with susceptor of silicon carbide (SiC) and stone charcoal powder has studied. The grain boundary of specimen at optimized, shown in fig.7.

6. CONCLUSIONS

This research work concludes the following observations-

- This technique complete experimental analysis by Taguchi method orthogonal L9 array.
- The effect of the type of material of susceptor and microwave power has significantly increased value of the hardness.
- Optimization of process parameters indicated that the maximum value of hardness has been achieved at 750W power, stone charcoal susceptor and 180 minutes heating time.
- The range of predicted optimal value of hardness is: 37.54 BHN to 59.29 BHN.

REFERENCES

1. Rajkumar K., Rajan P, and Charles J. Maria Antony,(2014) Microwave Heat Treatment on Aluminum 6061 Alloy- Boron Carbide Composites.Procedia Engineering 86, 34 – 41.
2. SinghShivinder, Belokar R. M, SuriN. M (2019) Fracture Analysis of Microwave Induced Al6061 Joints International, Journal of Engineering Trends and Technology (IJETT) - Volume 67 Issue 1.
3. Zaheerabbas B. Kandagal, Akkimardi V.G. and Sonnad A.N. (2020) Investigation on Mechanical Properties of Microwave Welded Al6061Graphite Metal Matrix Composites,International Journal of Applied Engineering Research ISSN 0973-4562 Volume 15, Number 7 pp. 682-689.
4. Adnan Khan, Motasem W. Abdelrazeq, Manohar Reddy Mattli, Moinuddin M. Yusuf, Abdullah Alashraf, Penchal Reddy Matli and R. A. Shakoor,(2020),Structural and Mechanical Properties of Al-SiC-ZrO2 Nanocomposites Fabricated by Microwave Sintering Technique.
5. Singh Satnam, Singh Praveen, Gupta Dheeraj, Jain Vivek, Kumar Rohit, Kaushal Sarbjeet,(2019) Development and characterization of microwave processed cast iron joint ,Engineering science and technology an international journal, 22,569-577.
6. Mishra and sharma, et, al (2019), "On mechanism of in-situ microwave casting of AA7031 and cast microstructure", Vol 72, pp104-120.

CHAPTER -35

IMPACT OF EXISTING TRANSPORTATION SYSTEMS ON ENVIRONMENT: NEED FOR SUSTAINABLE MODES OF TRANSPORTATION

Harsees Kaur[1], Prashant Maroju[1], Anil Carie Chetupally[1]

[1]Vellore Institute of technology – AP University,
Amaravati, Andhra Pradesh

harsees.21msd7020@vitapstudent.ac.in

INTRODUCTION

Transportation is defined as a medium for carrying goods, people and animals from one place to another and it has existed since humans stepped foot on this earth. A transportation network is the backbone of any economy, however, it has various environmental externalities which cannot be ignored. A major proportion of greenhouse gas emissions are carbon dioxide (CO2) emissions which are a result of transportation. This is the point where the concept of a sustainable transportation system comes into the picture. To achieve this, there is a need to harmonize economic growth, mitigate climate change, and environmental protection. It refers to energy-efficient, minimal emission modes of transport. However, which mode of transport requires an urgent need for sustainability is what will be discussed in this paper by analyzing on the basis of carbon dioxide (CO2) emissions thereby concluding the most sustainable vehicles. In this regard, various policies and decisions are made by various governments and legislators which leads to diversity in nature, and all these strategies are required to go through the recognition of consumer inclination towards particular transportation methods, and communication routes, among numerous others. Therefore, in addition, this paper also discusses how machine learning is applied to guide policy and decision-makers in making well-informed decisions while developing and maintaining a Sustainable Transportation Network.

MATERIALS AND METHODS

1. Analysis of CO2 emission levels from different transport sectors. In this step, we understand which mode of transport contributes to the highest level of CO2 emissions. The study employed is an exploratory analysis approach using Python and an interactive data visualization. Required libraries were imported such as - pandas to load the data and Matplotlib. For dataset preparation and analysis, Queensland's dataset of annual greenhouse gas emissions of carbon dioxide by the transport sector is taken.
2. This analysis focuses on comprehending message content as the basis from which inferences and conclusions about sustainable transport research are drawn in relevance to this paper. A review of data science and machine learning approaches with respect to transportation analytics is done from existing works including - Sustainable smart cities by Majumdar et al. [6], Balancing different modes of transportation in the city by Migliore et al. [7], Challenges in expanding the use of electric vehicles in the USA by Asensio et al. [2] among various others.

RESULTS AND DISCUSSION

From this paper, we conclude which sectors of transportation need the most sustainability measures from the Analysis part 1. The results obtained depict the top 4 modes of transport that are - Cars, Heavy-duty Trucks, Light commercial vehicles, and Domestic aviation contributing 49.0%, 21.9%, 12.9%, and 8.6% of CO_2 emissions respectively. Emissions from cars being the highest, call out the need for encouraging the use of electric cars.

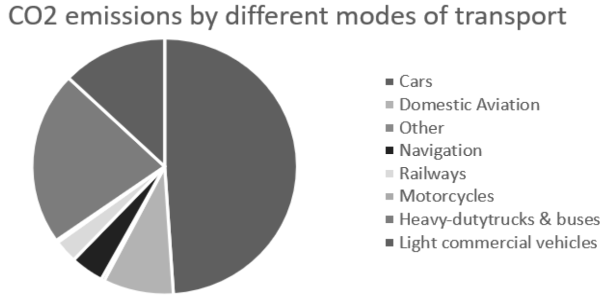

Figure 1. CO2 emissions by different modes of transport

It can be suggested to governments and policymakers that the above-mentioned 4 sectors of modes of transportation need more investment and attention as compared to others. We can also conclude that decision trees and neural networks have been employed repeatedly for prediction motives. It can be further said that the pollutant emissions can possibly be reduced by about 80% or even more by employing artificial intelligence algorithms and usage of 'green' energy source vehicles, electric cars for instance.

CONCLUSION

To mitigate the damage generated by CO_2 emissions generated by various modes of transport, in this paper, we conclude that cars and Heavy-duty Trucks and buses need the most attention for a sustainable transport system in terms of investment and inventions. We also conclude that an efficient combination of vehicle pooling practices and environment-friendly modes of transportation contributes to the reduction of traffic congestion, and unnecessary combustion of fuels thereby reducing CO_2 emissions to a great extent.

REFERENCES

1. Antoniou, C.; Dimitriou, L.; Pereira, F. Mobility patterns, big data and transport analytics: tools and applications for modeling; Elsevier, 2018.
2. Asensio, O.I.; Alvarez, K.; Dror, A.; Wenzel, E.; Hollauer, C.; Ha, S. Real-time data from mobile platforms to evaluate sustainable transportation infrastructure. Nature Sustainability 2020, pp. 1–9.
3. Darido, Georges & Torres-Montoya, Mariana & Mehndiratta, Shomik. (2014). Urban transport and CO2 emissions: Some evidence from Chinese cities. Wiley Interdisciplinary Reviews: Energy and Environment. 3. 10.1002/wene.71.
4. Liang, L.; Xu, M.; Grant-Muller, S.; Mussone, L. Household travel mode choice estimation with large-scale data—an empirical analysis based on mobility data in Milan. International Journal of Sustainable Transportation 2019, pp. 1–16.
5. Li, Y., Sun, Y. Modeling and predicting city-level CO2 emissions using open access data and machine learning.
   Environ Sci Pollut Res 28, 19260–19271 (2021).
6. Majumdar, S.; Subhani, M.M.; Roullier, B.; Anjum, A.; Zhu, R. Congestion prediction for smart sustainable cities using IoT and machine learning approaches. Sustainable Cities and Society 2020, 64, 102500
7. Migliore, M.; Burgio, A.L.; Di Giovanna, M. Parking pricing for a sustainable transport system. Transportation Research Procedia 2014, 3, 403–412.

ICATP 2022, ISBN 978-81-952903-0-7

CHAPTER -36

ANALYSIS OF GLOBAL WARMING USING QUADRATIC REGRESSION AND ARIMA MODEL

Hrishikesh, Puranik[1], and Kiran Kumar, Patra[2]

[1,2]VIT-AP University, Andhra Pradesh, India
Email: hrishikesh.21msd7008@vitapstudent.ac.in

Keywords: quadratic regression, ARIMA model, global warming, machine learning.

INTRODUCTION

In today's world it is critical to limit the impacts of global warming and fight to prevent its catastrophic consequences which can harm humans and living beings in the long run. Predicting the effects of global warming and wheather conditions in a long term run could be extremely useful in the field of climate science, agriculture and medicine. For eample the impact of climate change and weather in transport was studied by Mark and Piet (2009). A linear model of aquaculture of the crossroads of global warming was discussed by Miriam R. And et al. (2020). But the research work in this direction using multiple regression model were rarely found. This article is an attempt to find a prediction and forecasting of temerature and green house gases for upcoming years in India by suing a quadratic regression and ARIMA model (Radhika and Shashi (2009)).

MATERIALS AND METHODS

We provide statistical methodology based machine learning algorithm for predicting global temperature and best parabola fit for it from past years of collected global data in this study. The prime motive of this study is to analyse effects of global warming (Umair (2015)) in India for a long term period of approximately 60 years based on the available data recorded at different places like Kaggle, Data.gov.in, https://www.co2levels.org/, https://www.N2olevels.org/ and https://www.methanelevels.org/, etc. Following Deva et al.(2019), an appropriate quadratic regression and ARIMA model a best fit to the trending data of temperature in Indian climate is found in this work. This result can help to speculate the temperature of the future years.

RESULTS AND DISCUSSION

More than adequate accuracy is achieved for both the temperature forecast and the greenhouse gas prediction following a successful training of the temperature and greenhouse gas data. We have examined the results obtained by Deva et al.(2019), who conducted the processes using linear regression, with our findings using quadratic regression. If the prediction is accurate, the ARIMA model will be used to estimate India's temperature trend for the next years, and the matplot library will be used to create a graphical representation of the expected and forecasted data. The forecast graph shows that the linear pattern of regular temperature increases and physical forces contributing to global warming will continue.

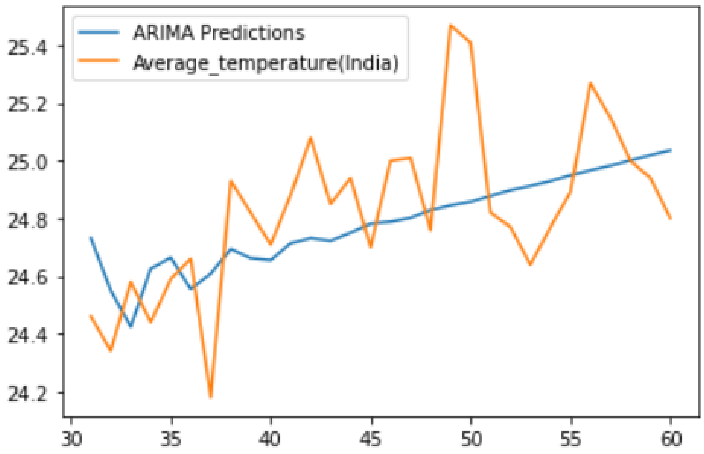

Figure:(Temperature trend using ARIMA)

CONCLUSION

In the present work, the authors analysed the temperature and green house data of 60 years using the quadratic regression and based on the findings form the analysis, we forecasted the average of the same for upcoming years. The expected and forecasted data are plotted using the Matplot package and the ARIMA model. As a result, it has been revealed that a model for predicting data for future years is trained and validated using a range of input variables, including temperature, carbon dioxide, methane, and nitrous oxide.

REFERENCES

Mark J.K., and Piet R., 2009. The impact of climate change and weather on transport: An overview of empirical findings. Transport research part D: Transport and Environment. 14: 205-221.

Miriam R. et al., 2020. Aquaculture of cross roads of global warming and antimicrobial resistance. 11:1870.

Deva, H., Anirban, P., Vineet, L., and Rajeev, G, 2019. Global Warming Prediction in India using Machine Learning. IJEAT, 9: 2249– 8958.

Radhika Y., Shashi, M., 2009. Atmospheric Temperature Prediction using Support Vector Machines. IJCTE, 1: 1793-8201.

Umair S.. 2015. Global Warming: Causes Effects and Solutions. Durre Samin Journal, 4: 1-7.

CHAPTER -37

ARDUINO UNO-BASED GSM SMART ENERGY METER

V. Manoj[1], G. Sudheshna[2], B.Yamini[3], M.Dheeraj[4], A.Upendra[5]

[*1]Assistant Professor, Department of Electrical and Electronics Engineering, GMR Institute of Technology, Rajam - 532127, Andhra Pradesh, India
[2,3,4,5]UG Student, Department of Electrical and Electronics Engineering, GMR Institute of Technology, Rajam - 532127, Andhra Pradesh, India

[1]manoj.v@gmrit.edu.in, [1]manojv287@gmail.com, [2]19341A0229@gmrit.edu.in, [3]19341A0214@gmrit.edu.in, [4]19341A0254@gmrit.edu.in, [5]19341A0205@gmrit.edu.in

INTRODUCTION

For past ten years, mart has been researching and developing electrical energy meter technology. Electricity consumption can be measured using a variety of technologies. The Energy Board will send the bill to customers by a variety of channels, including email, mail, and phone. Traditional electro-mechanical watt meters are still widely used in Malaysia, and the readings are not automated. To pay their electricity payment, customers will have to wait a month for the bill of energy consumption. Meter bill collectors typically visit each home at the end of the month to read the meter and hand out the bill. Electrical meter, or energy meters, are devices that measure the quantity of electricity used in a residential or commercial setting, such as a home or office.

MATERIALS AND METHODS

The full Smart Energy metering and billing system is implemented using Arduino and GSM technology in this article. It's the only spinning and digital energy meter that is used to monitor power and energy use.

Overall circuit:

The main circuit of this project consists of 6 units as follows:

- AC Supply unit
- Voltage measurement circuit (DC 5 V)
- Current sensor (ACS712) unit with Power supply
- Arduino unit
- Display unit
- GSM unit with Mobile

RESULTS AND DISCUSSION (headlines: TNR Bold, 12pt)

The system is made up of two components. Both the circuit for connecting an energy meter to Arduino and the interface for connecting a GSM module to Arduino were unified. The microcontroller had the correct programmed sequence and was able to run the circuit with no issues. To count the input, compute the bill, and save it in EEPROM, an Arduino board with an ATmega238 microcontroller was utilized. Every month, a Real Time Clock was used to reset the counter. When a sensor recognized an input, an LED indicator blinked. The LCD screen displayed the unit and bill price values according to the microcontroller's settings. We set a restriction for how many mobile

ICATP 2022, ISBN 978-81-952903-0-7

phone users were to receive a notification when the limit had been reached. Network plan SIM cards were used in GSM to transfer messages to mobile phones in GSM networks. The GSM module Tx and Rx were linked to Arduino pins 2 and 3 while the RTC utilised analogue pins A4 and A5 for CLOCK and RS correspondingly. Connecting LCD, LED, and light-to-voltage sensor to digital port 4 to 13 was the final step. It's easy for users to see their current energy bill by typing "my meter" into the command line and then sending it to their energy meter, as illustrated in Figure.

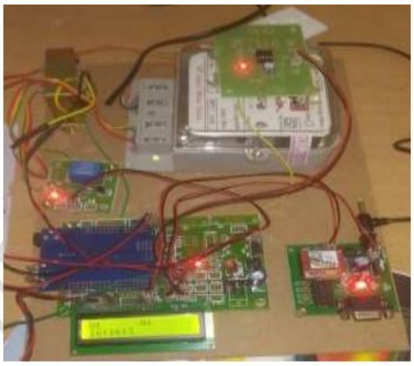

Figure 1. GSM Based Smart Energy Meter with Arduino Uno

CONCLUSION

In the proposed system, consumers who fail to pay their bills would have their electricity cut off by a wireless energy meter that constantly monitors the meter reading. There is no need for a human to take a reading, and you'll get accurate information. Information relevant to the user's actions is shown on the screen (LCD). At the end of the month, the client can pay his bill with a debit card using an SMS and the card reader built into the energy meter, all without leaving his house.

ACKNOWLEDGMENT

The authors would like to express their gratitude to the management of GMR Institute of Technology for providing the essential resources and facilities for completion of the project work.

REFERENCES

[1]. Aswatht D. R., C. Shabthi , “An Automated Energy Metering System Home Based Approach” International journal of Advance Research in Electrical, Electronics and Instruments Engineering-2017.

[2]. De Capua, C.et al., “A smart energy meter for power grids”, Conference Record - IEEE Instrumentation and Measurement Technology Conference, 2014, pp.878–883.

[3]. Ghaderi, M and Boutaba, “Call Admission Control in Mobile Cellular Networks : A Comprehensive Survey”, Wireless Communications and Mobile Computing, Vol. 6, No.1, 2006, pp 69-93.

[4]. Kumar Sehgal, V. et al, “Electronic energy meter with instant billing”, Proceedings – UK Sim 4th European Modelling Symposium on Computer Modelling and Simulation, EMS, 2010, pp.27–31.

[5]. Srividyadevi P., Pusphalatha D.V. and Sharma P.M. Gokaraju , “Measurement of Power and Energy Using Arduino”, Research Journal of Engineering Sciences. ISSN 2278 – Oct 24, 20 Vol. 2(10) /2018.

[6]. Sneha Salunkhe1, Dr.(Mrs.) S. S. Lokhande2, A Review: AUTOMATIC METER READING USING IMAGE PROCESSING, International Journal of Application or Innovation in Engineering & Management (IJAIEM), Volume 5, Issue 6, June 2016.

[7]. V.Preethi, G. Harish,” Design And Implementationof Smart Energy Meter”, Inventive Computation Technologies (ICICT), 26- 27 Aug. 2016.

CHAPTER -38

SPEECH EMOTION RECOGNITION USING WAVE PLOTS AND SPECTROGRAM ANALYSIS

[1] Sayak Karmakar, [1] Santanu Mandal

[1] School of Advanced Sciences, VIT-AP University

[1] santanu.mandal@vitap.ac.in

Introduction

Over the last few decades, one of the most intriguing challenges in speech processing has been speech emotion identification. Modeling the emotion recognition process helps to understand and evaluate the system's performance. The act of attempting to work on human emotion and the induced states from their speech is known as Speech Emotion Recognition, or SER. This takes use of the fact that voice tone and pitch frequently reflect underlying emotion [1]. This holds the same mechanism that animals such as horses and dogs use to interpret human emotion. In order to demonstrate the emotion recognition problem which is independent from the speaker, a speech emotion recognition approach is proposed that classifies four speech motions from coarse to fine, including sadness, rage, fear, and happiness. This paper introduces a method by analysis of wave plots and spectrograms of audio wave files and finding patterns between different emotions while narrating the same sentence. This is done by visualizing the audio waveforms with wave plots and spectrograms and compares the wave pattern and amplitude of each emotional speech waveform with other related ones.

MATERIALS AND METHODS

The dataset used in this paper consists of 6 different people speaking a single sentence in 4 different emotions. These audio recordings are from the CREMA-D [2] collection, which contains 7,400+ original clips performed by 91 actors. These clips featured 48 male and 43 female actresses between the age from 20 to 74, representing a diverse range of races and ethnicities. The audio files have been visualized using wave plots and spectrograms to find out similarities between each emotion. Various specific features like the amplitude, loudness (decibel) and the frequency spectrum of sound or other signals as it varies over time have been observed and the waveform patterns along with the loudness for each emotion has been inferred out in this method.

RESULTS AND DISCUSSION

The wave plots show how the amplitude of a signal changes over time. The spectrogram, on the other hand, shows how the frequencies of a signal change over time. The third dimension is then used to represent amplitude, which can be depicted with varying brightness or colour. It gives us a full perspective of audio, with time, frequency, and amplitude all represented on a single graph. A spectrogram can visually depict broadband, electrical, or intermittent noise in audio, allowing us to quickly distinguish between distinct patterns for different emotions [3].

We can primarily subcategorize the ‘fear’ and ‘angry’ emotions from ‘sad’ and ‘happy’ emotions based on their amplitude range in spectrograms. The former two have a range between 40 to –30 dB units whereas the latter two have the range between 0 to –60 dB units. Observing more, we could state that ‘angry’ and ‘happy’ emotions have a more spiked waveform as compared to ‘fear’ and ‘sad’.

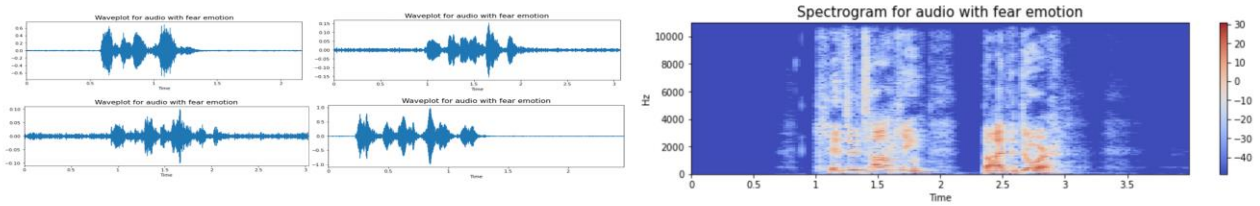

Figure 1. (a) Wave plots for ’fear’ emotion of 4 different persons. (b) Spectrogram for ‘fear’ emotion.

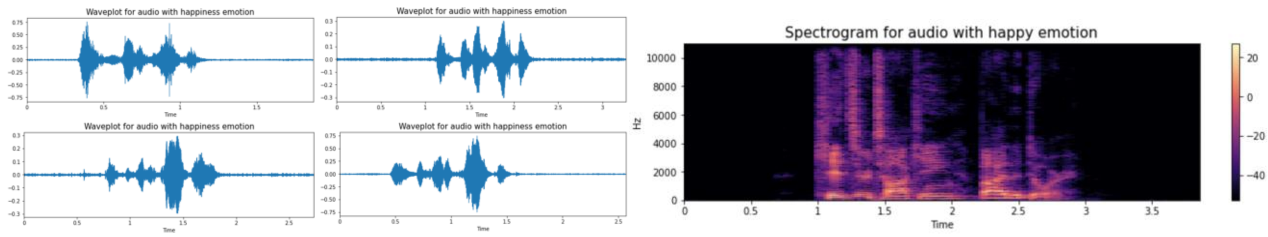

Figure 2. (a) Wave plots for ’happiness’ emotion of 4 different persons. (b) Spectrogram for ‘happiness’ emotion.

These plots have been visualized for all the four emotions for all six persons’ audio files and patterns between each emotion have been deduced.

CONCLUSION

The proposed method gives us identifiable patterns of audio waveforms for different waveforms. We first categorize the emotion based on the amplitude from the spectrogram into ‘fear/angry’ or ‘sad/happy’ categories, followed by observing the wave plot for the more spiked waveform, indicating either ‘angry’ or ‘happy’. A decision tree-based model [4] could be implemented using the findings of this work to classify the emotions based on the visualizations.

This method gives us the advantage of predicting and recognizing the emotion of a person by visually looking at the wave plots and spectrograms of that person’s speech which can be further worked on to develop Speech Emotion Recognition models using a wide and larger dataset.

Refernence

[1] Lijiang Chen, Xia Mao, Yuli Xue, Lee Lung Cheng. 2019. Speech emotion recognition: Features and classification models.
[2] Dataset: https://www.kaggle.com/code/shivamburnwal/speech-emotion recognition/data/input/cremad/AudioWAV/
[3] Dias Issa, M. Fatih Demirci, Adnan Yazici. 2020. Speech emotion recognition with deep convolutional neural networks.
[4] Agnes Jacob. Modelling speech emotion recognition using logistic regression and decision trees; 2019.

CHAPTER -39

Numerical Solution of coupled Lane-Emden-Folwer type equation by embeded Quasilinearization method with homotopy analysis method

Vikash Kumar Sinha[1], Prashanth Maroju[2]
[1]Department of Mathematics, School of Advanced Sciences, Vellore Institute of Technology, Amaravati, Andhra Pradesh, India
[2]Department of Mathematics, School of Advanced Sciences, Vellore Institute of Technology, Amaravati, Andhra Pradesh, India
E-mail(prashanth.m@vitap.ac.in)

Abstract
In this paper, we study the solution of the system of Emden-Folwer type equations by embedding the quasilinearization algorithm within the spectral homotopy analysis method. This approach easy to implement and converges to the solution very fast. The convergence analysis of our method is discussed in Banach space. Some Numerical examples of type highly nonlinear ordinary differential equations are taken to ensure the validity, generality, and accuracy of our proposed method. We calculate the approximate analytic solutions and compare with the existing Adomanian decomposition method. We observe that our approach gives better accuracy than the existing ADM.

CHAPTER -40

UNDERSTANDING FOREST FIRE SPREAD USING PERCOLATION MODEL

S. Sweta Reddy [1] and Santanu Mandal[1]

[1] School of Advanced Sciences, VIT-AP University, India.

santanu.mandal@vitap.ac.in

Introduction

The percolation theory was introduced in mathematics literature and physics to describe the nature of clustered components in random networks. Percolation is the most basic statistical mechanics model that exhibits phase transitions marked by the appearance of a massive linked component. An enormous study has been carried out on percolation theory and has been applied to large variety of social and natural systems, one of them being forest fire spread. This survey introduces a simple model for the propagation of fire through forests. It also consists of studying the burn patterns and characteristics of combustible sites.

Materials and Methods

Scrutinizing the percolation problem in a d-dimensional hypercubic lattice, Z^d. There exists a critical threshold p_c, satisfying, $0<p_c<1$ commonly known as percolation threshold. The connectedness of random network is elaborated by percolation model known as percolation network [Fig.1.]. The probability of one ignited tree to lit up its neighbors and spread the fire is taken as 'p' and of not lighting is '1-p'. The study investigated that the p value which highly effects the percolation spread of fire decreases exceptionally when the mean number of spread falls below the critical point. The critical point is said to be reached when the percolation threshold equals the p-value exactly. Here, the probability function is corrected mathematically to combat the exceptional variability [1]. The model is used to locate the hyperbolic tangents of the elements. Mathematically, it can be shown by,

$$\grave{P}=\frac{1}{2}\,[1+\tanh(t^*(p_{wind}-p_c))] \quad (1)$$

where t is the number of sweeps determining the how fast the network can percolate, p_{wind} is the reduction of the spread due to the speed of the wind blowing in a particular region. The value p_{wind} lies between 0 and 1 is the reduction of spread due to wind and is directed by,

$$p_{wind}=p_i{}^*\,a_w(x) \quad (2)$$

and,

$$p_i=(p_w(x=0)^*s_w{}^*p_w{}^T(x=0) \quad (3)$$

where, $p_w(x=0)$ denotes the initial area of the spread of the fire, s_w is the matrix of contact with the nearest-neighbor tree, all $a_w(x)$ are calculated based on the impact of the city's mitigating initiatives.

Results and Discussions

The study is carried out on the forest fire dataset [2], via which the parameters are considered. The model clearly explains with a graph [Fig.2] that for a low p_{wind} value, the corrected percolation function $\grave{P}\rightarrow 0$, implying zero loss of connectivity among the cluster of trees formed [3]. Hence, the lifetime of the fire increases and simultaneously increasing the burnt area (in km). The p_{wind} value gradually tending to the percolation threshold, increases $\grave{P}$ rapidly and at the highest p_{wind} regime, where more connections are lost among the clusters, $\grave{P}\rightarrow 1$. Each curves in Fig.2 is made for different

ICATP 2022, ISBN 978-81-952903-0-7

number of sweeps. Operating with 0.6 as the percolation threshold, the curve’s inflexion point is indicated [Fig.2].

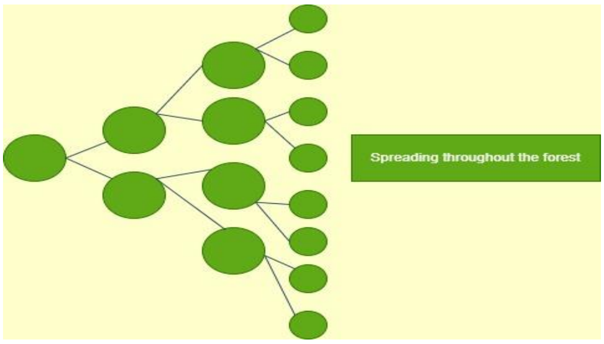

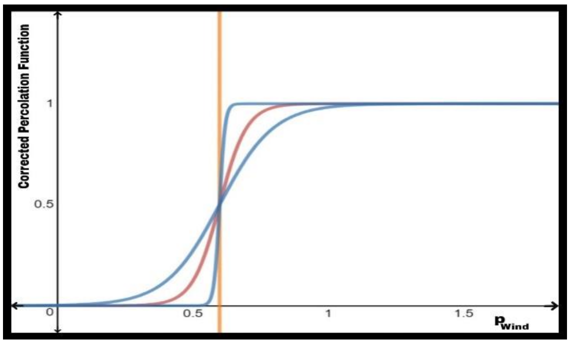

Fig.1. percolation network spread

Fig.2. Percolation correction function vs reduction of

Conclusion

The proposed model helps clearly understand the spread of fire by formation of percolating clusters and also lifetime of the fire. It enables us to understand the relation between percolation value and the reduction of spread which in turn defines clearly the highly prone areas for forest fire. Hence, helping the government in decision making for locating forest fire stations and improving fire safety services.

References

1. Caroline Franco at.al, 2022. Percolation across households in mechanistic models of NPI in SARS-COV-2 disease dynamics, 10.1016/j.epidem.2022.100551.
2. https://www.kaggle.com/datasets/balavashan/forest-fire-dataset
3. Saberi, Abbas, 2015. Recent advances in percolation theory and its applications. Physics Reports. 578. 10.1016/j.physrep.2015.03.003.

ICATP 2022, ISBN 978-81-952903-0-7

CHAPTER -41

K-Means Clustering based Forest Fire Image Classification to Detect Target Region for Primitive Measures

Pratibha Barnwal[1], Santanu Mandal[1], Shah Parth Mukeshbhai[1]
[1]School of Advanced Sciences, VIT-AP University, Amaravati, Andhra Pradesh, India

Introduction

Forest fires have instant and long-term impacts on the ecosystem, including biodiversity loss and increased global warming. Forest fire causes carbon dioxide emissions which pollute the air, reduce the oxygen level in the atmosphere, and cause detrimental effects on living beings [1]. This study proposes k-means clustering algorithm using Contrast Stretching to extract pixels [Fig.1] from a forest fire image and detect fire and smoky regions by forming different clusters. In this paper, the satellite image of California's deadliest fire [2] is taken to classify and detect the target region of the wildfire. The detection outputs allow forest fire mitigation experts and government to take immediate action to this disaster.

Materials and Methods

Satellite image of forest fire is segmented by partial contrast stretching (PCS) to increase image quality, using equation (1). Contrast stretching is an image processing technique that enhances the contrast of the image so that the image's features may be seen clearly [3].

$$I_o = (I_i - Min_i) * (((Max_o - Min_o)/(Max_i - Min_i)) + Min_o) \quad (1)$$

Where, I_i, I_o = Input, Output pixel value
And Min_i, Max_i, Min_o, Max_o = Min, Max pixel value of Input and Output image
Then on segmented image the k-means clustering algorithm is applied, using equation (2), between each centroid and every pixel in the image the Euclidean distance is measured. Consider a picture with (x x y) dimensions that must be grouped into k number of clusters. Let $p(x, y)$ represent the cluster input pixels and C_k represent the centers of the cluster, calculate using equation (3). The steps for k-means clustering algorithm are as follows:

a Initiate with k clusters and the center.

b Use Euclidean distance formula to find d between the image's center and every pixel, then based on d, allocate all pixels to the closest center.

$$d = \| p(x, y) - C_k \| \quad (2)$$

c Using this equation, recalculate the new position of the center.

$$C_k = \frac{1}{k} \sum_{y \in Ck} \sum_{x \in Ck} p(x, y) \quad (3)$$

d Continue the process until the error value is met. And resize the cluster pixels to fit the image.

So k-means clustering presents almost the same resemblance to a human eye and finally, the method resizes and reshapes the clusters into a single image where the target region is very prominent.

Fig.1. Flow diagram of the proposed algorithm

Results and Discussion

ICATP 2022, ISBN 978-81-952903-0-7

The proposed approach has been applied to Fig. 2. a) [2] to extract fire, and forest (green-land) region. Using PCS Fig. 2. b) and applying k-means clustering Fig. 2. c) is obtained as final output where the target region of fire is extracted successfully.

a) b) c)

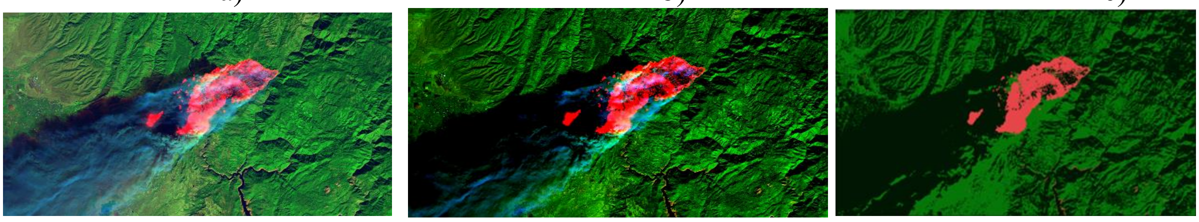

Fire , Forest

Fig.2. a) Original Image, b) PCS Image, c) Segmented image with k=3

Conclusion

The experimental results show that a combination of PCS with k-means clustering can be useful for the detection of fire-prone areas. This detection helps the immediate measure to prevent fire by detecting the location of the hotspot and actual region affected by the fire at that instant. Here PCS process filtering the input image for better performance and different cluster numbers can meet the requirement of various levels of the target region. Future research would focus on multiple clustering model integration and more advanced feature selection to acquire more relevant information.

References

[1] Abram, N.J., Henley, B.J., Sen Gupta, A. et al. Connections of climate change and variability to large and extreme forest fires in southeast Australia. Commun Earth Environ 2, 8, 2021.

[2] Stephanie Pappas, California's Deadliest Fire Is Seen Engulfing Paradise in 'Astonishing' Satellite Images, Live Science, 2018.

[3] Nameirakpam Dhanachandra, Khumanthem Manglem, Yambem Jina Chanu, Image Segmentation Using K -means Clustering Algorithm and Subtractive Clustering Algorithm, Procedia Computer Science, Volume 54, Pages 764-771, 2015.

CHAPTER -42

SPAM MAIL DETECTION USING MACHINE LEARNING

Akash Behera and Kiran Kumar Patra
VIT AP University
E-mail (akash.21msd7024@vitapstudent.ac.in)

INTRODUCTION

Email users are growing daily as a result of the expanding use of the internet. With the increase in email, usage has come issues brought on by spam, or pointless bulk email communications. On any computer system, it alters your search results and steals important information like our contact information from your contact list.

To distinguish between spam and non-spam emails in this system, the spam categorization system was developed. We occasionally receive spam, therefore it can be challenging to manually detect it each time. Consequently, we will employ some of the techniques in our suggested approach to identify.

Materials and Methods

There are numerous fields in the dataset, some of which are optional. Therefore, we got rid of several columns that weren't needed.

We created the graphs, histograms, and bar plots with the aid of NLTK (Natural Language Tool Kit) for text processing and matplotlib. As seen below, we separated the data into training and testing sets. A portion of the data set is utilized for training, while the remaining portion is used for testing.

The test data was then preprocessed in to distinguish between spam and non-spam emails. Python is employed as the backend technology, while the machine learning tools NLTK and Logistic Regression are used to detect spam.

Results and Discussion

The software determined whether or not the email was spam after receiving two inputs. “Thanks!” was used as the subject line in the initial run, which is not spam.

The module produced spam in the second run when the mail's subject line read “Call for the claim”
of lottery!" The findings are listed below.

```
Enter subject of the mail: >? Thanks !
Predicted class : Not Spam
Not Spam: 64.25221146216863%
Spam: 35.74778853783137%
```

Figure 1 shows the first run's input.

ICATP 2022, ISBN 978-81-952903-0-7

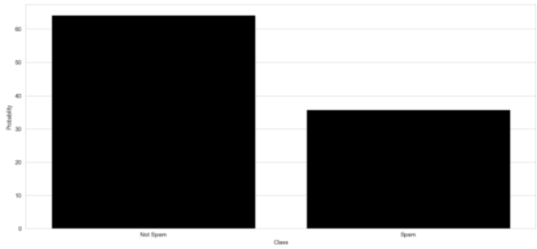

Figure 2: Results of the initial run, first bar displays the percentage of not spam, while the second bar displays the percentage of spam.

```
Enter subject of the mail: Call for the claim of lottery!
Predicted class : Spam
Not Spam: 41.607890105057145%
Spam: 58.392109894942855%
```

Figure 3: The second run's input.

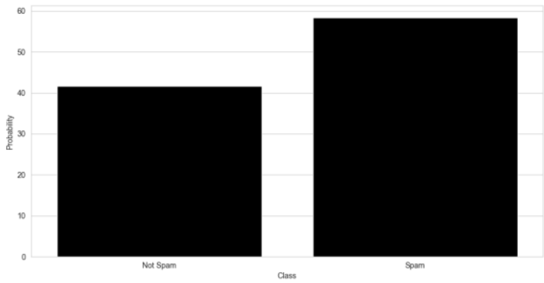

Figure 2: The second run's output first bar displays the percentage of not spam, while the second bar displays the percentage of spam.

Conclusion

We may infer from the work shown above whether or not the letter was classified as spam using NLTK and logistic regression.

References

Shukor Bin Abd Razak, Ahmad Fahrulrazie Bin Mohamad. 2013. Identification of Spam Email Based on Information from Email Header 13th International Conference on Intelligent Systems Design and Applications. (ISDA)

Mohammed Reza Parsei, Mohammed Salehi. 2015. E-Mail Spam Detection Based on Part of Speech Tagging 2nd International Conference on Knowledge-Based Engineering and Innovation. (KBEI).

CHAPTER -43

WASTE SEGMENTATION USING DENSLY CONVOLUTATED NEURAL NETWORK

[1] Abhasita Das Munshi, [1]Dr. Santanu Mandal
[1] School of Advance Science, VIT-AP University, India
[1]santanu.mandal@vitap.ac.in

INTRODUCTION

Waste classification is important in the waste treatment cycle because it allows for the separation of wastes to avoid environmental damage and the collection of recyclable wastes. Such concerns have prompted scientists to focus on technology advancements that would aid in the resolution of these issues. Some of the most important efforts are aimed at automating garbage classification at various stages. The scope of research might range from developing mobile apps to embedding classification algorithms in trash can cameras to automating industrial and mass waste treatment**.** This process is exceedingly complex in the context of waste management, and it requires a multidisciplinary approach, as well as the participation of local governments and communities, to be successful. We are going to concentrate on one component of this process for the rest of this post: *waste sorting using image classification*. Waste disposal is often a serious concern when in it comes to the context of pollution, segregating waste into organic and recyclable is necessary to avoid alarming conditions like eutrophication, toxic consumption of waste by animals and land, water and or air pollution. As different forms of garbage require different solutions, ensuring that waste is properly categorised is crucial in developing an effective and efficient waste management system.

MATERIALS AND METHODS

We have trained our model using waste classification dataset [1] (Dataset is divided into train data (85%) and test data (15%) Training data - 22564 images, Test data - 2513 images consisting of labelled images as *organic* or *recyclable*) from Kaggle using densely Convoluted Neural Network (densenet-121) with the help of PyTorch. PyTorch is basically a python framework that allows tensor computation with strong GPU acceleration for constructing deep neural networks. It provides flexibility and stability for deep learning. We have augmented the data which is cropping, flipping, and resizing the data to increase the accuracy of the learning algorithm. We have used transfer learning which is process of using already pre-trained models by tweaking last layers to classify images into organic and recyclable classes. Here we have used Densenet121 which is a powerful model with 121 layers. It connects each layer with other layer in a feed forward fashion. We have used 20 epochs to train the model. DenseNets have several compelling advantages, including the elimination of the vanishing-gradient problem, improved feature propagation, feature reuse, and a significant reduction in the number of parameters. [2]. A dense convolution network with only 3 dense network is shown in **Fig.1**. Transition layers are the layers that connect two neighbouring blocks and modify feature-map sizes through convolution and pooling.

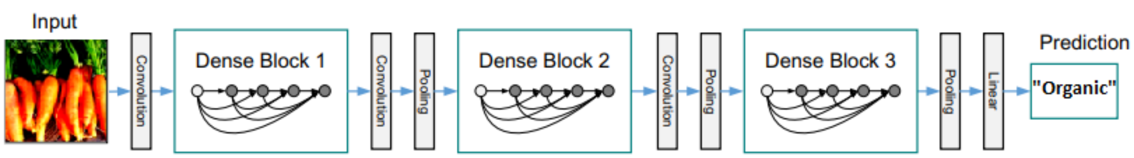

Fig.1. Three dense blocks in a deep DenseNet.

RESULTS AND DISCUSSION

We have used the test dataset for testing the accuracy of the classification. The model has accuracy of **91 %** for recyclable waste and **98 %** for organic waste. The test loss is **0.17**.

Fig.2. Classifying waste images as Recyclable (R) or Organic (O).

It has been seen that this model can clearly classify waste images efficiently and example has been shown in the **Fig.2.**, the predicted label is mentioned along with the true label in brackets for testing the accuracy of the model.

CONCLUSION

This proposed method of waste classification can identify classify waste images between *organic* and *recyclable* waste with an accuracy of 91% and 98% respectively with the help of densenet-121 (a pre trained densely convoluted neural network). This method can be implemented in the real-world scenario of waste segregation efficiently.

REFERENCES

[1] Dataset - https://www.kaggle.com/datasets/techsash/waste-classification-data

[2] G. Huang, Z. Liu, L. Van Der Maaten and K. Q. Weinberger, "Densely Connected Convolutional Networks," 2017 IEEE Conference on Computer Vision and Pattern Recognition (CVPR), 2017, pp. 2261-2269, doi: 10.1109/CVPR.2017.243.

CHAPTER -44

FLOW IN A PERMEABLE CHANNEL WITH REABSORPTION AT WALLS: ANALYTICAL AND NUMERICAL SOLUTION

Varunkumar Merugu
VIT-AP University, Amaravati-522237. Andhra Pradesh, India
E-mail: varunkumar.merugu@vitap.ac.in

INTRODUCTION

The research on fluid flow through a permeability tube/channel has piqued the interest of numerous researchers because to its significance in many experimental and theoretical investigations of engineering challenges. This study presents the effect of reabsorption on flow of steady incompressible viscous fluid through a permeable channel. The regular perturbation and finite difference techniques are used to provide approximations of the solutions for velocity, pressure drop, and streamlines. The graphs show how reabsorption affects velocity profiles, pressure drop, and streamlines.

Take into account the flow of a Newtonian incompressible viscous fluid through a channel that is L length and a half width a, as shown in Fig.1. The governing equations of present situation of fluid motion for momentum and continuity are given by

$$\frac{\partial u}{\partial x}+\frac{\partial v}{\partial y}=0$$
$$u\frac{\partial u}{\partial x}+v\frac{\partial u}{\partial y}=-\frac{1}{\rho}\frac{\partial p}{\partial x}+\nu\left(\frac{\partial^2 u}{\partial x^2}+\frac{\partial^2 u}{\partial y^2}\right)$$
$$u\frac{\partial v}{\partial x}+v\frac{\partial v}{\partial y}=-\frac{1}{\rho}\frac{\partial p}{\partial y}+\nu\left(\frac{\partial^2 v}{\partial x^2}+\frac{\partial^2 v}{\partial y^2}\right) \quad (1, 2, 3)$$

The boundary conditions are

$$v=0 \text{ and } \frac{\partial v}{\partial y}=0 \text{ at } y=0$$
$$u=0 \quad \text{at} \quad y=a$$
$$Q(x)=\int_0^a u(x,y)dy=Q_0e^{-\alpha x} \quad (4, 5, 6)$$

Eqs. (1)-(3) through (4)-(6) are solved analytically and numerically, and the behavior of flow through a channel when reabsorption at the permeable wall is present is then examined. The only significant difference between the two methods was 0.001 and both the numerical and analytical findings were in close agreement(Fig.1(a)). The primary characteristics of the reabsorption coefficient (α) on velocity, pressure, and stream function are all depicted and presented in graphs with reference to flow in renal tubules. The current study used modest reabsorption values (α=1.0-2.0) that were provided by the literature on physiological concerns.

RESULTS AND DISCUSSION

In this work, an effort is made to conceptually comprehend how reabsorption affects the flow of Newtonian fluid in a channel. In order to visualize the effects of reabsorption, perturbation solutions are constructed for velocities, pressure drop, and streamlines. The finite difference approach is also

ICATP 2022, ISBN 978-81-952903-0-7

used to try and quantitatively solve the governing flow equations. The transverse velocity profile numerical results were compared to the perturbation results. The largest discrepancy between the numerical and perturbation results is 0.0021, and both sets of results were in good agreement.

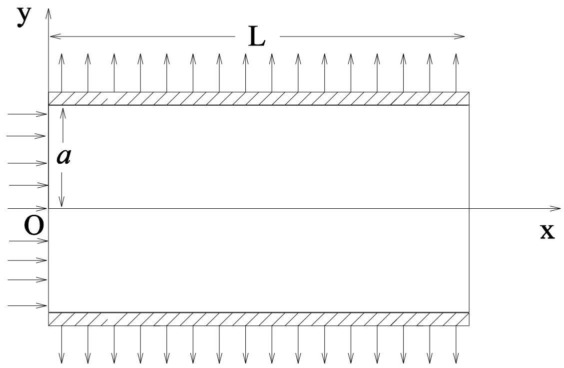

Figure 1. Geometrical representation of the problem

The following are the findings of the current investigation:
- The velocity *v* at the channel wall decreases as rise in α (Fig. 1(b)).
- Reabsorption at the wall greatly reduces the pressure drop throughout the channel (Fig. 2(a)).
- The streamline pattern reflects a change in flow direction brought on by a variation in α (Fig2(b)).

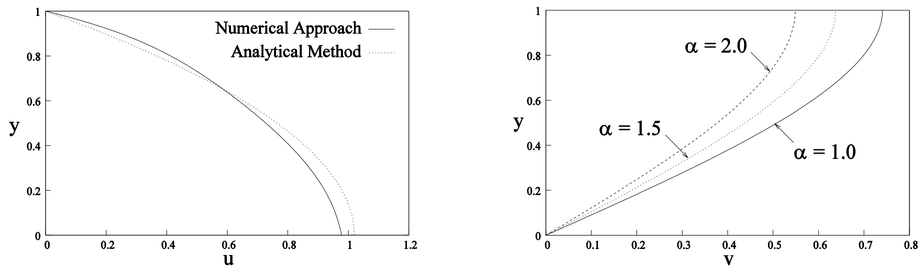

(a) (b)

Fig1. (a) Analytical method and numerical approach comparison (α = 1.0); (b) Axial velocity *v* with *y*, at *x = 0.30*.

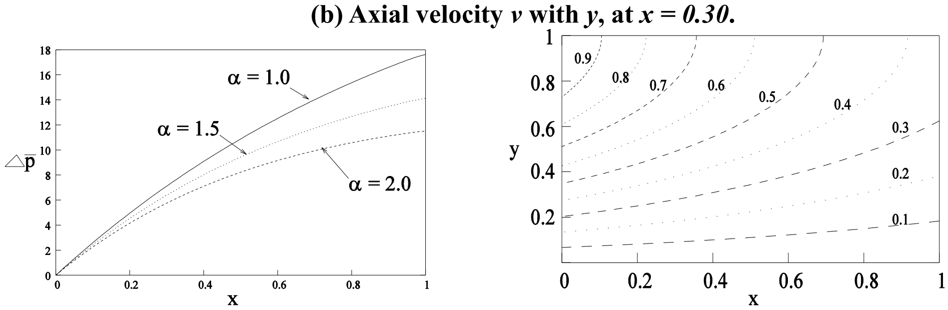

(a) (b)

Figure 2. (a) Mean pressure drop with *x*; (b) Streamlines distribution.

REFERENCES

Acharya, G. R. K., Peeyush, C. and Kaimal, M. R., 1981. A hydrodynamical study of the flow in renal tubules, Bull. of Math. Bio., 43: 151-163.

Chaturani, P. and Ranganatha, T. R., 1991. Flow of Newtonian uid in non-uniform tubes with variable wall permeability with application to ow in renal tubules, Acta Mech., 88: 11-26.

Siddiqui, A. M., Haroon, T. and Shahzad, A., 2016. Hydrodynamics of viscous fluid through porous slit with linear absorption, Applied Math. and Mech., 37-3: 361-378.

CHAPTER -45

A MODEL FOR BLOOD FLOW IN HUMAN FEMORAL ARTERIES

Debismita Nayak, Ketana K, T S L Radhika*
Department of Mathematics,
BITS Pilani, Hyderabad Campus, Hyderabad- 500078.
*corresponding author: radhikatsl@hyderabad.bits-pilani.ac.in

INTRODUCTION

Understanding the blood flow phenomenon in the human circulatory system has been a point of interest to researchers from diverse fields over several decades. While clinical practitioners have used the clinical data to comprehend the underlying mechanism of the system, lumped parameter models have become the engineers' tool to explore it. Mathematicians and Physicists have developed models using the physical laws governing the fluid (blood) flow in the human circulatory system to gain insight into the system's working.

In this paper, we worked on a mathematical model for the blood flow in the human arterial arteries. The three key features of the system, namely, the blood, have been modelled as a Newtonian fluid, and the blood flow is taken to be due to an oscillatory pressure gradient containing n-harmonics and the artery as a tapered elastic circular pipe. A mathematical model has been developed incorporating these features, and we have used the Homotopy Analysis Method to solve the model along with appropriate boundary conditions. Then, we computed the expressions for the two physical quantities, wall shear stress (WSS) and volumetric flow rate (QF) and computed the values with the help of publicly available anatomical data on the human femoral artery and the physiological behaviour of blood flow through it. The simulated data has been used to build statistical models that generate expressions for estimating the two physical quantities for any given set of model parameters which otherwise would involve tedious procedures.

RESULTS AND DISCUSSIONS:

For handiness, the inputs to the mathematical model, i.e., the model parameters, are categorized into flow-related parameters, fluid-related and material (artery)- related. Heart rate and the coefficients in the Fourier series representation of the pressure gradient driving blood flow in the human femoral arteries are flow-related parameters whose values are taken from references [1] and [2]. The values of the density and the viscosity of the blood, which are the fluid-related parameters, are taken from [2]. The expanding/ contracting parameter for capturing the dilation and the contracting states of the artery and the tapering fraction to describe the extent of the tapering of the femoral artery are the two material parameters that assume values based on specific mathematical requirements mentioned in [3,4]. We computed WSS and QF for this data and presented our findings below.

In both the expansion and dilation states of the artery, it has been observed that:

1. An increase in the heart rate (tachycardia) has decreased the value of the axial velocity component. The converse of this observation best interprets a physiological aspect of the CVS - its ability to compensate for poor blood circulation by increasing heart rate, i.e. when the heart fails to supply a sufficient amount of blood to the organs, it increases the rate at which it pumps the blood to compensate for the deficiency. Results show that the present model could capture this critical phenomenon.

2. An increased heart rate has resulted in a decrease in the WSS.

ICATP 2022, ISBN 978-81-952903-0-7

Moreover,

a. A 4% increase in the heart rate has decreased the average QF and the average WSS by 14.6%.

Furthermore,

b. In the expansion state, when the expansion parameter has been quadrupled, the average QF increased by 8%, and the average WSS by 1.96%.

c. In the dilation state, when the contraction parameter has become four times, the average QF decreased by 7.9% and the average WSS by 2.04%.

CONCLUSIONS

In this work, we explored the blood flow phenomenon in the human femoral artery by developing a mathematical model that captured the essential features of this physiological system. Simulations have been carried out using clinical data to gain an insight into its behaviour, and we presented our findings.

REFERENCES

1. Gayathri K and Shailendhra K., Pulsatile blood flow in large arteries: Comparative study of Burton's and McDonald's models, Applied Mathematics and Mechanics 35, 575-590, 2014.
2. Karthik, A., Radhika, T.S.L., Praveen Kumar, P.T.V. Mathematical Modeling of Blood Flow Through Human Femoral Arteries and the Analysis of Model Parameters. Int. J. Appl. Comput. Math 8**,** 30, 2022.
3. Karthik Alasakani, Radhika S.L. Tantravahi, Praveen Kumar P T V, On Refining the Input Data set to Mathematical Models Simulating Arterial blood flow in Humans, WSEAS Transactions on Fluid Mechanics, ISSN / E-ISSN: 1790-5087 / 2224-347X, Volume 16, 63-73, 2021.
4. M. Shriya, A. Karthik and T. S. L. Radhika, 2021 Mathematical Blood Flow Model - Simulations and Data Analysis, 2021 IEEE Bombay Section Signature Conference(IBSSC), 1-6, doi: 10.1109/IBSSC53889.2021.9673261.

CHAPTER -46

DISPERSION OF A SOLUTE IN NON-NEWTONIAN FLUID FLOW IN A CATHETERIZED ARTERY WITH MILD STENOSIS

Ajani Ausaru[1], P. Nagarani[1], A. Small[1,2] and Victor Job[1]

[1]Department of Mathematics, The University of the West Indies, Mona Campus, Kingston 7, Jamaica West Indies
[2]Faculty of Engineering, Caribbean Maritime University, Norman Manley Highway, Palisadoes Park, Kingston, Jamaica West Indies
ajani.ausaru02@uwimona.edu.jm

INTRODUCTION

Dispersion theory features prominently in a diversity of fields such as chemical engineering, environmental science, and physiological fluid dynamics. In this work, the varying flow pattern and dispersion of a solute for a pulsatile flow scenario in a narrow catheterized artery with stenosis is the studied. Localized narrowing occurring in the lumen of an arterial segment is termed stenosis. Stenosis can result in low blood flow in cells which can lead to serious circulatory problems. In the process of catheterization, minuscule tubes are inserted into the blood vessel and therefore into the circulatory system. The objective includes gaining information on blood flow such as measuring pressure within the heart chambers, taking blood samples to measure oxygen levels, and ascertaining if there are obstructions within the blood vessels.

METHODOLOGY

Consider a pulsatile, axisymmetric, fully developed flow of blood through a catheterized artery with stenosis, as shown in Figure 1. Here the radius of the artery is a and that of the catheter is ka with $k<1$. The flow is laminar and the fluid is considered as Casson fluid. The stenosis is considered axisymmetric and the geometry of the stenosis is modelled according to Young (1968).

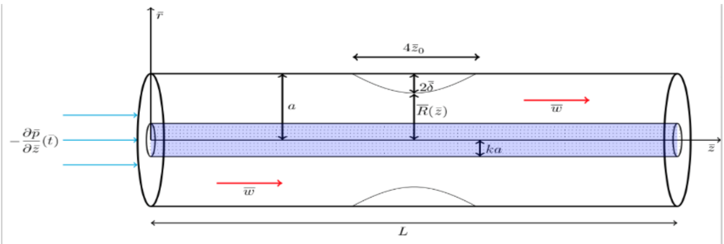

Figure 1. Stenosis geometry and coordinate system

The perturbation method is employed under the assumptions of low Womersley frequency parameter to solve the flow equations together with Casson's constitutive equation. Analytical expressions are derived for axial velocity, yield plane locations, and wall shear stress. The finite element method is used to solve the convection-diffusion equation by assuming the continuous supply of solute at the inlet. The effect of non-Newtonian rheology, unsteady flow, catheter radius, and stenotic region height on the yield plane locations and axial velocity are discussed. The effects of these flow parameters and slug input length of solute on local and mean concentrations are studied while keeping the Peclet and Schmidt numbers constant.

RESULTS AND DISCUSSION

An analysis of pulsatile flow is undertaken and results are attained experimenting with differing values of the Womersley frequency parameter a, the fluctuating component of the pressure gradient e, the yield stress t_y, the catheter radius k, and the stenotic depth d. The values of the parameters chosen are in a physiologically appropriate range. Increasing the yield stress affirms that the magitude of the velocity appreciably reduces. This is also true of the stenotic depth and catheter radius being varied. However, as the fluctuating component of the pressure gradient increases, we note an increase or a drop in the velocity magnitude depending on the time.

In this analysis there are two yield planes. In pulsatile flow, the yield plane locations l_1 and l_2 are time dependent, as different values of the pressure gradient are encountered and thus switch location during the course of motion.

The reverberations of the earlier mentioned parameters on the evolution of the dispersion are examined. Mathie (1982) intuits that information garnered from this examination can be used to understand the indicator dilution technique in a catheterized artery with partially decreased cross-sectionalarea.

Figure 2 attests that the smaller the value of the yield stress, the more stretched and extended is the dispersion trajectory. This means that the solute is able to travel much further axially for lesser values of the yield stress. Albeit, having an initial solute concentration of value 1 being continuously injected at the inlet of the artery, we observe that for all yield stress values, that the average concentration of the solute exceeds 1 at some point during its transport. This is probably due to the 'bottleneck' and obstruction in blood flow originated by the stenosis, resulting in a build-up of solute as the stenotic region is encountered. For a smaller yield stress value the fluid velocity is greater permitting the solute to disperse a much greater distance axially. Axial variation of the mean concentration for disparate values of the stenotic depth, d, reveals that there exists an inverse relationship vis a vis the values of the stenotic depth and the corresponding values of the average concentration. Sigmoid-like curve provide details about the time variation of the mean concentration. For the stenosis at prescribed depths we notice that mean concentration decreases with an increase in stenosis height up to certain time at which there is a change in concavity. This point of inflexion occurs at a certain time subsequent to which there is a reversal. This reversal is sustained up to a certain time, subsequent to which the mean concentration tends to an equilibrium value of 1. This reversal may be a consequence of the pulsatility associated with the flow.

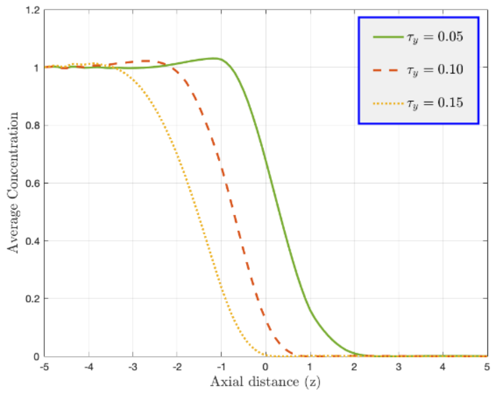

Figure 2. Axial varying of the mean concentration varying the rheological parameter while fixing other flow parameters

CONCLUSION

This work demonstrates that rheological properties of blood seriously impact the flow and dispersion phenomena, and this also applies to geometric properties contemplated in this study. This study applies in oxygen transport and drug therapy in blood flow.

REFERENCES

Mathie, R.T. 1982. Blood flow measurement in Man. *Castlehouse Publications*

Young, D.F. 1968. Effects of time-dependent stenosis on flow through a tube. *J. Eng. Ind. Trans. ASME*, 90: 248-254.

CHAPTER -47

Spatiotemporal linear stability of viscoelastic Saffman-Taylor flows

D. Bansal[1], T. Chauhan[1] and S. Sircar[1]

[1]Department of Mathematics, IIIT Delhi, India 110020

Email: dikshab@iiitd.ac.in (corresponding Author)

1 Introduction

Injecting a fluid into a more viscous fluid in a thin linear channel (or the Hele-Shaw cell) triggers a two-dimensional viscous fingering pattern which is characterized by increasingly long fingers undergoing tip splitting and branching events, also known as the Saffman-Taylor instability (STI). These complex structures are considered to be a paradigm for interfacial pattern formation and have continued to receive prolonged interest in theoretical and experimental studies as well as due to its practical applicability in crude oil recovery, surface coating and electrodeposition. We consider the linear stability of a steady fully developed flow of a low viscosity Newtonian fluid (fluid 1) displacing a high-viscosity viscoelastic fluid (fluid 2) inside a square Hele-Shaw cell of length and width, $2L$, and cell-gap, b. A rectilinear coordinate system with center as origin and x, y and z as flow, transverse and cell depth direction respectively.

$$\nabla \cdot \mathbf{v}_i = 0, \quad Re_j^* \left[\frac{\partial \mathbf{v}_j}{\partial t} + \frac{6}{5}(\mathbf{v}_j \cdot \nabla)\mathbf{v}_j \right] = -\mathbf{v}_j + \nabla \cdot \tau_j, \quad \text{j=1, 2,} \tag{1}$$

$$\tau_j = \begin{cases} -p_j \mathbf{I} + \mathbf{D}_j, & \text{j=1} \\ -p_j \mathbf{I} + \nu \mathbf{D}_j + (1-\nu)\mathbf{A}, & \text{j=2,} \end{cases} \tag{2}$$

$$\frac{\partial \mathbf{A}}{\partial t} + \mathbf{v}_2 \cdot \nabla \mathbf{A} - \nabla \mathbf{v}_2^T \cdot \mathbf{A} - \mathbf{A} \cdot \nabla \mathbf{v}_2 = \frac{\mathbf{D}-\mathbf{A}}{We^*}. \tag{3}$$

The governing two-dimensional, cell gap-averaged (along z-direction) continuity and momentum equations for both fluids, are given by a generalized Darcy's law in equation (1), where the extra stress tensor, τ, is given in equation (2), where I is the identity matrix. $D_j = \nabla v_j + \nabla v_j^T$ is the shear rate tensor and A is the elastic contribution to the stress tensor, satisfying the Oldroyd-B constitutive relation (3). The variables $v_j = (u_j, v_j), p_j$ are the velocity and pressure fields, respectively. The parameter, $\nu = \eta_s/(\eta_s + \eta_p)$ represents the viscous contribution to the total viscosity. Also, the kinematic boundary conditions at the interface are the equality of normal and tangential velocities and the normal velocity equal to the interface velocity. This present work significantly differs from the existing studies as we analyse the linear stability of Hele-Shaw flow of dilute polymer solutions through a spatiotemporal stability analysis (Shokri et al. (2017)) and aim to address questions about polymer relaxation conditions and time asymptotic response of the flow leading to the topological transition of the advancing interface?

2 Materials and Method

The equations (1)-(3) are linearized using a normal mode expansion of the disturbance $e^{i(\alpha x - \omega t)}$

ICATP 2022, ISBN 978-81-952903-0-7

and the resultant non-trivial solution wavenumber and frequency (α, ω) of linearized system is found by solving the corresponding dispersion relation $D(\alpha, \omega) = 0$. For spatiotemporal stability, α is allowed to be complex and the growth rate at the cusp point, ω_i^{cusp} is numerically evaluated, starting from the temporal growth rate, ω_i^{temp}. The cusp point in the ω-plane is a saddle pointsatisfying the criteria, $D(\alpha, \omega^{\text{cusp}}) = \partial D(\alpha, \omega^{\text{cusp}})/\partial\alpha = 0$, but $\partial^2 D(\alpha, \omega^{\text{cusp}})/\partial\alpha^2 \neq 0$. However, not all cusp points are unstable and, in particular, the evanescent modes are segregated from the regular cusp points using the Briggs idea of analytic continuation (Briggs (1964)). Notice that this spatiotemporal linear stability algorithm is solved via bivariate Newton-Raphson method (Bansal et al. (2021)).

3 Results and Discussion

This model has already been validated with the known set of experiments for Newtonian flows (Lindner (2006)). In the next subsections, we present our contribution to existing literature.

3.1 Neutral stability curves

For a fixed ν, as $E(1-\nu)$increases, Re_c decrease as per the scaling law outlined above until it reaches a minimum threshold value of $E(1-\nu)$ (see Figure 1). Beyond this threshold value, Re_c deviates from this scaling law and decreases rather sharply indicating flow to be unstable for all α beyond this threshold. However, threshold Re_c shifts to higher values of $E(1-\nu)$ and value of Re_c at the threshold also increases in the limit $\nu \to 1$. The last observation suggests that the viscoelastic Saffman-Taylor flows for strongly elastic dilute polymer solutions can become unstable for the entire wavenumber spectrum, at a critical value of Re which is much lower than that of their Newtonian counterpart.

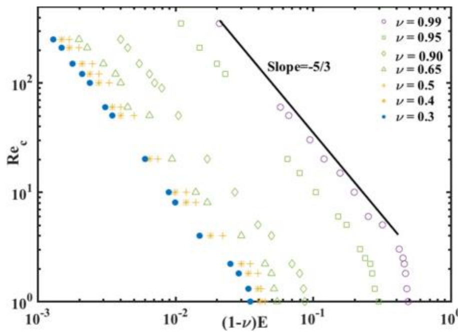

Figure 1. Variation of the critical parameters with $(1-\nu)$E for ν ranging from 0.3 to 0.99, where Re_c follows the scaling laws $Re_c \sim [(1-\nu)E]^{-3/2}$ below a threshold value of $(1-\nu)$E.

3.2 Spatiotemporal stability analysis

Spatiotemporal analysis is typically relevant when one introduces an impulse excitation locally in a flow and observes how that disturbance evolves with time. We evaluate the ω_i^{cusp} to identify the region of absolute instability, or the region indicating the topological reconfiguration and subsequent pinch-off of the advancing interface (see Figure 2). Here, we classified the nature of the instabilities by computing the boundaries of the evanescent modes (E), the convectively unstable (C) and the absolutely unstable regions (A) within a selected range of the flow-elasticity-viscosity parameter space. The flow stability phase diagram projected onto the $Re - E$ parameter space divulge the presence of absolutely unstable region at high values of Re and E, confirming our presumption that elasticity coupled with high fluid inertia has a destabilizing effect. Additionally, we report the presence of (E) at intermediate values of Re and E

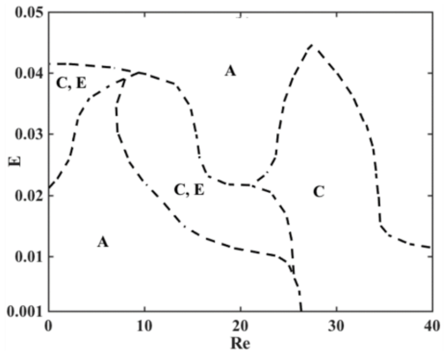

Figure 2: Stability phase diagram evaluated at spatial locations $\zeta_0 = 0.99$ and at fixed values of $\nu = 0.9$.

4 Conclusion

- The main conclusion is that the parameter regions susceptible to topological transitions, are primarily those driven by high inertia coupled with high elasticity.
- A number of simplifying assumptions were made, including the absence of non-linear terms, the numerical challenges posed in the regime of moderate to high E and the consideration of the Hele- Shaw flows of polymer melts.
- Experiments in vertically aligned Newtonian Hele-Shaw flows (Goldstein (1993)) suggest the importance of inertial effects in triggering a collapse of the moving interface.
- A deeper consideration of the impact of finite boundaries, including elastic boundaries on the evolution of the moving interface should be worthwhile in future.

References

Bansal D., Ghosh D. and Sircar S. 2021. Spatiotemporal linear stability of viscoelastic free shear flows: non-affine response regime. Phys. Fluids, 33: 054106.

Briggs R. J. 1964. Electron-stream interaction with plasmas. MIT Press, Cambridge.

Goldstein R. E., Pesci A. I. and Shelley M. J. 1993. Topology Transitions and Singularities in Viscous Flows. Phys. Rev. Lett., 70(20): 3043-3047.

Lindner A., Bonn D., Poire E. C., Ben Amar M. and Meunier J. 2002. Viscous fingering in non-Newtonian fluids. J. Fluid Mech. 469: 237-256.

Shokri H., Kayhani M. H. and Norouzi M. 2017. Nonlinear simulation and linear stability analysis of viscous fingering instability of viscoelastic liquids. Phys. Fluids 29: 033101.

ICATP 2022, ISBN 978-81-952903-0-7

Computational Study of Turbulent Flow Behavior in Two-Sided Lid-Driven Cavity

M.Gnanasekaran and A.Satheesh*
Department of Thermal and Energy Engineering, School of Mechanical Engineering, Vellore Institute of Technology, Vellore, Tamilnadu, INDIA-632014,
*Corresponding Author E-mail: satheesh.a@vit.ac.in

INTRODUCTION

The lid-driven cavity problem was developed to examine flow stability for many industrial and engineering problems in fluid dynamics like mixing, coating, flow over cuts, designs, roll coating systems, polymer melts, ceramic typecasting, drying applications, etc. Initially, the single side cavity problem was given more importance and is studied by several researchers like Botella and Peyret (1998), Arun and Satheesh (2015), etc. Later on, the double-side problem received significant attention and is studied by Kuhlmann et al. (1997), Hammami et al. (2018) and, Romanò et al. (2019), etc. Even though the majority of the researchers study laminar flow problems, most of the practical fluid problems deal with turbulent flow. Hence the present study used the k-ε turbulence model, to analyze the various turbulence features of the 2D steady-state incompressible two-side cavity flow with different speed ratios and higher Reynolds numbers for a constant aspect ratio. The flow behavior for the selected range is obtained by the streamline patterns, the turbulent kinetic energy, dissipation rate, turbulent viscosity, centerline velocity profiles, and Reynold stress.

NUMERICAL METHODOLOGY

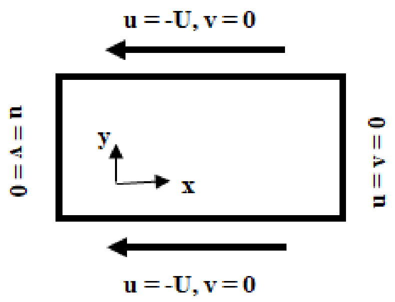

Figure 1. Geometrical configuration

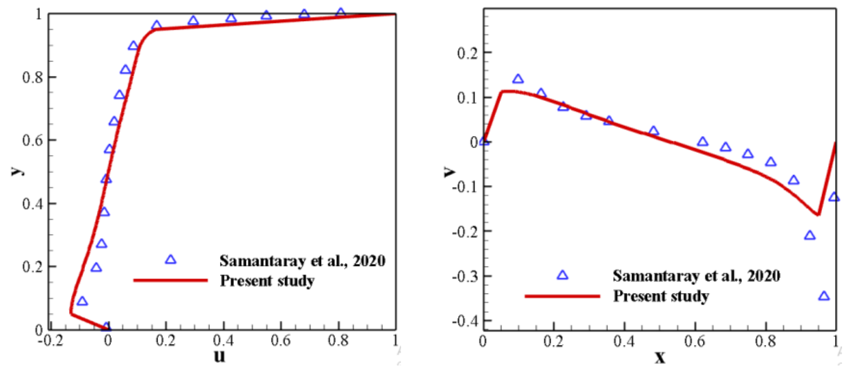

Figure. 2 Comparison of centerline velocity profiles Samantaray et al. (2020)

Fig.1 shows the geometrical model of the two-sided cavity. In that, the flow is driven by the top and bottom walls having equal velocities (-U) in the negative X-direction. The detailed numerical study of flow patterns has been performed by varying the Reynolds number ($1\times10^4 \leq Re \leq 1\times10^5$) and Speed Ratio (ratio between bottom wall to top wall velocities) ($0.05 \leq$ SR ≤ 1.0) with a constant aspect ratio (AR = 0.5) as shown in the Table. 1.

Table 1: Various parameters and their range used for the current study

Parameters	*Range*		
Speed Ratio (SR)	0.005,	0.5,	1.0
Reynolds Number (Re)	1×10^4,	5×10^4,	1×10^5
Aspect Ratio (AR)	0.5		
Both top and bottom wall motions	-X Direction		

The Reynolds averaged governing equations with k-ε turbulence modeling are solved using the Finite Volume Method (FVM) with staggered grid technique. Hybrid and QUICK Deferred

ICATP 2022, ISBN 978-81-952903-0-7

Schemes are used for discretizing the diffusion and convection respectively. The grid independence test for current C++ code is simulated for four different grid sizes, 81 × 81, 121 × 121, 161 × 161, and 201 × 201 with the aspect ratio of 1.0. A comparison of the centerline velocity profiles demonstrates that the grid size of 161 × 161 can be chosen for accuracy and its computational cost. All presented results in this numerical investigation have been converged to 10^{-8}.

RESULTS AND DISCUSSION

FVM code is used to compute the one-sided cavity flow for Re = 1× 10^4, AR = 1 to validate the present numerical problem. The comparison of the steady-state u and v centerline velocity profiles of the present study with Samantaray et al. (2020) is shown in Fig. 2, and are found to be in good agreement.

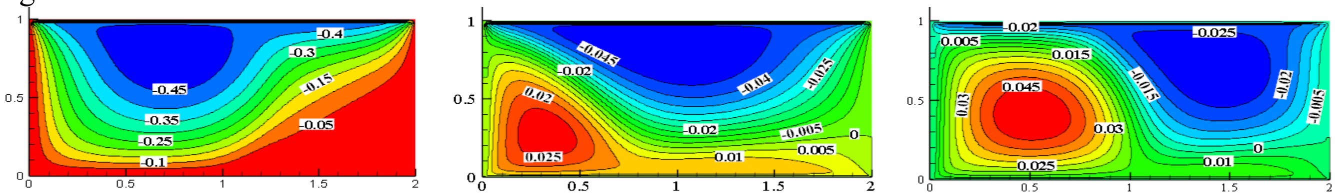

(a) SR = 0.05 **(b) SR = 0.5** **(c) SR = 1.0**

Figure 3. The variation of streamline contours for different SR at Re = 1 × 10^5

Fig 3. shows the streamlined contours for various speed ratios at Re = 1 × 10^5. For SR = 0.05, only one primary vortex was observed in the top left cavity. It was observed as the SR increases, the size of the secondary vortices in the bottom left cavity also increases. These vortices merged to form a new primary vortex that rotated in the opposite direction of the existing vortex at the cavity bottom. The main vortex drifted towards the cavity's middle due to an increase in its Reynolds number. For SR=0.05, the turbulent kinetic energy intensity decreases by increasing the Re, as shown in Fig 4(a). Similarly, the dissipation rate also decreased while an increase in Re which shows in Fig 4(b). The concentration of Reynolds stress is more on the left side of the cavity and its intensity increases by increasing the Re which is shown in Fig 4(c).

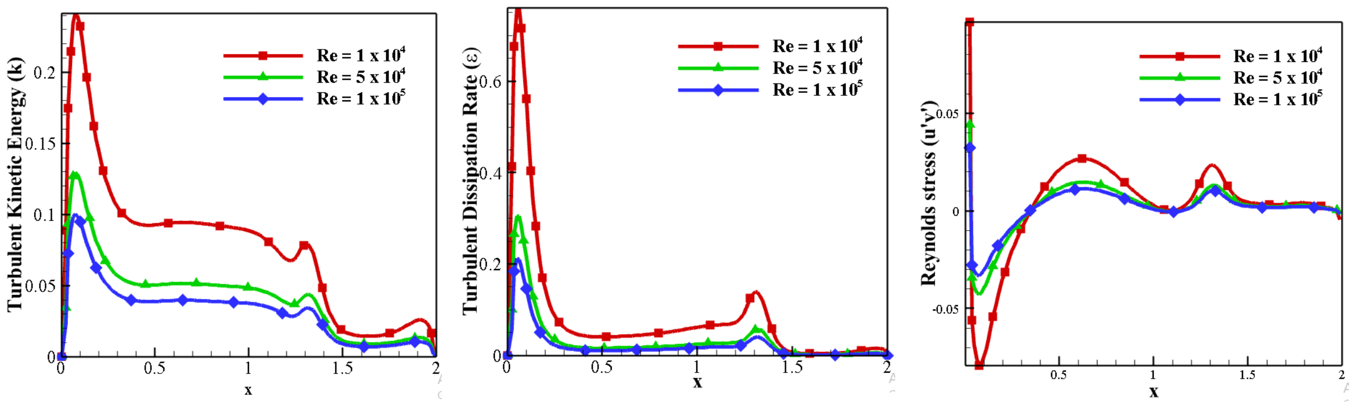

Figure 4. Effect of turbulent kinetic energy (k), dissipation rate (ε), and Reynolds stress components (u'v') for various Reynolds numbers at SR = 0.05 and AR = 0.5

CONCLUSIONS

Using the k-ε model, the present study investigated the turbulent flow behavior in a two-sided lid-driven cavity in the –X direction by varying the speed ratio and Reynolds Number. From the study, it is clear that the influence and intensity of the eddies obtained by lid motion are regulated by the speed ratio. The additional vortices generated from the cavity bottom wall are influenced by speed ratio as its size is observed to be decreasing at low-speed ratios. The intensity of Reynolds stress is influenced by the Re, as higher Reynolds stresses were generated at higher Re values. By increasing the Re from 1×10^4, the turbulent kinetic energy is decreased by 46.19% and 58.60% for Re = 5×10^4 and 1×10^5, respectively. Also, the turbulent dissipation rate decreased by 59.84% and 72.04%, respectively.

REFERENCES

Arun, S., and Satheesh, A. 2015. Analysis of flow behaviour in a two sided lid driven cavity using lattice boltzmann technique. *Alexandria Engineering Journal*, 54(4): 795–806.

Botella, O., and Peyret, R. 1998. Benchmark spectral results on the lid-driven cavity flow. *Computers and Fluids*, 27(4): 421–433.

Hammami, F., Ben-Cheikh, N., Ben-Beya, B., and Souayeh, B. 2018. Combined effects of the velocity and the aspect ratios on the bifurcation phenomena in a two-sided lid-driven cavity flow. *International Journal of Numerical Methods for Heat & Fluid Flow*, 28(4): 943–962.

Romanò, F., Kunchi Kannan, P., and Kuhlmann, H. C. 2019. Finite-size Lagrangian coherent structures in a two-sided lid-driven cavity. *Physical Review Fluids*, 4(2): 1–18.

Samantaray, D., Das, M. K., and Patel, D. K. 2020. Turbulence characteristics of high Reynolds number flow inside a three-dimensional cubic lid-driven cavity. *European Journal of Mechanics, B/Fluids*, 84: 23–39.

CHAPTER -49

Entropy Generation Analysis of Magnetohydrodynamic Bioconvective Radiative Non-Darcy Second Order Slip Flow of a Casson Nanofluid Containing Gyrotactic Microorganisms with Activation Energy and Hall Effects

Anindita Sahoo[1]
[1]Department of Mathematics, National Institute of Technology Jamshedpur,
Jamshedpur-831014, India
E-mail (anindita.sahoo1993@gmail.com)

INTRODUCTION

The bioconvection arises because of the macroscopic convective motion of the fluid created by the density gradient originated through the collective swimming of microorganisms. The bioconvection phenomenon dedicates various operative usages in many biological, environmental, and biotechnological areas. Mutuku and Makinde (2014) introduced a substantive model consisting of magnetohydrodynamic water-based nanofluid flow under the influence of bioconvection because of gyrotactic microorganisms.

Naturally, the measure of the system's disorderliness or consumption of the desired energy indicates entropy. The ruining of desired energy causes the reduction of competency of scientific equipment. The researchers are attracted to minimizing the entropy generation for overcoming several problems. Khan et al. (2020) established an operative mathematical model owing to clarifying entropy generation in radiative rolling motion of Casson nanofluid flow under the consequences of magnetic field and Joule heating.

The close surveillance of the previous explorations infers that the unsteady three-dimensional bioconvective Casson nanofluid flow passed over a stretching sheet under diacritic effects of Hall current, nonlinear thermal radiation, chemical reaction, and activation energy has not been explored yet. It is earnestly tried to fulfill this research gap in the present research article.

MATERIALS AND METHODS

Materials: activation energy, bioconvection, Hall current, motile gyrotactic microorganisms, second-order velocity slip, non-Darcy porous medium.

Methods: Proper similarity transformations [S. Shateyi and S. S. Motsa (2010)] are applied for achieving nonlinear ordinary differential equations. The produced nonlinear ordinary differential equations have been solved using one kind of robust numerical process named the spectral quasi-linearization method [A. Sahoo and R. Nandkeolyar (2021)].

RESULTS AND DISCUSSION

From Figure 1(a), the higher magnetic parameter (M) boosts up the temperature immensely. The potent magnetic field boosts elevating the Ohmic heating. As per Figure 1(b), the bioconvection Rayleigh number (Rb) has a favorable trend towards the motile microorganism profile. The strong buoyancy force's presence due to bioconvection creates a rise in the motile microorganism field because of upsurging the bioconvection Rayleigh number.

ICATP 2022, ISBN 978-81-952903-0-7

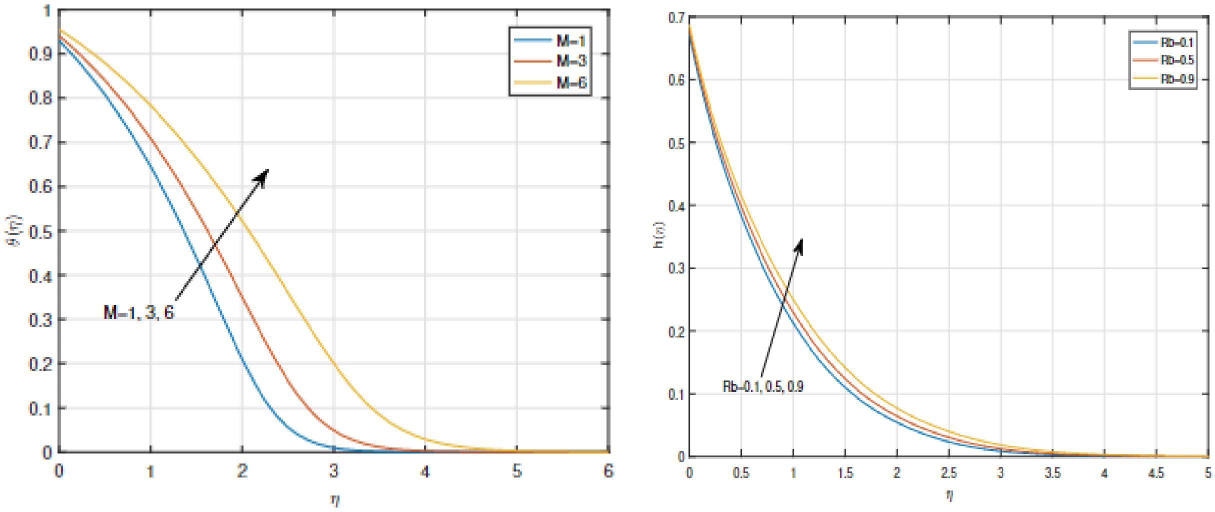

(a) **(b)**

Figure 1. Impact of (a) M on the temperature field and (b) Rb on the motile microorganism profile.

CONCLUSION

The interesting findings of the present research study are revealed below

- The strong magnetic field resists fluid movement but enlarges transverse velocity at the sheet's neighborhood.
- The enlarging tendency of the bioconvection Rayleigh number to motile microorganism's concentration is observed, indicating the motile microorganism boundary layer thickness to be thicker.
- The Casson parameter opposes entropy production far from the sheet.

REFERENCES

A. Khan, Z. Shah, E. Alzahrani, and S. Islam. 2020. Entropy generation and thermal analysis for rotary motion of hydromagnetic Casson nanofluid past a rotating cylinder with Joule heating effect. Int. Commun. Heat Mass Transf., 119:104979.

A. Sahoo and R. Nandkeolyar. 2021. Entropy generation in convective radiative flow of a Casson nanofluid in non-Darcy porous medium with Hall current and activation energy: The multiple regression model. Appl. Math. Comput., 402:125923.

S. Shateyi and S. S. Motsa. 2010. Variable viscosity on magnetohydrodynamic fluid flow and heat transfer over an unsteady stretching surface with Hall effect. Bound. Value Probl., 2010:1-20.

W. N. Mutuku and O. D. Makinde. 2014. Hydromagnetic bioconvection of nanofluid over a permeable vertical plate due to gyrotactic microorganisms. Comput. Fluids, 95:88-97.

CHAPTER -50

A BIOCONVECTION MODEL OF AN UNSTEADY MHD MICROPOLAR FLUID WITH WATER BASED METALLIC OXIDE NANOPARTICLES THROUGH A SQUEEZING CHANNEL

Srinivasu, M[1], and Sastry, D.R.V.S.R.K[2*]

[1]Department of Mathematics, Aditya College of Engineering, Surampalem – 533437, India
[2*]Department of Mathematics, SASTRA Deemed University, Thanjavur – 613401, India
drvsrksastry@gmail.com

INTRODUCTION

The unsteady flow through a squeezing channel, originated by the moving boundary under the influence of external normal stresses, is often encountered in the process of manufacturing hydro-dynamical machines, accelerators, lubrication equipment, and so on. Initial investigation on squeezing flow is made by Stefan (1874). Later, research has been carried out by several researchers successively for various geometrical configurations. Moore (1965) extended the Stefan equation for viscous fluid through a squeezing channel. Hayat et al.(2016) have analyzed the problem of a squeezing flow in MHD Jeffery nanofluid. Ali et al.(2013) have discussed the effect of radiations on un-steady free convection magnetohydrodynamics flows of the Brinkman kind fluids in a porous medium have Newtonian heat. Khan et al. (2016) observed thermal radiation consequence on squeezing flow Casson fluid among parallel disks. Srinivasacharya (2015) has been investigated both the effects in the vertical curly surface at existing of the porous medium.The term “bio-convection” was stated by Platt (1963) from the beginning with the streaming patterns detected in the dense cultures of free-swimming microorganisms. Zuhra et al. (2018) explained the mechanism of gyrotactic microorganisms with magnetohydrodynamic second grade nanofluid flow under the passively controlled nanofluid model boundary conditions by using convectively heated vertical surface.

PROBLEM FORMULATION AND SOLUTION

The problem consists of two plates at a distance $h(t)=l\sqrt{(1-\alpha t)}$. The upper plate moving with velocity ${dh}/{dt}$ touches the lower plate at $t=1/\alpha$. The micropolar nanofluid flow between two parallel plates with embedded nanoparticles, where the base fluid water is considered. Assume constant temperature H_1 at the upper plate and no heat flux at the center of the channel. The magnetic field acts in the direction of the horizontal plates. The governing equations along with the boundary conditions are first converted to a set of nonlinear ordinary differential equations with the aid of similarity transformation and then, are numerically solved by means of RK method equipped with the shooting technique.

RESULT ANALYSIS

An analysis is carried out over temperature, microrotation, concentration, and density of microorganisms(see the figure1 to figure4) when the upper plate is moving towards lower plate(squeezing case). It is found that temperature increases and microroation decreases with increase in magnetic parameter. This is due to the Lorentz force developed by magnetic field. Iron nanoparticles’ temperature distribution is found high(fig.1) and futher, observed a high spin in copper nanoparticles(fig.2). Concentration increases with increase in concentration parameter and noticed high when the distance between the plates is large. It is very clear from the fig.4 that the Schmidt number enhances the density of microorganisms.

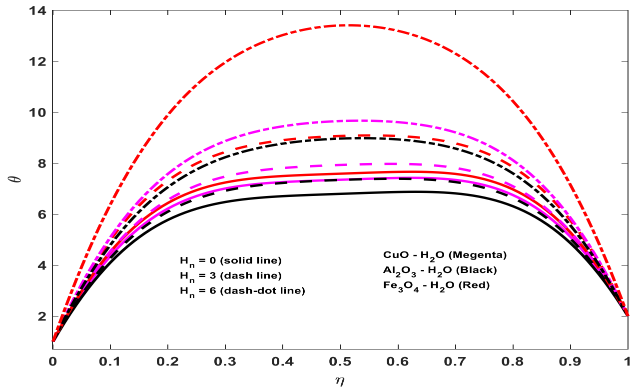

Figure 1: θ vs η **for different** H_n

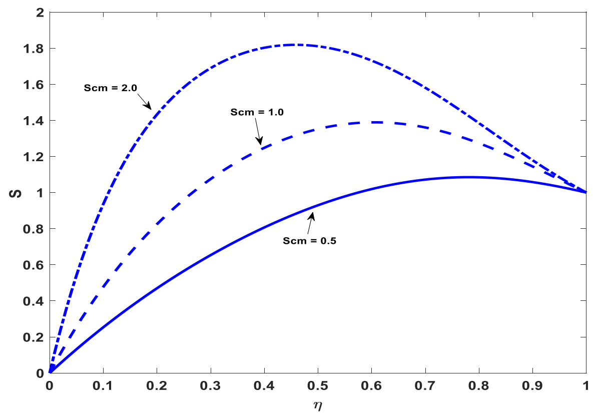

Figure 4: S vs η **for different** Scm

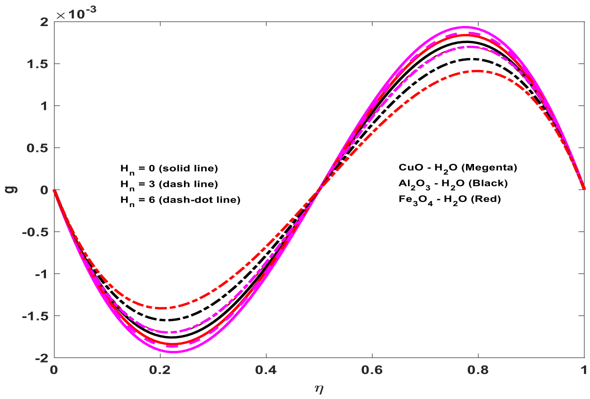

Figure 2: g vs η **for different** H_n

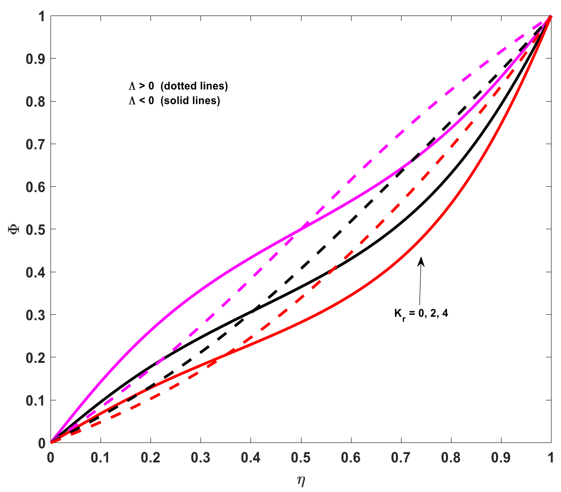

Figure 3: Φ vs η **for different** K_r

CONCLUSION

1) Temperature distribution is found high in Iron-water nanofluid particles.
2) The magnitude of microrotation is found less in Iron-water nanofluid particles.
3) The species concentration is increasing with chemical reaction parameter

REFERENCES

Stefan, J. 1874. Versucheuber die scheinbare adh ¨ asion, ¨ Akadenie deer Wissenschaften in Wien. Math.-Naturw, 69: 713– 721.

Moore, D.F. 1965. A review of squeeze films, Wear, 8(4): 245–263.

Hayat T, Abbas T, Ayub M, Muhammad T, Alsaedi A. 2016. On squeezed flow of jeffrey nanofluid between two parallel disks. Appl. Sci. 2016;6:346.

Ali F, Khan I, Haq SU. Shafie S. 2013. Influence of Thermal Radiation on Unsteady Free Convection MHD Flow of Brinkman Type Fluid in a Porous Medium with Newtonian Heating. Mathematical Problems in Engineering; 2013. DOI.org/10.1155/2013/632394.

Khan SI, Khan U, Ahmed N, Mohyud-Din ST. 2016. Thermal Radiation Effects on Squeezing Flow Casson Fluid between Parallel Disks. Comm. in Numerical Analysis. 92-107.

Srinivasacharya D, Mallikarjuna B, Bhuvanavijaya R. 2015. Soret and Dufour effects on mixed convection along a vertical wavy surface in a porous medium with variable properties. Ain Shams Engineering. 6:553-564

Platt, J.R.1963. Bioconvection patterns in cultures of free-swimming microorganisms, Science 133, 1766–1767.

Zuhra, S., N. S. Khan, S. Islam, 2018. Magnetohydrodynamic second grade nanofluid flow containing nanoparticles and gyrotactic microorganisms, Computational and Applied Mathematics 37, 6332–6358. https://dx.doi.org/10.1007/s40314-018-0683-6.

CHAPTER -51

Computational Modeling and Simulation of Tumor Dynamics: Current Status and Future Outlook

Gobinda Debnath[1,*] and B. Vasu[1]
[1]Department of Mathematics, Motilal Nehru National Institute of Technology Allahabad, Prayagraj 211004, U.P., India
*E-mail (gobinda.2021rma02@mnnit.ac.in)

Abstract

Nowadays throughout the world studying biological processes through mathematical modeling become significant since it is used to simulate the dynamics of biological processes which will strengthen the quantitative and analytical understanding of biomedical research. Currently, mathematical modeling of phenomena like tumour growth and its treatments in cancer dynamics become very hot issues in the biomedical research world. The main intent of the paper is to provide an extensive review of tumor dynamics, mathematical models of tumor dynamics, dynamics of cancer cells. Also the review explores their interaction with the Immune system, and different types of discrete and hybrid models. This review also focuses on its treatment resistance evolution, challenges, and related treatment models. It also considered the simulation of tumor dynamics, significances, and opportunities of model-based study. The evolution of advancements in cancer research which helps in overcoming treatment troubles and resistance due to the complex tumor dynamical system leads to more hope to treat cancer.
Keywords: Mathematical Models, Tumor Dynamics, Treatment Resistance Evolution.

Introduction

According to American Cancer Society data approximately 1.6 lakh new cancer cases and 50 thousand deaths estimated in every months in the US in 2022. This data also estimated around 19 lakh new cancer cases and more than 6 lakh deaths will happen in the US in 2022 (Seigal et al. 2022). Even in India, according to the data of Indian Council of Medical Research (ICMR) - National Centre for Disease Informatics and Research, there were an estimated 1.39 million cancer cases in India in the year 2020.
Mathematical modelling has been the most dominant tool to study the behaviour of tumour development, parameters that influence its progress, and its bio interaction with the host tissue in the living organism (Gatenby 1996; Anderson et al. 2000; Anderson 2005). An intensive study of biological phenomenon through mathematical modelling helps biomedical research to make a better world. The biological characteristics of tumour dynamics are very complex, it shows various kinds of resistance and challenges to its treatment. Continuous never-ending progress is going on to overcome such resistance and hence improvement in therapy brings a better life to living beings. (Hahnfeldt et al. 1999; Enderling et al. 2006; Meral and Surulescu 2013; Meghdadi et al. 2016).

Mathematical Models and Background

This review throughly studied the ODE and PDE-based models of tumor growth, derivation of such models and how they can be used to simulate tumor growth and treatment purpose, and dynamics of growth rates (Enderling and Chaplin, 2014). A combined analysis of mathematical modeling, simulation of tumor dynamics with drug interventions has been studied by (Unni and Seshaiyer, 2019) in which the mathematical model that combines important interactions between tumor cells and cells in the immune systems including natural killer cells, dendritic cells, and cytotoxic $CD8^+$ T cells combined with drug delivery to these cell sites is also considered in this review. This review also consider the following equation (Unni and Seshaiyer, 2019) that has been used to describe the dynamics of various types of cell population.

$$\frac{\partial[.]}{\partial t} + \nabla.(\vec{u}[.]) - \delta_D \nabla^2[.] = f(.) - g(.) - K_{[.]} z(M)[.] \qquad (1)$$

Numerical Simulation of Tumor Dynamics

To study the dynamical behavior of tumor cell population progress and its interaction with the other type of cells in the host tissue numerical simulation is done. Unni and Seshaiyer, (2019) have shown the detailed dynamics of these cells which include interactions between each other as well as dynamics generated by interaction with chemotherapy as well immunotherapy drug concentrations in the bloodstream. Gulnihal Meral and Christina Surilescu, (2013) have proposed a mathematical model for the influence of heat shock proteins on tumor invasion which studied the both analytical and numerical simulations of the model, this found a fine agreement with the expected behavior of invasion for the different choices of time delay.

Clinical Importance

Despite a huge effort from the researchers towards the development of advanced mathematical models, very few clinical achievements have been found over the years. These models can be used to discover the important biological parameters, which will help to predict the treatment outcome. Over the years all the conventional way of treatments for cancer has a substantial amount of challenges and a very small amount of success rate has been recorded. The improvements in mathematical modeling-based research help in controlling its treatment and anti-cancer drug delivery. Thus it shows a notable reduction in the number of new cases and deaths over the years.

Discussion and Conclusion

Day-by-day improvements in mathematical modeling give a better insight into understanding how it causes and how to tackle it. İn the present review article discussed different mathematical models which illustrate the dynamics, surroundings environment interaction, and how to reduce the difficulties in its Clinical implementation. Based upon rigourous studies from the literature it is found that the results may aid the model-based anticancer treatment reaction analysis. An ultimate general model structure controlling al this aspect would be big advantage for optimizing anticancer treatment.

References

Anderson, A. R., Chaplain, M. A., Newman, E. L., Steele, R. J., & Thompson, A. M. (2000). Mathematical modelling of tumour invasion and metastasis. *Computational and mathematical methods in medicine*, *2*(2), 129-154.

Anderson, A. R. (2005). A hybrid mathematical model of solid tumour invasion: the importance of cell adhesion. *Mathematical medicine and biology: a journal of the IMA*, *22*(2), 163-186.

Enderling, H., Anderson, A. R., Chaplain, M. A., Munro, A. J., & Vaidya, J. S. (2006). Mathematical modelling of radiotherapy strategies for early breast cancer. *Journal of Theoretical Biology*, *241*(1), 158-171.

Gatenby, R. A., & Gawlinski, E. T. (1996). A reaction-diffusion model of cancer invasion. *Cancer research*, *56*(24), 5745-5753.

Mathur, P., Sathishkumar, K., Chaturvedi, M., Das, P., Sudarshan, K. L., Santhappan, S., Nallasamy, V., John, A., Narasimhan, S., Roselind, F. S., & ICMR-NCDIR-NCRP Investigator Group (2020). Cancer

ICATP 2022, ISBN 978-81-952903-0-7

Statistics, 2020: Report From National Cancer Registry Programme, India. *JCO global oncology*, *6*, 1063–1075.

Meghdadi, N., Soltani, M., Niroomand-Oscuii, H., & Ghalichi, F. (2016). Image based modeling of tumor growth. *Australasian physical & engineering sciences in medicine*, *39*(3), 601-613.

Meral, G., & Surulescu, C. (2013). Mathematical modelling, analysis and numerical simulations for the influence of heat shock proteins on tumour invasion. *Journal of Mathematical Analysis and Applications*, *408*(2), 597-614.

Siegel RL, Miller KD, Fuchs HE, Jemal A. Cancer statistics, 2022. *CA Cancer J Clin*. 2022; 72(1): 7– 33.

Unni, P., & Seshaiyer, P. (2019). Mathematical modeling, analysis, and simulation of tumor dynamics with drug interventions. *Computational and mathematical methods in medicine*, *2019*.

Yin, A., Moes, D. J. A., van Hasselt, J. G., Swen, J. J., & Guchelaar, H. J. (2019). A review of mathematical models for tumor dynamics and treatment resistance evolution of solid tumors. *CPT: pharmacometrics & systems pharmacology*, *8*(10), 720-737.

CHAPTER -52

NUMERICAL INVESTIGATION OF LIQUID PLUG DEPOSITION IN HUMAN RESPIRATORY AIRWAY

Sourav Sudhakaran[1], Md. Asif[1], Kishore Singh Patel[1*]
[1,] Department of Mechanical Engineering, National Institute of Technology, Rourkela
[*]E-mail: patelks@nitrkl.ac.in; kishpatel.mech@gmail.com; Mob. No. +91-9945676486

INTRODUCTION

As of May 2022, COVID-19 pandemic has resulted in almost 62 lakh fatalities worldwide. Across the world, scientific communities are working to better understand the mechanism of virus infection and treatments to reduce its impacts. According to the preliminary research on COVID-19 infection, the SARS-CoV-2 virus infects AE2 cells in the alveolus just like other members of the corona family. This, in turn, causes a lack of natural pulmonary surfactants in the airways, which might lead to the formation of blockages in the airways due to increased surface tension of the inner lining fluid or liquid film. This leads to acute respiratory distress syndrome (ARDS) in the patients, which is a typical symptom of COVID-19 infection. Considering this, a drug delivery technique based on surfactant replacement therapy (SRT) (Grotberg et al. 2011) is being investigated. This work aims to computationally optimize the pulmonary drug delivery mechanism as per the lung conditions of different COVID-19 patients.

Previous studies in this field have analyzed the propagation of the liquid plug analytically, numerically, and experimentally. However, most of the studies focused on examining the peak stresses produced during the rupture and ways to reduce the tissue damage associated with it. The current work aims to optimize the propagation of liquid plug for the better deposition of containing the drug inside the pulmonary airway. For the drug to be deposited, the liquid plug must be pushed through the airway until its contents are deposited on the walls of the airways and reach a point where the plug ruptures. A generation number of 7/8 is chosen for the study. The choice of generation is based on the smallest size Bronchoscope (drug deposition medium) available as of now.

METHODOLOGY

The coupled Navier-Stokes and Cahn-Hilliard Phase field equations are numerically solved using an in-house developed multiphase solver. This diffuse interface multiphase model readily handles the dynamics of liquid plug propagation and rupture inside the airways. Since the Reynolds number of flow being considered is in the range of 200 – 300, laminar flow is assumed inside the respiratory pipe. Hence the domain is solved using a 2D axisymmetric approach.

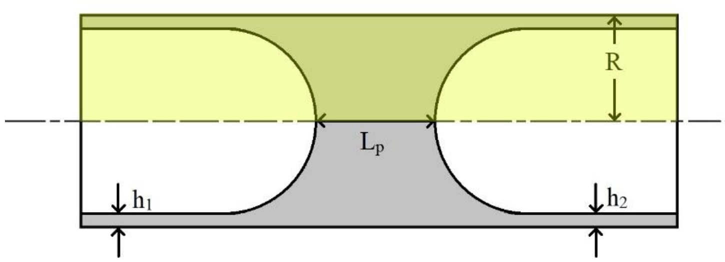

Figure 1: Schematic diagram of computational domain.

The schematic of computational domain is highlighted in Figure 1. The parameters such the optimal dosage, the time until the plug ruptures, and the volume rate of drug deposition are being studied to optimize the drug deposition. The results were validated by comparing the time variation of plug width with previous studies. A parabolic velocity profile is applied at the inlet and a constant pressure boundary condition is applied at outlet.

RESULTS AND DISCUSSION

In this work, the preliminary results obtained from the studies are discussed. Figure 2 shows the time evolution comparison of liquid plug width with reference results reported by Hassan et al. (2010). The initial non-dimensional plug width (L_p /R) of liquid plug is kept 1, and the leading film thickness (h_2/R) along the inner surface of the wall is 0.13. A pressure gradient (ΔP) of 1 (inertial scaling) is applied across the plug. After the validation of the computational setup, a time evolution of the liquid plug profile (Figure 3) is studied for the parabolic velocity inlet condition with the overall volume flow rate of 20 liter/min. The leading-edge film thickness, in this case, is kept h_2/R = 0.9. Figure 3 shows the evolution profile of pressure contours along with the exact location liquid-air interface (solid black line). As can be seen, at around non-dimensional time (tU/R) of 40 steps, the contents of liquid plug have already been deposited on the walls of the airway, leading to the thinning of the liquid plug and its eventual rupture.

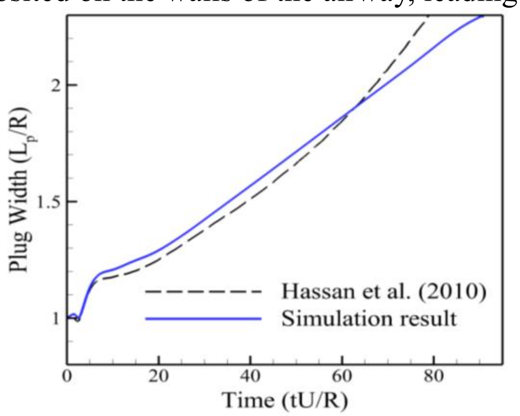

Figure 2: Validation plot compares the variation in liquid plug width with evolution time for h_2=0.13R.

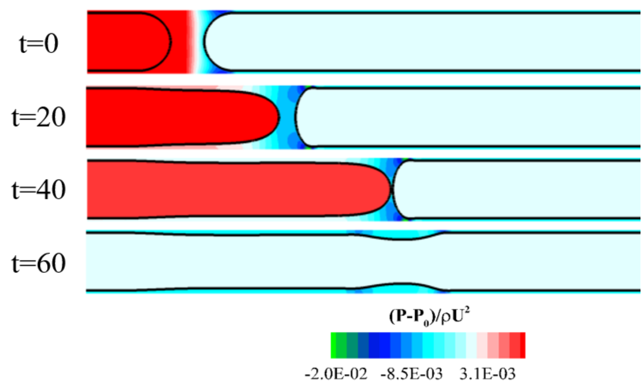

Figure 3: The pressure contours showing time evolution of the liquid plug propagation leading to its rupture.

Further, simulations are conducted with different inlet velocities, and it has been found that a cut-off velocity exists below which deposition does not occur. Counterintuitively, the liquid plug collects fluid from the walls leading to an increase in plug width during its propagation. The velocity study identifies the cut-off velocities for different film thicknesses, and the time required for the rupture is investigated. It has been found that the time required for rupture decreased with increasing inlet velocity, which shows a similar trend for the drug deposition area. However, the volume rate of deposition increases with the velocities.

CONCLUSION

The study shed light on the dynamics of liquid plug propagation and the drug deposition trends for different inlet velocities and liquid film thicknesses. The existence of a cut-off velocity was found out below which the deposition ceases to occur. From the study results, the amount of drug that can be deposited for a patient with a particular pulmonary film thickness (which depends on the patient's disease situation) can be found for different breathing rates.

REFERENCES

E. A. Hassan, E. Uzgoren, H. Fujioka, J. B. Grotberg, and W. Shyy, "Adaptive Lagrangian-Eulerian computation of propagation and rupture of a liquid plug in a tube," *Int. J. Numer. Methods Fluids*, vol. 67, no. 11, pp. 1373–1392, Dec. 2011, doi: 10.1002/fld.2422.

J. B. Grotberg, "Respiratory fluid mechanics," *Phys. Fluids*, vol. 23, no. 2, 2011, doi: 10.1063/1.351773.

CHAPTER -53

Reliability Analysis of the Shafts when Shear Stress follows Weibull Distribution

Md. Yakoob Pasha[1], M. Tirumala Devi[2], and T. Sumathi Uma Maheswari[3].
[1]Department of Mathematics, Kakatiya University, Warangal-506009, Telangana, India.
[2]Department of Mathematics, Kakatiya University, Warangal-506009, Telangana, India.
[3]Department of Mathematics, Kakatiya University, Warangal-506009, Telangana, India.
E-mail: mypasha139@gmail.com

INTRODUCTON

Reliability of a system is the probability that a system perform its intended purpose for a given period of time under stated environment conditions. In some cases system failures occur due to certain type of stresses acting on them. Anil Misra et al. [1] discussed with the view of developing methods for reliability based design, the finite difference technique was combined with the Monte-Carlo simulation method to create a probabilistic load–displacement analysis. The Monte-Carlo simulation method was used, in lieu of other closed-form probabilistic techniques, due to the complexity of the load–displacement analysis. Dr. Edward E. Osakue et al. [2] studied fatigue shaft design verification for bending and torsion. Dr. R. K. Bansal [3] discussed shear stress produced in a circular shaft subjected to torsion, torque transmitted by a circular solid shaft and a hollow circular shaft. E. Balagurusamy [4] discussed stress dependent hazard models. K. C. Kapur and L.R. Lamberson [5] discussed design of a shaft subjected to torsion, when a shaft is subjected to a torque a shearing stress is produced in the shaft. M. E. Ghitany et al. [6] studied Lindley distribution and its application.

MATERIALS AND METHODS

The probability density function (pdf) of the Weibull distribution is

$$f(t) = \left(\frac{k \times t^{k-1}}{\lambda^k}\right) \left[\exp\left(-\frac{t}{\lambda}\right)^k\right]$$

where $t \geq 0, k > 0$ is the shape parameter and scale parameter $\lambda > 0$ is the characteristic life.
The reliability function and the hazard rate functions of Weibull distribution are respectively

$$R(t) = \exp\left(-\frac{t}{\lambda}\right)^k \text{ for } t \geq 0 \text{ and}$$

$$h(t) = \frac{k}{\lambda^k} \times t^{k-1}$$

The reliability function of shear stress produced in a circular shaft subjected to torsion is

$$R(t) = \exp\left[-\left(\frac{t}{\lambda}\right)^k \times \left(\frac{R \times C \times \theta}{L}\right)\right]$$

The reliability function of torque transmitted by a circular solid shaft is

$$R(t) = \exp\left[-\left(\frac{t}{\lambda}\right)^k \times \left(\frac{16T}{\pi D^3}\right)\right]$$

The reliability of torque transmitted by a hollow circular shaft is

ICATP 2022, ISBN 978-81-952903-0-7

$$R(t) = \exp\left\{-\left(\frac{t}{\lambda}\right)^{k} \times \left[\frac{16T \times D_0}{\pi(D_0^4 - D_i^4)}\right]\right\}$$

Table 1
k =1.9622, λ=0.8,
R=16 mm, L=64 mm,
C=73.1 GPa, θ=0.0698 radian.

t	R(t)
0.1	0.978669741
0.2	0.919418557
0.3	0.83014411
0.4	0.720820864
0.5	0.602172759
0.6	0.484146672
0.7	0.374722548
0.8	0.279264756
0.9	0.200437429
1.0	0.138570467

Figure 1

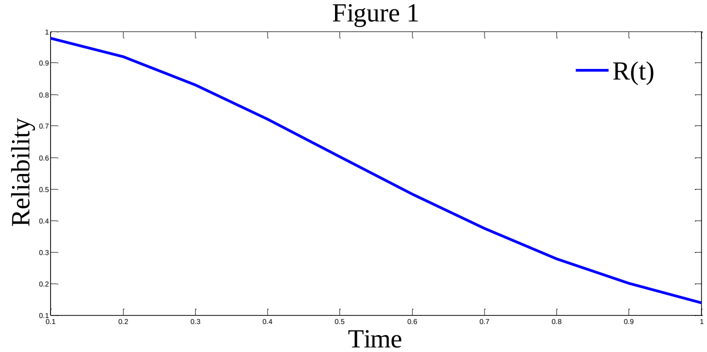

CONCLUSION

The reliability of a circular shaft subjected to torsion when shear stress follows Weibull distribution has been derived. The reliability analysis of torque transmitted by a circular solid shaft and a hollow circular shaft has been derived. It is observed that the reliability of the shaft decreases when time, twisting moment and modulus of rigidity increases and the reliability decreases when external diameter and length of the shaft decreases. Reliability of the shaft increases when internal diameter and total torque decreases.

REFERENCES

[1] Anil Misra et al., "Reliability analysis of drilled shaft behavior using finite difference method and Monte Carlo simulation", Geotech Geol Eng, Springer Science+Business Media B.V., pp. 493–506, 2007.

[2] Dr. Edward E. Osakue, D. L. Anetor and D. C. Odetunde, "Fatigue Shaft Design Verification for Bending and Torsion," International Journal of Engineering Innovation and Research, vol. 4, no. 1, pp. 197-206, 2015.

[3] Dr. R. K. Bansal, "Strength of Materials (Mechanics of Solids)", Laxmi Publications (Private) Limited, New Delhi, 1996.

[4] E. Balagurusamy, "Reliability Engineering", McGraw Hill Education (India) Private Limited, New Delhi, 1984.

[5] K. C. Kapur and L. R. Lamberson, "Reliability in Engineering Design", Wiley India Private Limited, New Delhi, 1997.

[6] M. E. Ghitany, B. Atieh, and S. Nadarajah, "Lindley distribution and its application", Mathematics and Computers in Simulation (Elsevier), pp. 493-506, 2008.

CHAPTER -54

An impact of MHD on casson nanofluid flow with heat source/sink and first order chemical reaction

T. Maranna[1*] & U.S. Mahabaleshwar[2]

[1] *Department of Mathematics, Davangere University, Shivagangothri, Davangere, 577 007*
Email: marannat4@gmail.com
[2]*Department of Mathematics, Davangere University, Shivagangothri, Davangere, 577 007*
Email: u.s.m@davangereuniversity.ac.in

Abstract

The primary goal of this research is to examine the effect of MHD casson nanofluid flow on the thermosolutal Marangoni boundary with heat source/sink with first order chemical reactions. The flow is studied as a result of nonlinear thermal radiation. In order to obtain analytic outcomes. The ruling PDE's are reconstructed through to ODE's using correct non-dimensional variables. The problem of continuous, laminar flow of an electrically conducting MHD casson nanofluid is investigated analytically in the presence of first-order chemical reactions, heat generation or absorption, and a magnetic field. Temperature and concentration are thought to be proportional to surface tension. Graphs depict physical factors such as heat generation/absorption coefficient, velocity, temperature, concentrations, and suction/injection qualities.

Key words: MHD, Casson fluid, Nanofluid, Marangoni boundary conditions, heat source/sink, First order chemical reaction.

CHAPTER -55

AN MHD CASSON GAS FLOW OVER A STRETCHING/SHRINKING SHEET WITH INDUCED SLIP CONDITION

G. P. Vanitha, Research Scholar, Department of Mathematics, Davangere University, Davangere-577007.
U. S. Mahabaleshwar, Professor, Department of Mathematics, Davangere University, Davangere-577007.

ABSTRACT
Theoretical investigation is carried out in this paper, to analyse the MHD Casson gas flow and heat transfer over a linearly stretching/shrinking sheet under induced slip condition and radiation effect. The closed form solution is obtained for the governing equations under the boundary layer conditions. The explicit solution to the MHD flow are obtained analytically and explained. Variations in physical parameters such as induced slip parameter, suction/injection, Chandrasekhar number, radiation number, and shear stress are analysed and presented graphically. The effects of induced slip parameter and inclined magnetic field on the flow are also demonstrated. Flows in slip reign have numerous applications in micro and nanoscale level problems, as well as flows with minute particles. This problem, which involves MHD effects and aids in fluid motion control, is technically excellent and has applications in industries and research laboratories.

Keywords
Casson model, induced slip, stretching/shrinking sheet, inclined MHD, suction/injection, analytical solution.

CHAPTER -56

SOLUTE TRANSPORT IN A MAGNETOHYDRODYNAMICS COUETTE FLOW UNDER THE EFFECT OF REVERSIBLE REACTION

Nanda Poddar [1,*], Subham Dhar[1], and Kajal Kumar Mondal[1]

[1] Department of Mathematics, Cooch Behar Panchanan Barma University, Cooch Behar, West Bengal, India-736101

[*]E-mail: nandapoddarcr7@gmail.com

INTRODUCTION

Over the last several decades, the study of the mixing of solute particles in different flow geometry has been given special care due to their practical importance in a number of fields, such as environmental, biomedical and chemical engineering, as well as the pharmaceutical industry. The solute transport phenomena in a magnetohydrodynamics (MHD) flow under the impact of chemical reaction plays important roles in drug targetting, glass blowing, polymer solutions, food processing and paper manufacturing industries. Thus, the this types of real world application problems on MHD flow with chemical reaction are significant to investigate. In recent time, the effect of reversible phase exchange kinetics in open channel flow and Couette flow are studied by several resaerchers (Ng and Bai, 2001; Barik and Dalal, 2021; Poddar et al. 2022). Transport of solute in MHD flow are discussed by Poddar et al. 2021; Dhar et al. 2022. But, from the literature review, it is observed that no work has been reported on transport of solute in a MHD Couette flow with the aid of a transverse magnetic field under the effect of reversible reaction.

In the present research, the transport phenomena in a MHD couette flow wherein the soluable particles may undergoes a reversible phase exchange between the immobile phase (stationary boundary bed phase) and mobile phase (fluid phase) is explored. To show the effects of phase exchange kinetics and retardation factor in apperance of transverse magnetic field on transport coefficient as well as in the two-dimensional longitudinal and transverse concentration distributions, the analytical expressions are found by multiple-scale homogenization technique. It is seen that with the enhancement of Damkohlar number and Hartmann number the transport coefficient diminishes remarkably

KEYWORDS: Transport, MHD Couette flow, Reversible reaction, Homogenization technique.

MATERIALS AND METHODS

For the current research a steady, laminar plane Couette flow between two parallel plates of viscous incompressible electrically conducting liquid in apperance of transverse magnetic field H_0 is considered. The plates are separated by a distance h. The $\overline{x}$ and $\overline{y}$ axes are taken as along longitudinal and transverse directions (see Figure 1). At $\overline{y} = 0$, the lower plate is assumed to be stagnent, where the upper plate moves with a constant velocity U in its own plane. The velocity distribution of MHD Couette flow in dimensionless form is given by,

$u = \frac{\overline{u}}{U} = \frac{SinhMy}{SinhM}$. Where $y = \frac{\overline{y}}{h}, M$ represents the Hartmann number, which describes the correlation into magnetic and viscous forces.

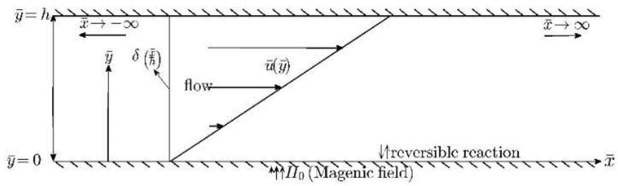

Figure 1. Schematic diagram of steady MHD Couette flow with reversible reaction.

When a reactive soluble particles with constant molecular diffusion coefficient D through the above mentioned flow is released, the transport problem of the reactive solute in dimensionless form is given by,

$$\frac{\partial C}{\partial t} + \epsilon u Pe \frac{\partial C}{\partial x} = \epsilon^2 \frac{\partial^2 C}{\partial x^2} + \frac{\partial^2 C}{\partial y^2}$$

The initial and boundary condition is taken as $C(x,y,t) \vee_{\; t=0} = \Delta\left(\frac{x}{\epsilon}\right)$

$$\frac{\partial C}{\partial y} = 0 at y = 1 \text{ and } \frac{\partial C}{\partial y} = \frac{\partial C_s}{\partial t} = Da(\theta C - C_s) \text{at} y = 0.$$

Here $\epsilon = \frac{h}{L} (\ll 1)$ is used as a perturbation parameter. The dimensionless parameters are $x = \frac{\bar{x}}{L}, y = \frac{\bar{y}}{h}, u = \frac{\bar{u}}{U}, t = \frac{\bar{t}}{h^2/D}, Pe = \frac{Uh}{D}, Da = \frac{\gamma h^2}{D}, \theta = \frac{\bar{\theta}}{h}$. Where C and C_s are concentration of mobile and immobile phases respectively; $\gamma$is the reversible reaction rate; $\bar{\theta}$ is the retention parameter or partition coefficient which represents the relation between the C and C_s; Da is the Damkohler number.

In order to solve the problem multi scale homogenization method is employed with three distinct time scales associated with two length scales (Barik and Dalal, 2021). The method consists of techniques used to create effective macro-scale models from complex micro-scale models and it is applied to get a sample of the same composition and structure throughout the volume.

RESULTS AND DISCUSSION

It is seen from the Figure 2 that lower kinetics of sorptive exchange i.e. when Da is larger, transport coefficient is smaller. It is significant to note that when the phase exchange kinetics is slow ($Da \ll 1$, the dispersion coefficients are large in comparison to that of the phase exchange kinetics is fast ($Da > 1$). It is also seen that as M increases, a resisting Lorentz force also increases in the flow, so the transport process reduces significantly. It is observed that with increment of retardation factor θ the transport coefficient initially enhances and after a certain value of θ it reduces. The amplitude of the real concentration distribution increases with the increment of Da, actually, from the immobile phase the tracer particles progresses rapidly in flow and enhance it in the mobile phase.

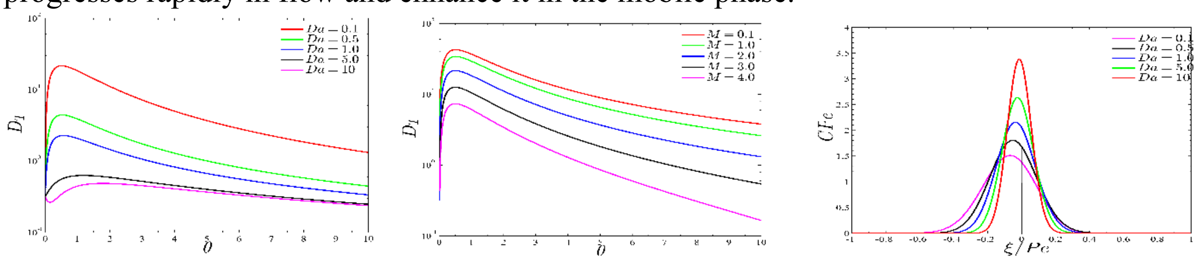

Figure 2. Variations of transport coefficient with θ for different Da and M and Longitudinal real concentration distribution for different Da.

CONCLUSION

The transport of reactive solute in MHD Couette flow with reversible reaction is discussed analytically by multi-scale homogenization method. The limiting case of the present outcome is compared with the previous analytical results of Bandyopadhyay and Mazumder, 1999; Ng and Bai, 2001; Poddar et al. 2022 and it achieved a remarkable agreement. The results shows the effect of Damkohler number

ICATP 2022, ISBN 978-81-952903-0-7

(phase exchange kinetics), Hartmann number, retention factor, dispersion time on transport coefficient, longitudinal and transverse real concentration distributions.

ACKNOWLEDGMENT

The first author is thankful to UGC, India for financial support.

REFERENCES

Barik, S., Dalal, D. C. Analytical solution for concentration distribution in an open channel flow with phase exchange kinetics. Acta Mechanica Sinica, 1.(2021).

Dhar, S., Poddar, N., Mondal, K.K., Mazumder, B. S.: On dispersion of solute in a hydromagnetic flow between two parallel plates with boundary absorption. Physics of Fluids. 33, 083609 (2021).

Ng, C.O., Bai, Y.C.: Dispersion in oscillatory Couette flow with sorptive boundaries. Acta Mechanica, 178(1-2), 65-84 (2005).

Poddar, N., Dhar, S., Mondal, K., K.,. Effect of reversible reaction on concentration distribution of solute in a Couette flow. Nonlinear Dynamics and Applications, Springer Proceedings in Complexity, (2022). (Accepted).

Poddar, N., Dhar, S., Mazumder, B. S., Mondal, K. K.: An Exact Analysis of Scalar Transport in Hydromagnetic Flow between Two Parallel Plates: a Multi-scale Approach. Proc. R. Soc. Lond. A. 477 (2248), 20200830 (2021).

CHAPTER -57

CONVECTIONAL FLOW OF NON-NEWTONIAN FLUID OVER THE SURFACE WITH CATTANEO-CHRISTOV MODEL

Atul Kumar Ray[*], **Minakshi Poonia** and **Divya Chaturvedi**

Engineering Mathematics and Computing, Madhav Institute of Technology and Science Gwalior, Madhya Pradesh-474005, India

Corresponding Author Email: akray18490@gmail.com, atulray@mitsgwalior.in

Abstract

The mathematical formulation and semi-numerical approach of two-dimensional steady convectional flow of non-Newtonian Jeffrey fluid over surface with modified Buongiorno model and Cattaneo-Christov heat flux is analysed. The influence of thermal relaxation is taken under consideration. Suitable transformation is introduced which turns into coupled and non-linear system of ordinary differential equation which are then solved using the Homotopy Analysis Method. The convergence of solution obtained from the method is significantly discussed using special curve in HAM method. Homotopy solutions are obtained for the velocity, surface temperature and concentration profiles. The nature of the flow of non- Newtonian fluid for different fluid parameter and thermal relaxation are elaborated through figures and table. The analysis reveals that thermal relaxation of CCF model can be applied to control the rise in temperature under difficult situation instead of Fourier Model of heat conduction.

Keywords: Cattaneo-Christov Heat Flux, Thermal Relaxation, Buongiorno Model

Mathematical Modeling

The transformed set of ordinary differential equations and associated boundary conditions

$$f''' + (1+\lambda)(ff'' - f'^2) + \beta\left(f''^2 - ff'''\right) = 0 \tag{1}$$

$$\frac{1}{\Pr}\theta'' + f\theta' + \frac{Ec}{(1+\lambda)}\left[f''^2 + \beta(f'f'' - ff'f''')\right] - \gamma(ff'\theta' + f^2\theta'') + Nb\theta'\phi' + Nt\theta'^2 = 0 \tag{2}$$

$$\frac{1}{Sc}\phi''(\eta) + f(\eta)\phi'(\eta) + \frac{Nt}{Nb}\theta'' = 0 \tag{3}$$

The boundary conditions become

$$\text{At } \eta=0 \quad f'=1, \quad f=0 \quad \theta=1, \quad Nb\phi'+Nt\theta'=0, \tag{4}$$

$$\text{At } \eta\to\infty \quad f'=0, \; f''=0, \; \theta=0, \; \phi=0 \tag{5}$$

Methodology

Homotopy Analysis Method is used to solved the system of equations. Residual error is decreasing with increase in number of approximation.

Result and Analysis

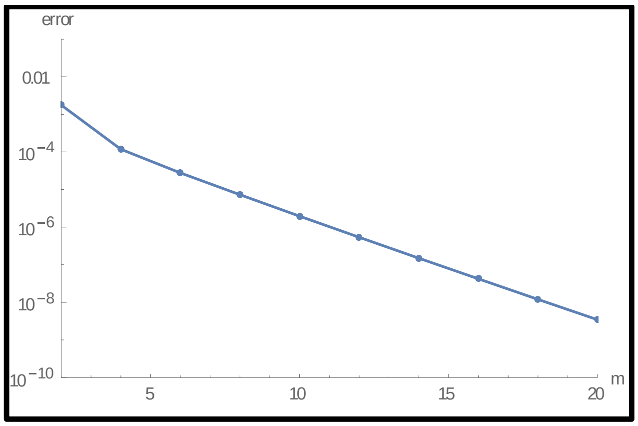

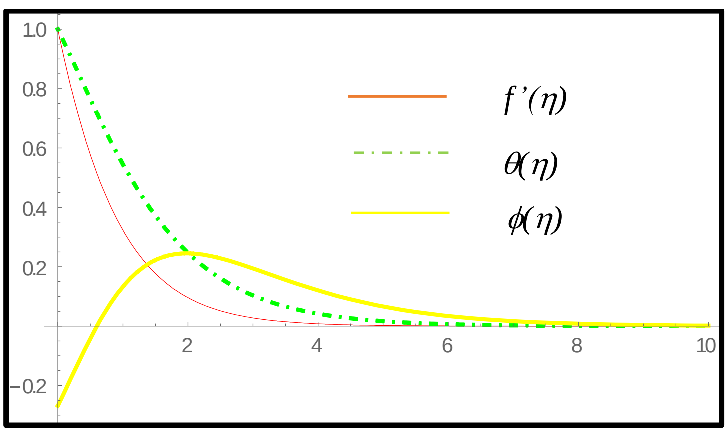

ICATP 2022, ISBN 978-81-952903-0-7

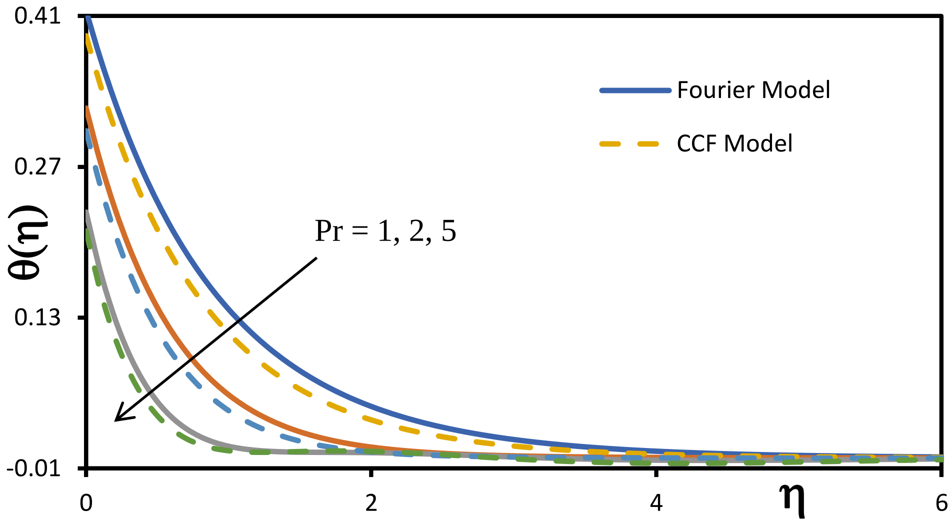

Conclusion

1) CCF model can be applied in order to control the temperature instead of Fourier Model of heat conduction.
2) Residual error is decreasing with increase in number of approximation which shows the convergence of homotopy series solution.

ICATP 2022, ISBN 978-81-952903-0-7

CHAPTER -58

BROWNIAN MOTION, THERMOPHORESIS EFFECTS ON MHD PULSATING FLOW OF CASSON NANOFLUID IN A VERTICAL CHANNEL

Suripeddi Srinivas[1], Kalyan Kumar Challa[2, *], and Anala Subramanyam Reddy[3]

[1] Department of Mathematics, School of Advanced Sciences, VIT-AP University, Inavolu, Vijayawada-522237, India.

[2] Department of Mathematics, Narayana Engineering College, Gudur-524101, SPSR Nellore, India.

[3] Department of Mathematics, School of Advanced Sciences, Vellore Institute of Technology, Vellore- 632014, India.

E-mail (kalyankumar.challa@gmail.com)

ABSTRACT

The Buongiorno model was used in the current study to analyse the MHD pulsatile Casson nanofluid flow along a vertical channel with chemical reaction and thermal radiation. Viscous dissipation and Joule heating effects are considered. The governing partial differential equations of the Casson nanofluid flow are converted to ordinary differential equations using the perturbation method and solved using the shooting technique with Runge–Kutta fourth-order method. According to the analysis, the velocity decreases with the rising applied magnetic field. The temperature profile falls with an increase in Hartmann number and rises for a given increase in thermophoresis and Brownian motion parameters. Additionally, the distribution of nanoparticle concentrations rises for a given increase in the Brownian motion parameter but falls for a given increase in the Lewis number and chemical reaction parameter.

Keywords: Casson nanofluid, Pulsatile flow, Lewis number, Thermophoresis, Brownian motion parameter.

ABOUT VIT-AP UNIVERSITY

VIT-AP University offers several avenues to explore your interests and identify core competencies through its flexible courses and a unique teaching-learning experience. The institute's curriculum focuses on practical learning and providing holistic education and growth. With state-of-the art facilities, continuous assessments, a student-oriented mentoring scheme, extracurricular activities, several international collaborations, placement opportunities and much more, VIT-AP ensures that students are informed, inspired, and engaged at the institute. Consistently ranked among the top educational institutes in the country, the VIT group of institutions have a proud tradition of pursuing knowledge and excellence. In a similar vein, the leadership at VIT-AP demonstrates a dynamic blend of academic initiative and industry partnership with a vision of creating one of the finest academic destinations in the world. With several years of educational, industrial, and administrative experience, VIT-AP is helmed by Dr. G. Viswanathan, Chancellor, founder of VIT group of institutions; along with the core group comprising Dr. Sekar Viswanathan, Vice-President; Dr. Sandhya Pentareddy, Executive Director; Dr. S. V. Kota Reddy, Vice-Chancellor; and Dr. Jagadish Chandra Mudiganti, Registrar.

For further details of VIT-AP University visit the official website: https://vitap.ac.in/

ABOUT THE SCHOOL OF ADVANCED SCIENCES

The School of Advanced Sciences (SAS) is one of the premier Schools of VIT-AP and it houses the Departments of Mathematics, Physics, and Chemistry. Our school aims at providing a solid foundation in natural Sciences by training the graduate, postgraduate, and PhD students in recent scientific and technological developments. Deploying the technique of project-based learning (PBL), we teach our students to think critically and encourage them to question, explore, and research across various disciplines of sciences. We aspire to be a valuable contributor towards the nation's growth and development by producing highly skilled professionals and charismatic leaders. We believe that our quality of education and research will foster ethical and professional standards in students and hone their logical-thinking and problem-solving skills which are essential to counteract the professional challenges of today and the future.

Further details of School of Advanced Sciences can be obtained from the website: http://vitap.ac.in/school-of-advanced-sciences/

VIT-AP University Location:

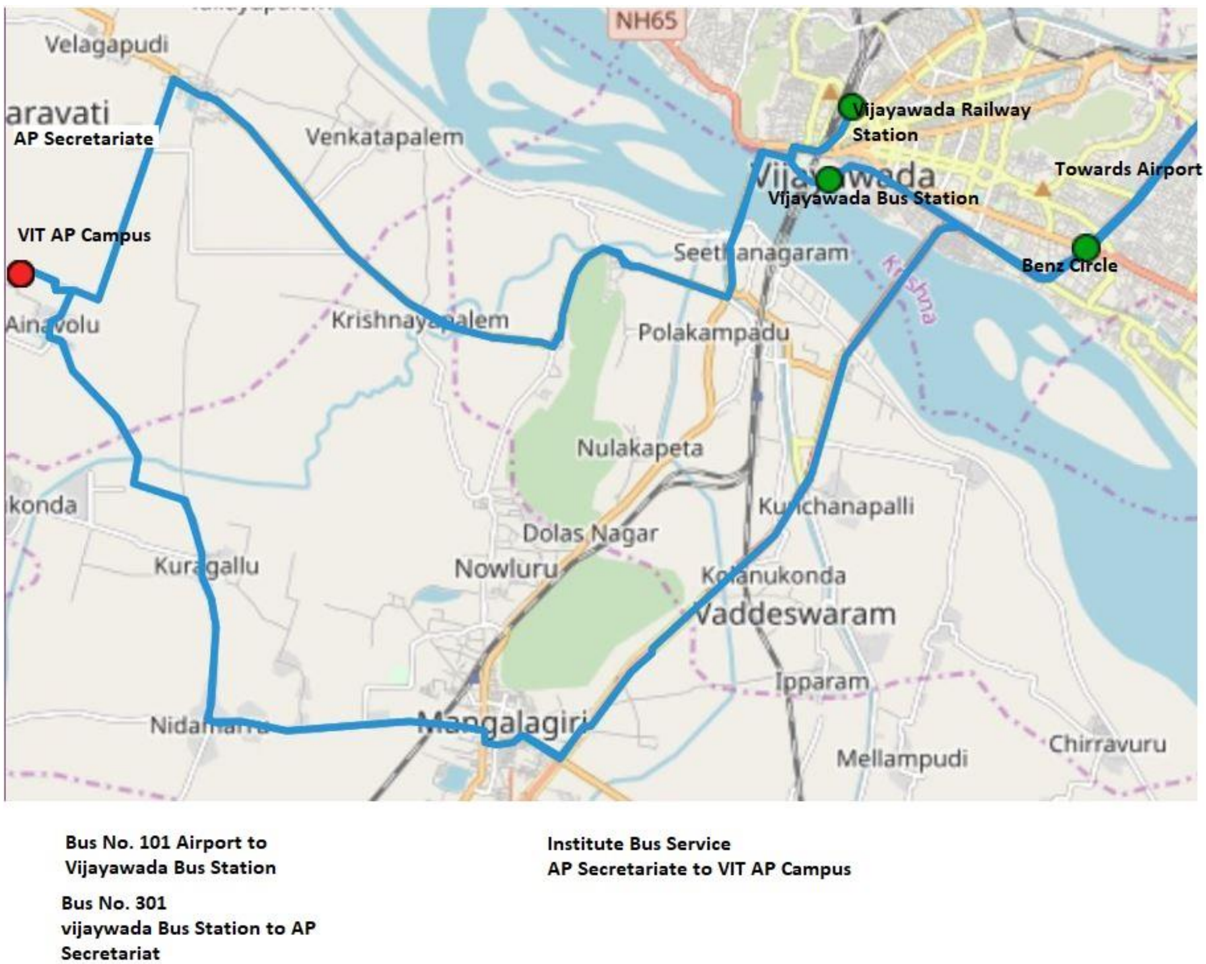

School of Advanced Sciences
VIT-AP University,
Andhra Pradesh-522237, India

https://vitap.ac.in/school-of-advanced-sciences/

secretary.sas@vitap.ac.in

ISBN 978-81-952903-0-7

9 788195 290307

www.openbookspublisher.com